Nonlinear Controller Design for Regulating Systems

A Dissertation

Presented to

the Faculty of the Department of Mechanical Engineering

University of Houston

In Partial Fulfillment

of the Requirements for the Degree

Doctor of Philosophy

in Mechanical Engineering

by

Fatemeh Zamanian

August 2015

Nonlinear Controller Design for Regulating Systems

Fatemeh Zamanian

Approved:

Chair of the Committee
Dr. Matthew A. Franchek, Professor,
Mechanical Engineering

Committee Members:

Co-chair of the Committee
Dr. Karolos Grigoriadis, Professor,
Mechanical Engineering

Dr. Jagannatha R. Rao, Associate Professor
Mechanical Engineering

Dr. Gangbing Song, Professor,
Mechanical Engineering

Dr. Robert S. Provence, Lecturer,
NASA, Johnson Space Center,
Electrical and Computer Engineering

Dr. Suresh K. Khator, Associate Dean,
Cullen College of Engineering

Dr. Pradeep Sharma, Professor and Chair
Mechanical Engineering

Acknowledgements

I would like to take this opportunity to offer my sincere thanks to all those individuals without whom this work would not have been possible.

First and foremost, I would like to thank my advisor, Dr. Matthew Franchek. It has been an honor and a great pleasure to work under his supervision. I appreciate his contributions of time, ideas and his continuous guidance and motivation throughout the course of my studies. I would like to thank my committee members Dr. Grigoriadis, Dr. Song, Dr. Rao, and Dr. Provence for their time and comments on reviewing my dissertation. I would also like to thank the staff of the Mechanical Engineering Department and all my lab-mates and friends at UH for their supports and helps.

Most importantly, I would like to thank Mehdi, my husband, for all of the encouragement he gave me to get through this adventure. His endless support made the completion of this work achievable. Lastly, I would like to thank my parents, Masoumeh and Ali, my sisters Mahboubeh and Faezeh, and my brother, Mohammad, for guiding and supporting me so that I could achieve my lifelong goals. This dissertation is dedicated to my family for their unconditional love and support.

Nonlinear Controller Design for Regulating Systems

An Abstract

of a

Dissertation

Presented to

the Faculty of the Department of Mechanical Engineering

University of Houston

In Partial Fulfillment

of the Requirements for the Degree

Doctor of Philosophy

in Mechanical Engineering

by

Fatemeh Zamanian

August 2015

Abstract

Presented in this dissertation is a nonlinear controller synthesis methodology based on the inverse Sinusoidal Input Describing Function (SIDF) for a class of regulating systems. The design goal is to improve regulating performance beyond what is achievable by a linear control for a predicted level of disturbance step size. The controller design is executed using open loop frequency domain information and is applicable when the frequency response of a linear design cannot satisfy the designed open loop gain and phase characteristics. The gain and phase differences between the designed open loop frequency response and that of a linear design is treated as SIDF distortions. The inverse describing function approach is employed to identify an isolated explicit nonlinearity that is associated with obtained gain and phase distortions.

For this, a computational solution to the inverse SIDF for a broad class of hysteresis or memoryless explicit nonlinearities is developed. The proposed numerical solution uses gain and phase distortions as a function of input amplitude size to identify the nonlinearity, and does not require *a priori* knowledge of the nonlinearity in the estimation process. The output from the algorithm is a non-parametric model of the nonlinearity from which a parametric model can be recovered.

To illustrate the proposed nonlinear controller design technique, the idle speed control of a V-6 fuel injected engine model subject to an external torque load disturbance is considered. The closed loop performance is validated through simulation and the closed

loop stability in the sense of the bounded-input-bounded-output (BIBO) is assessed using Circle Theorem.

Table of Contents

List of Figures

List of Tables

Chapter 1. Introduction

The controller design for a system is considered an open-ended problem. In general, controller design addresses imposing the performance requirements on the closed loop system. More specifically, a feedback controller provides one or more of the followings: (i.) stabilization of unstable systems, (ii.) tracking of reference inputs, (iii.) rejection of external disturbances, and (iv.) prevention of actuator saturation.

Typically, the controller design process provides a trade-off between the controller complexity and the closed loop performance requirements. A block diagram of a generalized control system is shown in Figure 1-1, where p denotes the derivative operator. Without loss of generality, this block diagram excludes sensor noises and input disturbances.

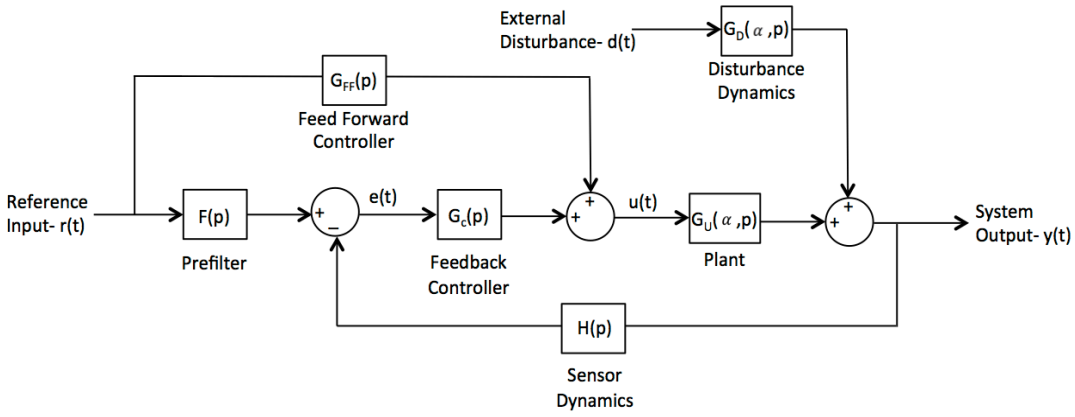

Figure 1-1 Block Diagram of a General Control System.

The dynamics between the controlled output, $u(t)$, and the system output, $y(t)$, are denoted by $G_U(\alpha, p)$, where α represents parametric uncertainties in the system. The dynamics between the external disturbance, $d(t)$, and the system output, $y(t)$, are denoted by $G_D(\alpha, p)$. Typically, these dynamics are given *a priori* to the controller design process and are considered fixed. The sensor dynamics, $H(p)$, provides a proper translation of the system output for the feedback controller.

For a single input single output (SISO) control system, there are generally three types of controllers available. (i.) The feed-forward controller, $G_{FF}(p)$, that provides a direct actuation of the reference input signal, $r(t)$, to the plant. This type of controller can be considered as a proactive response to a reference input. (ii.) The prefilter, $F(p)$, that is used to include additional dynamics to the reference input signal to improve the tracking performance of the closed loop system. (iii.) The feedback controller, $G_C(p)$, that is used to provide disturbance rejection, reduce sensitivity of the system to the uncertainty, and provide stability for the closed loop system. The amount of feedback control specified during controller design procedure is proportional to the degree of uncertainty in the system and the magnitude of the external disturbance [1].

The controller design techniques can be classified in different ways, depending on the type of information available for the open loop system and the performance requirements on the closed loop system. One general way to categorize these techniques is in the time domain and in the frequency domain. There is a tremendous knowledge base concerning both methods for linear systems. For example reference [2] provides a complete

discussion on the classical time domain and frequency domain controller design techniques for linear systems.

As the closed loop performance requirements become more stringent, linear controller design techniques prove inadequate and nonlinear controller design procedures are desirable. Nonlinear feedback control methodologies have been proven effective in dealing with a large variety of real world issues such as (i.) rate and magnitude saturation of actuators, (ii.) restricted controller bandwidth, (iii.) sensor noise, (iv.) time delays, (v.) disturbances, and (vi.) system uncertainties associated with feedback maximization [3].

There is a vast knowledge base of the literature available in the area of time domain nonlinear feedback controller design. One way to deal with the nonlinearities in the feedback system is to remove their effect with feedback control. This is formulated as the feedback linearization method [4]. In this method, the nonlinear dynamics of the system will be transformed into a linear form using state feedback. For this method to be fully effective, the full states of the system must be measurable. Another shortcoming associated with this method is related to the nonlinear systems with uncertainties, in which the issue of robustness is not guaranteed.

To address the uncertainty in the nonlinear systems, other approaches have been developed. The uncertainty in the system can be related to either parametric uncertainties (unknown parameters of the system) or unstructured uncertainties (due to un-modeled dynamics). The issue of parametric uncertainty is considered in the robust control area such as the Sliding Mode Control (SMC) methodology. A robust controller is generally comprised of a nominal part and an additional term aimed for model uncertainties. For

unstructured uncertainties, on the other hand, the adaptive control methodology is useful, in which the structure of the controller is very similar to those in robust control but in addition, the model itself will be updated based on the performance measurements during the operation of the system [4]. These adaptation techniques can also be incorporated into the feedback linearization methodologies to address the robustness issues [5].

The so-called bifurcation controller design methodology develops nonlinear controllers that modify the stability point behavior of a nonlinear system. These methods have been employed to design the feedback controllers to modify the nature of the bifurcation. The design is conducted in the phase plane using equilibrium point analysis with the goal of designing nonlinear controller that transforms one form of bifurcation to another (e.g., subcritical bifurcation to a supercritical bifurcation) [6, 7]. Similar to feedback linearization, this methodology requires an accurate knowledge of the system nonlinearities. Although this method changes the fundamental nature of the nonlinear system, it does not address the performance issue and only focuses on the stability [8].

There is also a vast knowledge base of the literature available in the area of nonlinear controller design in the frequency domain that is of the interest of this dissertation as well. The frequency domain analysis of nonlinear systems is formulated as the Describing Function (DF) method [9-11]. The most deployed DF in the literature is the Sinusoidal Input Describing Function (SIDF). In simple words, SIDF is the quasi-linearization of a nonlinear system that represents the nonlinear systems in terms of the gain and phase distortions of the nonlinear element response due to the harmonic input. The SIDF can be considered as the equivalence of transfer functions in the linear control

systems. However, unlink linear systems, SIDF can be function of both amplitude and frequency of the input signal.

The inverse SIDF has been utilized for designing nonlinear controllers for nonlinear plants. Different methods are suggested that yield to a great flexibility in the design of nonlinear controllers by adjusting their gain and phase distortions [12]. In this regard, one possible structure for the nonlinear controller to consider is a combination of a static nonlinearity and a dynamic linear controller. One application for this is to reduce the closed loop sensitivity to the input amplitude in a certain range of operation. In other words, the nonlinear controller is designed such that the gain and phase distortions due to the nonlinear controller will cancel the effect of the gain and phase distortions due to the nonlinearity in the plant. Different nonlinear controller structures such as PID or Fuzzy can be obtained by this method [13-15]. There are multiple design methods proposed to obtain gain and phase distortions of the nonlinear controller: (i.) M-circle method, (ii.) Error Criterion (EC) method, and (iii.) Frequency Constraint (FC) method [13-16]. In the first method, the gain and phase distortions of the nonlinear controller are calculated such that they all required touching a pre-specified M-circle in the Nichols chart at the same frequency. In the other two methods, on the other hand, the gain and phase distortions of the nonlinear controller are obtained by minimizing an error function over a certain frequency range.

Another important issue to consider is the possibility of utilizing nonlinear controllers, similar to those described above, to improve the closed loop performance of a linear system beyond what is achievable by a linear controller. In this regard, nonlinear

controller design methodologies in the frequency domain are developed. In [1, 8, 17, 18], a Volterra series representation is used to design a nonlinear controller in the frequency domain for a class of linear regulating systems subject to time domain constraints. The use of Volterra series limits the class of nonlinear controllers to the continuous functions. Their proposed strategy involves two steps: (i.) designing a linear controller that balances the trade-off between output performance and required actuation, and (ii.) augmenting the linear controller with a nonlinear controller that has the characteristics of an odd cubic polynomial. The coefficients for the nonlinear term are calibrated such that the gain and phase distortions associated with the augmented open loop plant meet the time domain constraints.

Additionally, in [19] a controller design technique is proposed that utilizes actuator saturation to meet output performance specification for linear regulating systems subject to time domain constraints. The proposed nonlinear controller saturates for large disturbance sizes while it operates linearly for smaller disturbance sizes. The gain and phase distortions of the nonlinear controller are obtained by enforcing time domain constraints in the frequency domain. Since the structure of the nonlinearity (saturation element) is known, the amplitude of the input signal to the nonlinearity is obtained by relating the characteristics of the analytical formulation of SIDF of the saturation element to the required gain and phase distortions.

In this dissertation, a novel nonlinear controller design methodology is developed for a class of linear regulating systems subject to time domain constraints. The proposed nonlinear controller design methodology is executed in the frequency domain. The design

methodology allows for an increase in the external disturbance size (beyond what is predicted for a linear controller) by imposing required gain and phase distortions on the linear open loop transfer function to assure that the time domain constraints are satisfied. Doing so, the closed loop performance will be improved.

In the proposed methodology, the time domain performance constraints will be translated in to the frequency domain tolerances. Additionally, the increase in the disturbance step size will be translated in terms of gain and phase distortions due to a nonlinearity. To identify the nonlinearity, a computational method for solving inverse SIDF problem is developed that estimates an isolated explicit nonlinearity from its gain and phase distortions information.

1.1 Connection between Time Domain Performance and Frequency Domain Characteristicts

The performance requirements of a system are usually defined in the time domain. To accommodate designing the controller in the frequency domain, translating the time domain properties in to the frequency domain characteristics is necessary.

In general, enforcing time domain specifications in the frequency domain is not trivial, due to intrinsic incompatibilities between these two domains. However, some of the classical time domain performance specifications can be translated to the frequency domain characteristics for a limited class of systems. For this, consider a unity feedback second order system shown in Figure 1-2.

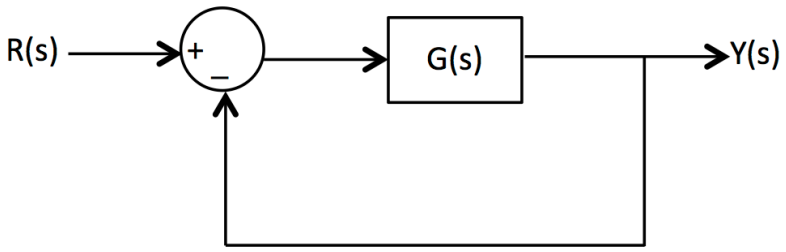

Figure 1-2 Block Diagram of a Unity Feedback System.

In Figure 1-2, the second order system dynamics are represented by

$$G(s) = \frac{\omega_n^2}{s(s + 2\xi\omega_n)}, \tag{1.1}$$

where ω_n is the natural frequency and ξ is the damping ratio of the system. Equation (1.1) represents many different dynamic systems such as DC motors. For this system, a direct connection between the closed loop characteristics such as phase margin (ϕ_M), overshoot (OS), and crossover frequency (ω_c), and the properties of the open loop system such as damping ratio and natural frequency can be formulated by [20]

$$\phi_M = tan^{-1}\left(\frac{2\xi}{\sqrt{\sqrt{4\xi^4 + 1} - 2\xi^2}}\right), \tag{1.2}$$

$$OS = \exp(\frac{\pi\xi}{\sqrt{1 - \xi^2}}), \tag{1.3}$$

and

$$\omega_c = \omega_n\sqrt{\sqrt{4\xi^4 + 1} - 2\xi^2}. \tag{1.4}$$

During the controller design process in the frequency domain, the relationships in Eqs. (1.2) to (1.4), can be utilized to impose required gain and phase characteristics on the frequency response of the open loop system such that the closed loop system meet the pre-specified time domain characteristics.

Although the performance specifications in Eqs. (1.2) to (1.4) have proved to work well, more detailed performance measures (such as output performance and actuator saturation) are needed for the design of modern higher performance feedback systems. Enforcing these time domain performance requirements in the frequency domain requires a new level of complexity in the control design methodologies and will be discussed later in Chapter 4.

1.2 Problem Statement

The class of systems considered in this dissertation is the linear SISO regulating systems. For regulating systems, with the reference input held constant (see Figure 1-1), only the feedback controller is needed. Consider the block diagram of this type of system shown in Figure 1-3.

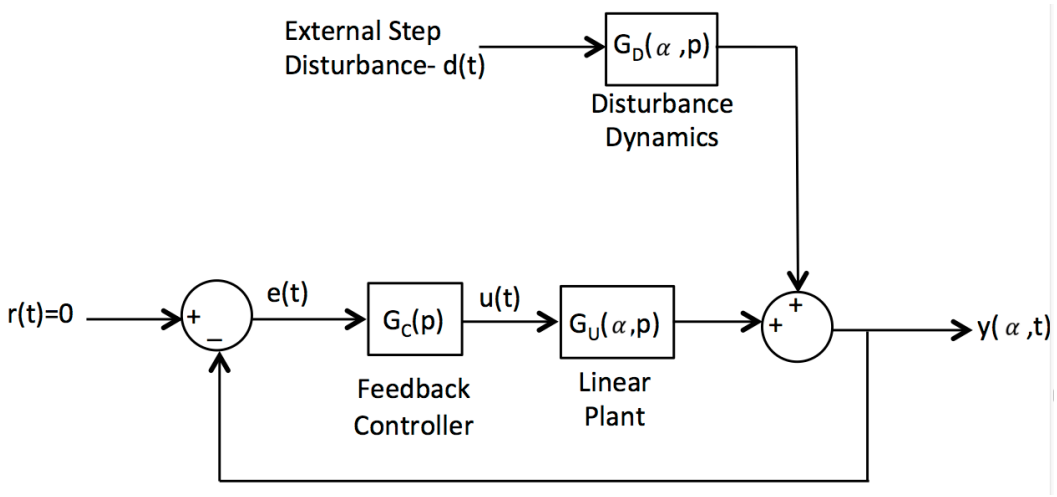

Figure 1-3 Block Diagram of a Regulating System.

For a system shown in Figure 1-3, the typical performance objectives are to maintain the regulated output variable $y(t)$ and the controlled output $u(t)$ with a pre-specified tolerances about their fixed set points despite the size of the external disturbance.

The objective is to design a nonlinear controller to improve the closed loop regulating performance of the system described in Figure 1-3, beyond what is achievable by a linear controller for a predicted level of disturbance step size. The nonlinear controller will be appended to the linear controller that is designed for the predicted level of disturbance step size. The nonlinear feedback controller must be able to satisfy performance objectives for a given value of the disturbance step size, γ, that is greater than the predicted level, γ^* for the designed linear controller.

The time domain performance specifications will be translated in terms of upper and lower amplitude bounds on the open loop system (feedback controller $G_C(p)$ in series combination with the plant dynamics $G_U(p)$ in Figure 1-3) in the Nichols chart. This

enables designing a controller in the frequency domain through the use of performance weights in H_∞ controller synthesis method.

The main focus of this dissertation is aimed at designing a nonlinear controller for a linear regulating system to improve the closed loop performance. The proposed approach is within the frequency domain and includes time domain performance specifications. The proposed solution is an extension of the classical linear robust control methodologies (QFT, H_∞).

The proposed nonlinear controller synthesis methodology imposes required gain and phase distortions on the frequency response of the linear open loop transfer function to achieve higher closed loop performances. These gain and phase distortions will be treated as the SIDF information. To identify the nonlinear controller from its SIFD representation, an inverse SIDF algorithm is utilized. For this, a computational solution for the inverse SIDF problem is developed that estimates an isolated explicit (static) nonlinearity from its gain and phase distortions information. The formulation of the inverse SIDF and the synthesis of the nonlinear controller comprise the main content of this dissertation.

1.3 Organization of the Dissertation

The proposed controller design in this dissertation is separated into two major sections. First, the extension of the frequency response analysis for nonlinear systems is introduced. This is covered in Chapter 2 and Chapter 3. More specifically, Chapter 2 introduces describing function (DF) methodology and its application in the analysis of

nonlinear systems. It explains the process of characterizing nonlinear systems with the notion of the frequency response. Chapter 3 presents a numerical method to solve the inverse SIDF problem and it motivates the benefit of using it for nonlinear controller design.

In the second section of this dissertation, the methodology of designing controller for the class of linear regulating systems is presented. Chapter 4 serves to motivate and describe the linear controller design technique in the frequency domain. Transforming the time domain specifications in to the frequency domain is discussed, followed by the linear controller design procedure. In Chapter 5, the nonlinear frequency based controller synthesis methodology is proposed. It presents the utilization of the developed inverse SIDF algorithm in designing a nonlinear controller to improve the closed loop performance.

In Chapter 6, the stability analysis of the designed nonlinear feedback systems in the sense of bounded-input-bounded-output (BIBO) is addressed. Conclusions and contributions are presented in Chapter 7.

Chapter 2. Describing Function Method

The frequency response analysis of linear feedback systems is a well-established methodology. The utility of linear frequency response methods was extended to nonlinear systems in late 1940s and early 1950s [21-26]. This method has been formulated as the describing function (DF) method. This chapter serves to provide a brief overview of the DF method for analysis of nonlinear systems.

2.1 Introduction to Describing Function Method

Describing function is a quasi-linearization of the nonlinear system that approximates the nonlinear function with a linear representation. DF minimizes the mean square error between the nonlinear system response and its linear description. The DF characterization of a nonlinear system has been developed for specific input signals such as harmonic excitation, random input signal, Gaussian input, and biased inputs [9-11, 27]. The most deployed DF in the literature is the Sinusoidal Input Describing Function (SIDF), which is defined as the fundamental response of a nonlinear system at steady state for a single sinusoidal input [10]. SIDF characterizations produce descriptive gain and phase distortions of a nonlinear system that are function of the input amplitude, A, and frequency, ω.

A typical application of the SIDF in a feedback loop is shown in Figure 2-1, where the plant nonlinearity, $P[u(t)]$, is replaced by a SIDF representation, $P[A(u(t)), \omega(u(t))]$.

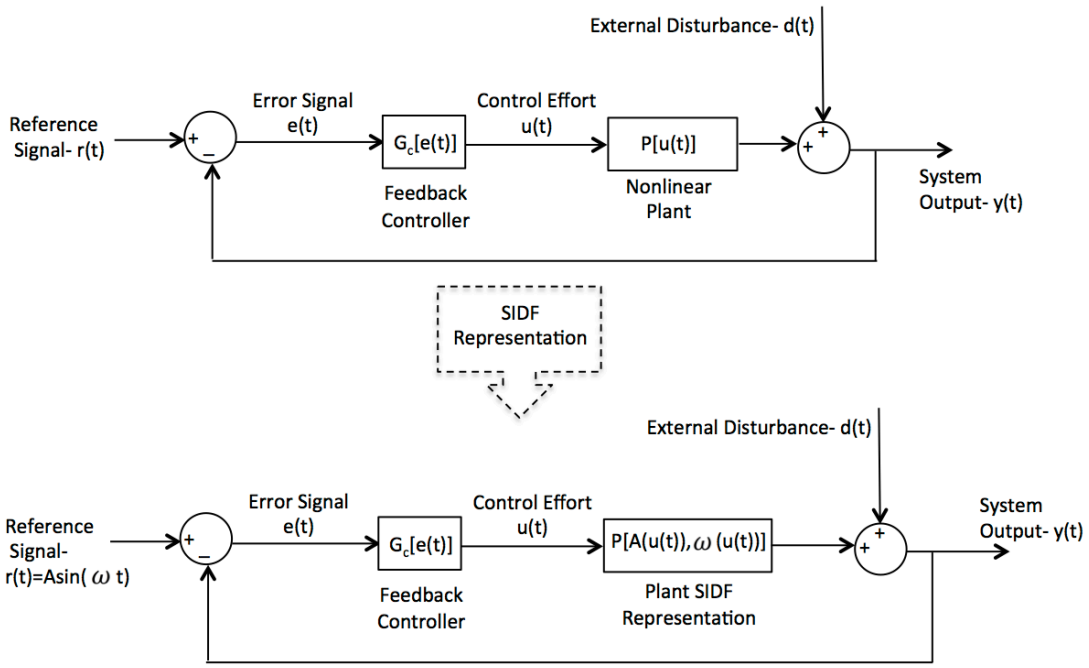

Figure 2-1 Application of the SIDF in a Feedback Loop.

The generalized SIDF parallels transfer function ideas in linear systems. In fact, SIDF is an approximation of the nonlinear system by linear time invariant transfer functions. However, unlike linear systems, the characteristics of these representative transfer functions depend on the amplitude and frequency of the input signal. In the following section, the formulation for computing describing function is presented.

2.2 Computation of Describing Function

The development of the DF is based on the estimation of a linear filter, $w(t)$, that approximates a nonlinear differential equation functional, $n[x(t)]$, for a particular input wave, $x(t)$, such that the mean square of the error signal, $e(t)$, is minimized (Figure 2-2) [1, 9]. The procedure for calculating the optimal filter is presented below. This derivation closely follows the derivation of the unified theory of describing function in [9] with the modification for a single input signal.

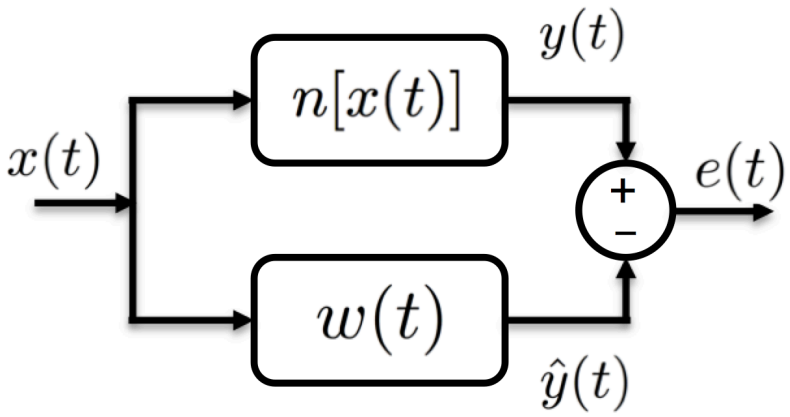

Figure 2-2 Describing Function Representation.

The DF is defined as the selection of an optimal filter, $w(t)$ that minimizes

$$\overline{e^2(t)} = \overline{(y(t) - \hat{y}(t))^2} = \overline{y(t)^2} - 2\overline{\hat{y}(t)y(t)} + \overline{\hat{y}(t)^2}, \tag{2.1}$$

where

$$e(t) = y(t) - \hat{y}(t), \tag{2.2}$$

$$\hat{y}(t) = \int_{-\infty}^{\infty} w(\tau)x(t-\tau)d\tau, \tag{2.3}$$

and $\overline{v(t)}$ denotes the expected value of a given signal $v(t)$ defined as, $\overline{v(t)} = \int_{-\infty}^{\infty} v(t)p_v dv$, in which p_v is the probability density of $v(t)$. The expected value of a signal is a measure of its mean value.

To find $w(t)$, consider expanding all terms in Eq. (2.1),

$$\begin{aligned} \hat{y}(t)^2 &= \int_0^{\infty} w(\tau_1)x(t-\tau_1)d\tau_1 \int_0^{\infty} w(\tau_2)x(t-\tau_2)d\tau_2 \\ &= \int_0^{\infty}\int_0^{\infty} w(\tau_1)w(\tau_2)x(t-\tau_1)x(t-\tau_2)d\tau_1 d\tau_2, \end{aligned} \tag{2.4}$$

and

$$\begin{aligned} \overline{\hat{y}(t)^2} &= \int_0^{\infty}\int_0^{\infty} w(\tau_1)w(\tau_2)\overline{x(t-\tau_1)x(t-\tau_2)}d\tau_1 d\tau_2 \\ &= \int_0^{\infty}\int_0^{\infty} w(\tau_1)w(\tau_2)\phi(\tau_1-\tau_2)d\tau_1 d\tau_2, \end{aligned} \tag{2.5}$$

where $\phi(\tau_1 - \tau_2) \triangleq \overline{x(t-\tau_1)x(t-\tau_2)}$. Following same procedure, the followings can be obtained.

$$\hat{y}(t)y(t) = \int_0^{\infty} w(\tau)y(t)x(t-\tau)d\tau \tag{2.6}$$

and

$$\overline{\hat{y}(t)y(t)} = \int_0^\infty w(\tau)\overline{y(t)x(t-\tau)}d\tau. \tag{2.7}$$

Substituting Eqs. (2.5) and (2.7) into Eq. (2.1) yields

$$\overline{e^2(t)} = \int_0^\infty \int_0^\infty w(\tau_1)w(\tau_2)\phi(\tau_1-\tau_2)d\tau_1 d\tau_2 - 2\int_0^\infty w(\tau)\overline{y(t)x(t-\tau)}d\tau + \overline{y(t)^2}. \tag{2.8}$$

Next step is to find the necessary condition for the optimal set of filters. To minimize the error function, $\overline{e^2(t)}$ must be stationary with respect to variations in $w(t)$. To formulate this requirement, $w(t)$ is expressed by

$$w(t) = w_0(t) + \delta w(t), \tag{2.9}$$

where $w_0(t)$ is the optimal filter, and $\delta w(t)$ is an arbitrary (but physically realizable) variation of the optimal filter. Using similar notation for the error function, the expanded square error function can be written as

$$\overline{e^2(t)} = \overline{e_o^2(t)} + \overline{\delta e^2(t)} + \overline{\delta^2 e^2(t)}. \tag{2.10}$$

Using Eq. (2.8), the firs term in the right hand side of Eq. (2.10) can be written as

$$\overline{e_o^2(t)} = \int_0^\infty \int_0^\infty w_0(\tau_1)w_0(\tau_2)\phi(\tau_1-\tau_2)d\tau_1 d\tau_2 - 2\int_0^\infty w_0(\tau)\overline{y(t)x(t-\tau)}d\tau + \overline{y(t)^2}. \tag{2.11}$$

Additionally, the second term in the right hand side of Eq. (2.10) is given by

$$\overline{\delta e^2(t)} = \int_0^\infty \int_0^\infty [w_0(\tau_1)\delta w(\tau_2) + w_0(\tau_2)\delta w(\tau_1)]\phi(\tau_1 - \tau_2)d\tau_1 d\tau_2 - 2\int_0^\infty \delta w(\tau)\overline{y(t)x(t-\tau)}d\tau. \tag{2.12}$$

Assuming $\phi(\tau_1 - \tau_2) = \phi(\tau_2 - \tau_1)$, Eq. (2.12) is reduced to

$$\overline{\delta e^2(t)} = 2\int_0^\infty \delta w(\tau_1)\left[\int_0^\infty w_0(\tau_2)\phi(\tau_1 - \tau_2)d\tau_2 - \overline{y(t)x(t-\tau_1)}\right]d\tau_1. \tag{2.13}$$

Moreover, the third term in the right hand side of Eq. (2.10) is given by

$$\overline{\delta^2 e^2(t)} = \int_0^\infty \int_0^\infty \delta w(\tau_2)\delta w(\tau_1)\phi(\tau_1 - \tau_2)d\tau_1 d\tau_2. \tag{2.14}$$

Based on Eq. (2.14), $\overline{\delta^2 e^2(t)}$ is not a function of the optimal filter, $w_0(t)$, and is positive; therefore, it cannot be "designed" to reduce the error. Hence, the square error in Eq. (2.10) can only be reduced by means of Eq. (2.13), i.e., by setting $\overline{\delta e^2(t)} = 0$. This yields

$$\int_0^\infty w_0(\tau_2)\phi(\tau_1 - \tau_2)d\tau_2 = \overline{y(t)x(t-\tau_1)}. \tag{2.15}$$

Therefore, to minimize the error function, Eq. (2.15) must be satisfied. This equation can be solved for different input signals. In the following section, the formulation for sinusoidal input signal is presented which yields to the formulation of SIDF.

2.2.1 Computation of Sinusoidal Input Describing Function

To find the SIDF, the input signal is set to $x(t) = A\sin(\omega t)$ in Eq. (2.15). For this harmonic input, $\phi(\tau)$ is evaluated as [9]

$$\phi(\tau) = \frac{\omega}{2\pi}\int_{\frac{-\pi}{\omega}}^{\frac{\pi}{\omega}} A^2 \sin(\omega t)\sin(\omega t + \omega\tau)\, dt = \frac{A^2}{2}\cos(\omega\tau). \tag{2.16}$$

Consequently the expression for $\phi(\tau_1 - \tau_2)$ is given by

$$\phi(\tau_1 - \tau_2) = \frac{A^2}{2}\,[\cos(\omega\tau_1)\cos(\omega\tau_2) + \sin(\omega\tau_1)\sin(\omega\tau_2)]. \tag{2.17}$$

For the harmonic input, the right hand side of Eq. (2.15) can be written as

$$\overline{y(t)x(t-\tau_1)} = A\cos(\omega\tau_1)\,\overline{y(t)\sin(\omega t)} - A\sin(\omega\tau_1)\,\overline{y(t)\cos(\omega t)}. \tag{2.18}$$

Substituting Eqs. (2.17) and (2.18) into Eq. (2.15) produces two equations

$$\frac{A}{2}\int_0^\infty w_0(\tau_2)\cos(\omega\tau_2)\, d\tau_2 = \overline{y(t)\sin(\omega t)} \tag{2.19}$$

and

$$\frac{A}{2}\int_0^\infty w_0(\tau_2)\sin(\omega\tau_2)\, d\tau_2 = -\overline{y(t)\cos(\omega t)}. \tag{2.20}$$

The optimal filter, $w(t)$, must simultaneously satisfy Eqs. (2.19) and (2.20). One possible solution given in [9] is

$$w(\tau_2) = \frac{2}{A}\overline{y(t)\,sin(\omega t)}\,\delta(\tau_2) + \frac{2}{\omega A}\overline{y(t)\,cos(\omega t)}\,\dot{\delta}(\tau_2), \tag{2.21}$$

where $\delta(.)$ and $\dot{\delta}(.)$ are the so-called Dirac Delta and Doublet functions, respectively. The transfer function representations of Eq. (2.21) is given by

$$W(s) = \frac{2}{A}\left[\overline{y(t)\,sin(\omega t)} + \frac{1}{\omega}\overline{y(t)\,cos(\omega t)}\,s\right]. \tag{2.22}$$

It is to be noted that Eq. (2.21) is not the only solution for Eqs. (2.19) and (2.20). However, the transfer function representation of any other solution has also the characteristics of a Proportional plus Derivative (PD) path, as Eq. (2.22) does [9].

An alternative form of Eq. (2.22) can be considered as a complex gain, which distorts the input signal. This can be obtained by setting $s = j\omega$ in Eq. (2.22) that yields to

$$W(j\omega) = \frac{2}{A}\left[\overline{y(t)\,sin(\omega t)} + j\,\overline{y(t)\,cos(\omega t)}\right]. \tag{2.23}$$

Additionally, the SIDF can be obtained by considering the Fourier transformation of Eq. (2.21) as

$$N(A,\omega) = \frac{C'(A,\omega) + jS'(A,\omega)}{A}, \tag{2.24}$$

where

$$C'(A,\omega) = \frac{1}{\pi}\int_0^{2\pi} y(A\sin(\omega t))\sin(\omega t)\,d(\omega t) \tag{2.25}$$

and

$$S'(A,\omega) = \frac{1}{\pi}\int_0^{2\pi} y(A\sin(\omega t))\cos(\omega t)\, d(\omega t). \tag{2.26}$$

Collectively, Eqs. (2.24) to (2.26) can be written as

$$N(A,\omega) = \frac{j}{\pi A}\int_0^{2\pi} y(A\sin(\omega t))\, e^{-j(\omega t)} d(\omega t). \tag{2.27}$$

The SIDF representation by Eq. (2.27) is valid provided that $y(t)$ is periodic and its derivative is piecewise smooth on the periodic interval $0 \leq \omega t \leq 2\pi$.

For system with nonlinearities, if $y(t)$ is known, the SIDF can be directly calculated using integral equations in Eq. (2.27). It is to be noted that, this SIDF representation implies the gain and phase distortions (per Eqs. (2.25) and (2.26), respectively) of the fundamental output of the periodic response $y(t)$, due to the nonlinearity subject to a harmonic input.

If the nonlinearity is single-valued (memoryless), then its SIDF representation is associated with only gain distortions, i.e., $S'(j\omega) = 0$. In the case of a double-valued nonlinearity (hysteresis), on the other hand, the SIDF representation is associated with both gain and phase distortions.

For an explicit (static) nonlinearity, the nonlinear function depends only on the input signal, i.e., $x(t)$, and its SIDF representation is only a function of the input signal amplitude. On the other hand, for an implicit (dynamic) nonlinearity, the nonlinear

function depends on the input signal as well as its derivatives, and its SIDF representation is function of both amplitude and frequency of the input signal.

2.3 Applications of Describing Function

The DF method has many important applications in the analysis and design of nonlinear feedback systems. They are powerful tool for the investigation of possible existence and stability of the limit cycles in the nonlinear systems [28-30]. To illustrate this, consider a closed loop system with a single nonlinear element denoted by $N.L.$ and a linear dynamic denoted by $G(p)$ shown in Figure 2-3.

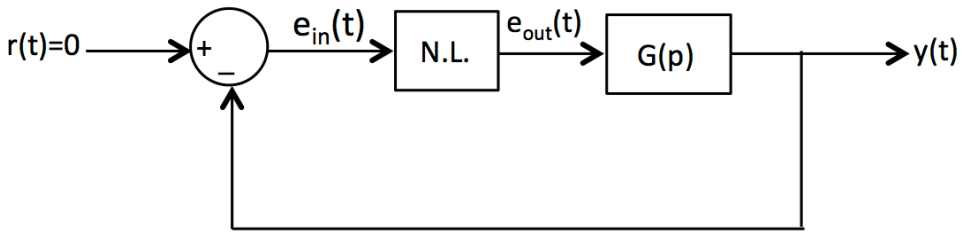

Figure 2-3 General Block Diagram of a Feedback System with Nonlinear Element in the Loop.

Let $e_{in}(t) = A\sin(\omega t)$ and the SIDF representation of the nonlinear element be $N(A,\omega)$, then the feedback equation for the block diagram of Figure 2-3 can be written as [11]

$$N(A,\omega)G(j\omega) = -1. \tag{2.28}$$

Equation (2.28) provides a condition for the existence of the limit cycle for the closed loop system. In other word, if Eq. (2.28) holds, then the system oscillates. Moreover, if a

limit cycle exists, solving Eq. (2.28) gives both amplitude and frequency of the oscillations.

Additionally, Eq. (2.28) can be used to investigate the stability of the oscillations. This can be viewed as the extended Nyquist criterion, meaning that, instead of considering the encirclements of the critical point (i.e., $-1 + j0$), the encirclements of $\frac{1}{N(A,\omega)}$ must be examined.

It is to be noted that, the reliability of conditions determined by Eq. (2.28) are contingent upon a clear (i.e., not tangential) intersection between $G(j\omega)$ and $\frac{-1}{N(A,\omega)}$ plots, due to the approximate nature of the SIDF. For a special class of systems, sufficient conditions are formulated in [31] under which the use of SIDF for examining the existence and stability of limit cycles are justified.

2.4 Chapter Summary

Presented in this chapter is an overview of the describing function method and its applications in the analysis of nonlinear systems. More specifically, the SIDF formulation is presented that represents the frequency response of a nonlinear system. It is shown that the SIDF representation of a nonlinear system can be considered as the gain and phase distortions in the response of the nonlinearity to the harmonic input signal. These gain and phase distortions will be utilized in Chapter 3 to present a numerical solution to the inverse SIDF problem that can identify an isolated static nonlinearity.

Chapter 3. Numerical Solution to the Inverse Sinusoidal Input Describing Function

Beyond the SIDF pseudo-linearization presented in Chapter 2, is the inverse problem, i.e., recovering a nonlinear function from its gain and phase distortions information. The main focus of this chapter is to develop a numerical solution for the inverse SIDF to identify a non-parametric model for an explicit nonlinear function based on its gain and phase distortions. The proposed solution can be used in designing a nonlinear controller in a compensatory network to improve the closed loop performance of the system.

3.1 Introduction

The goal of inverse SIDF problem is the identification of a nonlinear function whose gain and phase distortions information is available. That is, if the gain and phase distortions are known, one can obtain the nonlinear function associated with the gain and phase distortions by using the developed inverse SIDF algorithm. The inverse SIDF solution developed in this chapter will be utilized in Chapter 5, to develop a methodology for synthesizing nonlinear controllers for regulating systems to improve their closed loop performance.

3.2 Overview of Inverse Describing Function

Inverse describing functions have important applications in the analysis and design of systems with nonlinear elements [13-16, 32-27]. Several methods for estimation of nonlinear functions using inverse describing functions have been proposed. The simplest inverse SIDF method employs a linear interpolation technique for the estimation of the nonlinear function for an isolated explicit single-valued nonlinearity with the characteristic of a slope-bounded function defined as [10, 14]

$$a_1 \leq \frac{n[x_1(t) + \varepsilon] - n[x_1(t)]}{\varepsilon} \leq a_2, \tag{3.1}$$

where $n[x(t)]$ denotes a nonlinear function, $x(t)$ is the input signal, a_1 and a_2 are finite real numbers, and ε is an arbitrary small number.

Another method uses the gain distortions to recover a piecewise linear function [9, 15, 34, 36]. The nonlinearities applicable for this inverse SIDF method include isolated explicit single-valued nonlinearities that have the characteristics of a gain-changing continuous function. The analytical SIDF used for this class of nonlinearities is

$$N(A) = \frac{4M}{\pi A} + \sum_{i=1}^{n-1} (m_i - m_{i+1}) f\left(\frac{x_i}{A}\right), \tag{3.2}$$

where $f\left(\frac{x_i}{A}\right)$ is the so-called saturation function with unit limits and unit slope defined as

$$f\left(\frac{x_i}{A}\right) = \begin{cases} \frac{2}{\pi}\left[\sin^{-1}\left(\frac{x_i}{A}\right) + \left(\frac{x_i}{A}\right)\sqrt{1-\left(\frac{x_i}{A}\right)^2}\right] & \text{for } \frac{x_i}{A} \le 1 \\ 1 & \text{for } \frac{x_i}{A} > 1 \end{cases}, \tag{3.3}$$

where m_i, x_i and M are parameters of a piecewise continuous nonlinearity with n different segments (Figure 3-1L) [1, 9].

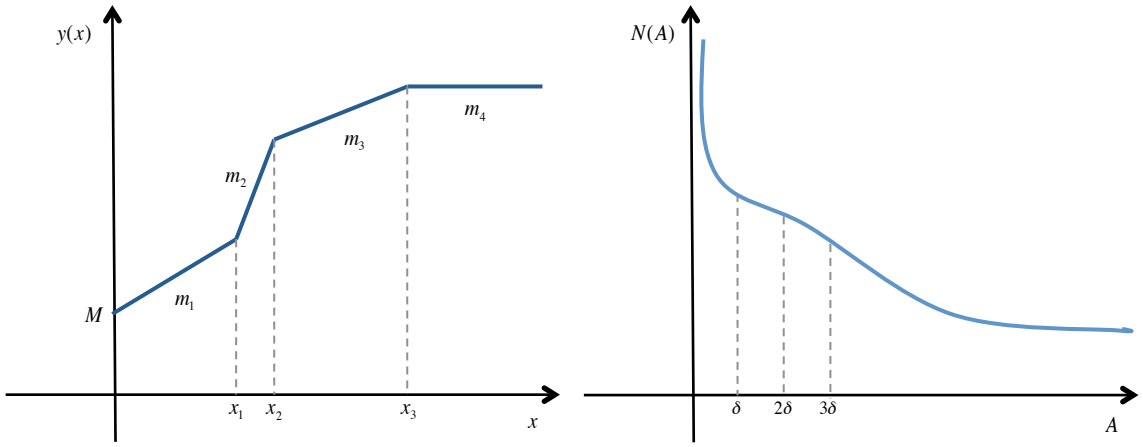

Figure 3-1 (L) Piecewise Continuous Nonlinearity and (R) Corresponding SIDF.

To initiate the inversion process, the gain distortions, $N(A)$ are divided into equal discrete segments (Figure 3-1R). Then the SIDF in Eq. (3.2) is used to evaluate the resulting gain distortions at the discretized amplitudes of $A = \frac{\delta}{2}, \frac{3\delta}{2}, \ldots$ to generate the set of equations

$$\begin{bmatrix} 1 & 0 & 0 & \dots & 0 \\ f\left(\frac{2}{3}\right) & 1-f\left(\frac{2}{3}\right) & 0 & \dots & 0 \\ f\left(\frac{2}{5}\right) & f\left(\frac{4}{5}\right)-f\left(\frac{2}{5}\right) & 1-f\left(\frac{4}{5}\right) & \dots & 0 \\ \vdots & \vdots & \vdots & \dots & \vdots \end{bmatrix} \begin{bmatrix} m_1 \\ m_2 \\ m_3 \\ m_4 \\ \vdots \end{bmatrix} = \begin{bmatrix} N\left(\frac{\delta}{2}\right) \\ N\left(\frac{3\delta}{2}\right) \\ N\left(\frac{5\delta}{2}\right) \\ N\left(\frac{7\delta}{2}\right) \\ \vdots \end{bmatrix}. \quad (3.4)$$

Using Least Square Estimation (LSE) method, Eq. (3.4) can be solved to obtain the parameters of the nonlinear piecewise function, $y(x)$ (Figure 3-1L). The accuracy of this approximation is contingent upon the selection of δ. This method effectively estimates a piecewise nonlinearity provided the nonlinearity is a piecewise continuous function.

Additional SIDF inversion algorithms have been suggested for other classes of nonlinearities such as polynomials. In the case of a polynomial function, the analytical formulation of the SIDF itself is a polynomial. Therefore, a LSE curve-fit method can be employed to the gain distortions to recover the nonlinear polynomial function [9]. Alternatively, inverse describing function method for multiple inputs and random inputs have also been developed. Determination of the inverse random describing function for a Gaussian input has been interpreted as the inverse Laplace transform. Same concepts have been extended to the case of multiple inputs, when the independent inputs are either random Gaussian input or signals with the probability density of a sinusoidal input [38-40]. These methods have been formulated for a class of odd-symmetric single-valued nonlinearities, thereby only gain distortions are considered.

In [41], an inverse SIDF algorithm is proposed for nonlinearities with and without memory. This algorithm employs a preconceived structure for the nonlinearity (e.g., memoryless or hysteresis, piecewise linear or polynomial) as well as an initial estimate for its parameters. The structure of the nonlinearity is selected from a catalogue of functions considered in the analysis. Based on the selected structure for the nonlinearity and initial estimate of its parameters, the proposed algorithm finds the "best" parameters for the nonlinearity by minimizing the squared error between the estimated and actual gain and phase distortions. This algorithm has been employed in [16, 32, 33, 35 and 37].

In general, the inverse SIDF solutions appearing in the open literature have one similarity; an assumed nonlinearity structure is required. Developing a more general algorithm to solve the inverse SIDF problem without *a priori* information at the nonlinearity would further advance the knowledge base. In this regard, a numerical algorithm to solve the inverse SIDF problem for explicit odd single-valued nonlinearities is presented in [13]. This algorithm only utilizes the SIDF gain distortions to estimate the nonlinearity by numerically solving its analytical inverse SIDF integrals.

The main focus of this chapter is to develop a more general numerical solution for the inverse SIDF. The proposed computational method directly utilizes the gain and phase distortions and numerically recovers a non-parametric model of the nonlinearity. Unlike other methods, the structure of the nonlinearity is an output from the proposed method and will be identified from the non-parametric model, therefore it is not known *a priori*. The class of nonlinearities applicable to the proposed method is isolated explicit nonlinearities.

3.3 Analytic Solution to the Inverse SIDF

In this section, an analytical approach upon the solution of the inverse SIDF for explicit nonlinearities is presented. This is done by transformation of SIDF in a form that the inverse SIDF problem will be presented in terms of Volterra integral equations [42, 43].

The analytical solution to the inverse SIDF applies to explicit nonlinearities. Consider a class of nonlinear functions given by

$$y = n(x), \tag{3.5}$$

where $n(x)$ has the most general form of an explicit nonlinear function including double-valued nonlinearities, yet excludes the frequency dependency (i.e., implicit nonlinearities). In other words, $n(x)$ is a function of input signal $x(t)$, but not its derivatives. One such a function is shown in Figure 3-2.

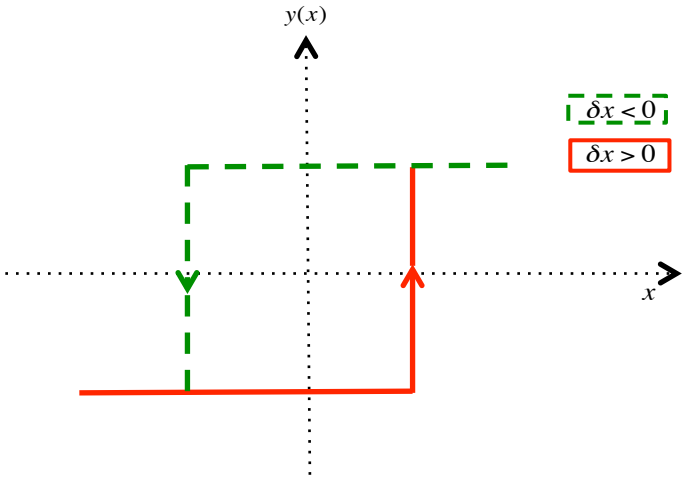

Figure 3-2 Example of an Explicit Double-valued Nonlinearity.

If $n(x)$ is a double-valued function (Figure 3-2), it can be decomposed into two single-valued functions as

$$n(x) = \begin{cases} n_1(x) & \delta x < 0 \\ n_2(x) & \delta x > 0' \end{cases} \tag{3.6}$$

where δx is a small increment of the input signal. Provided the input to the nonlinear function is a harmonic wave $(x(t) = A\sin(\omega t) = A\sin(\alpha))$, $y(t)$ will be a periodic function with period 2π. Its Fourier expansion is

$$y(t) = \frac{a_0}{2} + a_1\cos(\alpha) + b_1\sin(\alpha) + H.O.T., \tag{3.7}$$

where a_0, a_1 and b_1 are the Fourier coefficients, and $H.O.T.$ represents the higher order terms that are neglected in the SIDF method [31]. This assumption is valid by considering the low-pass filter hypothesis. The SIDF is defined as the ratio of the fundamental harmonic output to the amplitude of the input [9] and can be written in terms of the Fourier coefficients

$$M(A) = \frac{a_0}{2A} = \frac{1}{2\pi A}\int_0^{2\pi} n(A\sin(\alpha))\, d\alpha, \tag{3.8}$$

$$C(A) = \frac{b_1}{A} = \frac{1}{\pi A}\int_0^{2\pi} n(A\sin(\alpha))\ \sin(\alpha)\ d\alpha, \tag{3.9}$$

and

$$S(A) = \frac{a_1}{A} = \frac{1}{\pi A}\int_0^{2\pi} n(A\sin(\alpha))\ \cos(\alpha)\ d\alpha. \tag{3.10}$$

The SIDF of the nonlinear function is given by Eqs. (3.8) to (3.10), where $M(A)$ is related to the offset term in the Fourier series expansion (which is considered zero in the SIDF formulation, i.e., it is not accounted for), $C(A)$ is the real part of the SIDF, and $S(A)$ is the imaginary part of the SIDF.

The inverse SIDF problem solves Eqs. (3.8) to (3.10) to recover the nonlinear function, $n(x)$. In general, the solution is not trivial, owing to the double-valued nature of $n(x)$. The procedure of solving Eqs. (3.8) to (3.10) is to determine $n(x)$ based on the method in [43-45].

Considering the sign of δx in different segments of interval 0 to 2π, and using Eq. (3.6), Eqs. (3.8) to (3.10) can be decomposed as

$$M(A) = \frac{1}{2\pi A}\left[\int_0^{\frac{\pi}{2}} n_2(A\sin(\alpha))\, d\alpha + \int_{\frac{\pi}{2}}^{\pi} n_1(A\sin(\alpha))\, d\alpha + \int_{\pi}^{\frac{3\pi}{2}} n_1(A\sin(\alpha))\, d\alpha + \int_{\frac{3\pi}{2}}^{2\pi} n_2(A\sin(\alpha))\, d\alpha\right], \tag{3.11}$$

$$C(A) = \frac{1}{\pi A}\left[\int_0^{\frac{\pi}{2}} n_2(A\sin(\alpha))\sin(\alpha)\, d\alpha + \int_{\frac{\pi}{2}}^{\pi} n_1(A\sin(\alpha))\sin(\alpha)\, d\alpha + \int_{\pi}^{\frac{3\pi}{2}} n_1(A\sin(\alpha))\sin(\alpha)\, d\alpha + \int_{\frac{3\pi}{2}}^{2\pi} n_2(A\sin(\alpha))\sin(\alpha)\, d\alpha\right], \tag{3.12}$$

and

$$S(A) = \frac{1}{\pi A}\left[\int_0^{\frac{\pi}{2}} n_2(A\sin(\alpha))\cos(\alpha)\,d\alpha + \int_{\frac{\pi}{2}}^{\pi} n_1(A\sin(\alpha))\cos(\alpha)\;d\alpha\right.$$
$$+ \int_{\pi}^{\frac{3\pi}{2}} n_1(A\sin(\alpha))\cos(\alpha)\;d\alpha \qquad (3.13)$$
$$\left. + \int_{\frac{3\pi}{2}}^{2\pi} n_2(A\sin(\alpha))\cos(\alpha)\;d\alpha\right].$$

The single-valued functions $n_1(x)$ and $n_2(x)$, can be written as the summation of odd and even functions

$$n_1(x) = p_1(x) + q_1(x) \qquad (3.14a)$$

and

$$n_2(x) = p_2(x) + q_2(x), \qquad (3.14b)$$

where p_i denotes an even function, i.e., $p_i(-x) = p_i(x)$ and q_i denotes an odd function, i.e., $q_i(-x) = -q_i(x)$ and $q_i(0) = 0$.

Substituting Eq. (3.14) in Eqs. (3.11) to (3.13), performing appropriate change of variables, and using the properties of odd, even, and trigonometric functions, all integrals in Eqs. (3.11) to (3.13) can be transformed to compact integrals with the same interval of 0 to $\frac{\pi}{2}$.

In Eq. (3.13), consider $S_1(A) = \int_0^{\frac{\pi}{2}} n_2(A\sin(\alpha))\cos(\alpha)\,d\alpha$, $S_2(A) = \int_{\frac{\pi}{2}}^{\pi} n_1(A\sin(\alpha))\cos(\alpha)\;d\alpha$, $S_3(A) = \int_{\pi}^{\frac{3\pi}{2}} n_1(A\sin(\alpha))\cos(\alpha)\;d\alpha$, and $S_4(A) = \int_{\frac{3\pi}{2}}^{2\pi} n_2(A\sin(\alpha))\cos(\alpha)\;d\alpha$. $S_1(A)$ is already in the interval of 0 to $\frac{\pi}{2}$ and can be expressed as

$$S_1(A) = \int_0^{\frac{\pi}{2}} [p_2(A\sin(\alpha)) + q_2(A\sin(\alpha))]\cos(\alpha)\;d\alpha. \tag{3.15}$$

For $S_2(A)$, consider applying a change of variable as $\alpha = \pi - \beta$ and using the properties of trigonometric functions of $\cos(\pi - \beta) = -\cos(\beta)$ and $\sin(\pi - \beta) = \sin(\beta)$, and considering the properties of odd and even functions, $S_2(A)$ can be written as

$$S_2(A) = \int_0^{\frac{\pi}{2}} [-p_1(A\sin(\alpha)) - q_1(A\sin(\alpha))]\cos(\alpha)\;d\alpha. \tag{3.16}$$

Similarly, for $S_3(A)$, consider applying a change of variable as $\alpha = \pi + \beta$ and using the properties of trigonometric functions of $\cos(\pi + \beta) = -\cos(\beta)$ and $\sin(\pi + \beta) = -\sin(\beta)$, and considering the properties of odd and even function, $S_3(A)$ can be written as

$$S_3(A) = \int_0^{\frac{\pi}{2}} [-p_1(A\sin(\alpha)) + q_1(A\sin(\alpha))]\cos(\alpha)\;d\alpha. \tag{3.17}$$

Finally, for $S_4(A)$, consider applying a change of variable as $\alpha = 2\pi - \beta$ and using the properties of trigonometric functions of $\cos(2\pi - \beta) = \cos(\beta)$ and $\sin(2\pi - \beta) =$

$-\sin(\beta)$, and considering the properties of odd and even function, $S_4(A)$ can be written as

$$S_4(A) = \int_0^{\frac{\pi}{2}} [p_2(A\sin(\alpha)) - q_2(A\sin(\alpha))]\cos(\alpha)\ d\alpha. \tag{3.18}$$

Using Eqs. (3-15) to (3-18) in Eq. (3-13), $S(A)$ is reduced to

$$S(A) = \frac{-2}{\pi A}\int_0^{\frac{\pi}{2}} P(A\sin(\alpha))\cos(\alpha)\ d\alpha. \tag{3.19}$$

Using the exact same procedures for Eqs. (3-11) and (3-12), $M(A)$ and $C(A)$ can also be reduced to

$$M(A) = \frac{1}{\pi A}\int_0^{\frac{\pi}{2}} P^*(A\sin(\alpha))d\alpha \tag{3.20}$$

and

$$C(A) = \frac{2}{\pi A}\int_0^{\frac{\pi}{2}} Q(A\sin(\alpha))\sin(\alpha)\ d\alpha, \tag{3.21}$$

where in Eqs. (3.19) to (3-21)

$$P^*(x) = p_1(x) + p_2(x), \tag{3.22a}$$

$$P(x) = p_1(x) - p_2(x), \tag{3.22b}$$

and

$$Q(x) = q_1(x) + q_2(x). \tag{3.22c}$$

Note that $Q(x)$ is an odd function and $P(x)$ and $P^*(x)$ are even functions.

By returning to the original input variable, i.e., x, Eqs. (3.19) to (3.21) can be written as

$$M(A) = \frac{1}{\pi A}\int_0^A \frac{P^*(x)}{\sqrt{A^2 - x^2}}\, dx, \tag{3.23}$$

$$C(A) = \frac{2}{\pi A^2}\int_0^A \frac{x\, Q(x)}{\sqrt{A^2 - x^2}}\, dx, \tag{3.24}$$

and

$$S(A) = \frac{-2}{\pi A^2}\int_0^A P(x)dx. \tag{3.25}$$

The sets of equations in Eqs. (3.8) to (3.10) have been transformed into sets of equations in Eqs. (3.23) to (3.25), in which $P^*(x), Q(x)$ and $P(x)$ are all single-valued functions.

To recover the inverse SIDF problem, the integral equations in Eqs. (3.23) to (3.25) must be evaluated. The solution of Eq. (3.25) for $S(A)$ is immediate while the other two equations are special forms of Volterra's integral equation of the first kind (The details of the solutions are outlined in Appendix A). The solutions to Eqs. (3.23) to (3.25) are [44]

$$P^*(x) = 2\frac{d}{dx}\int_0^x \frac{z^2 M(z)}{\sqrt{x^2 - z^2}}\, dz, \tag{3.26}$$

$$Q(x) = \frac{1}{x}\frac{d}{dx}\int_0^x \frac{z^3 C(z)}{\sqrt{x^2 - z^2}}\, dz, \tag{3.27}$$

and

$$P(x) = \frac{-\pi}{2}\frac{d}{dx}[x^2 S(x)]. \tag{3.28}$$

The functional transformation given by Eqs. (3.23) to (3.25) and Eqs. (3.26) to (3.28) are not one-to-one, meaning that the solution for inverse SIDF is not unique. This is immediate since the SIDF is an approximate measure of the nonlinearity [9]. A solution to $Q(x)$ in Eq. (3.27) is developed in [13]. Presented in the following section is the numerical solution of Eqs. (3.26) to (3.28) to identify the nonlinear function $n(x)$.

3.4 Numerical Solution to the Inverse SIDF

Given the analytical expressions for SIDF, $M\,(A)$, $C\,(A)$, and $S\,(A)$, Eqs. (3.26) to (3.28) can be directly solved to obtain $P^*(x)$, $Q(x)$, and $P(x)$, respectively. However, in the present case, the values of $M\,(A)$, $C\,(A)$, and $S\,(A)$ are available in discrete sets. Therefore a numerical approach is developed. This section presents the numerical solution to the inverse SIDF problem and addresses the computational difficulties.

3.4.1 Numerical Solution for $Q(x)$

In solving Eqs. (3.26) and (3.27), the integrands approaches infinity at the upper bound limit. This causes some difficulties to solve these equations. To resolve this problem, a graphical integration method known as *method of cursors* is used.

3.4.1.1 Method of Cursors

The method of cursors is a graphical integration approach, in which the numerical solution of an integral in the form of

$$I_s = \int_{z=0}^{z=\theta} h(z)\, d[A_s(z)], \tag{3.29}$$

is given in [11, 46-48] as

$$I_s \cong \frac{A_\theta}{\eta} \sum_{i=1}^{\eta} h(z_i), \tag{3.30}$$

where A_θ is the total change in $A_s(z)$ between $z = 0$ and $z = \theta$ (Figure 3-3), η is the number of equal points into which A_θ is divided, and z_i are values of z at the midpoints of the intervals.

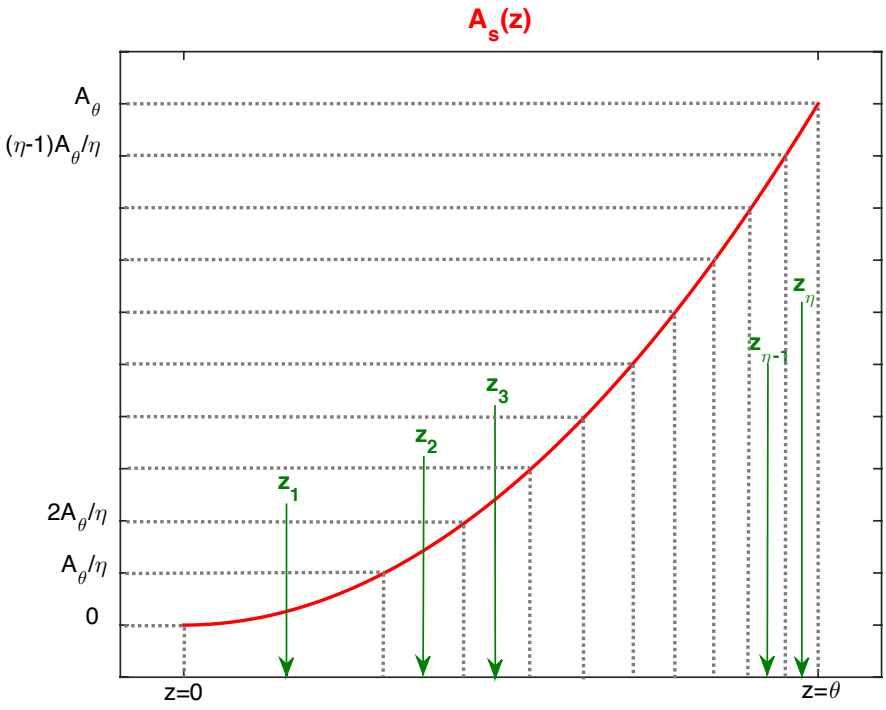

Figure 3-3 Illustration of the Method of Cursor.

Applying the method of cursors to the inverse SIDF to solve $Q(x)$ requires some transformations. Applying integration-by-parts and Leibniz integral rules to Eq. (3.27), gives, the following (details are outlined in Appendix B)

$$\frac{d}{dx}\int_0^x \frac{z^3 C(z)}{\sqrt{x^2-z^2}}\,dz = x\int_0^x \frac{1}{\sqrt{x^2-z^2}}\,d\big(z^2C(z)\big). \tag{3.31}$$

Substituting Eq. (3.31) into Eq. (3.27) yields

$$Q(x) = \int_0^x \frac{d\big(z^2C(z)\big)}{\sqrt{x^2-z^2}}. \tag{3.32}$$

Since $Q(x)$ must be solved at each values of x, i.e., $x = x_j$, Eq. (3.32) can be written as

$$Q(x_j) = \int_0^{x_j} \frac{d[z^2 g(z)]}{\sqrt{x_j^2 - z^2}}. \tag{3.33}$$

Comparing Eqs. (3.29) and (3.30) with Eq. (3.33) and employing method of cursors, $Q(x_j)$ can be estimated. Defining $A_s(z) \triangleq z^2 C(z)$ and $h(z) \triangleq \frac{1}{\sqrt{x_j^2 - z^2}}$, the $Q(x_j)$ estimation is

$$Q(x_j) \cong \frac{A_\theta}{\eta} \sum_{i=1}^{\eta} h(z_i). \tag{3.34}$$

Equation (3.34) is solved for all values of x_j in the range of the amplitude of the input signal.

3.4.2 Numerical Solution for $P^*(x)$

Through additional transformations, the method of cursor can also be utilized to solve $P^*(x)$. Applying integration-by-parts and Leibniz integral rules to Eq. (3.26) gives the following (see Appendix B)

$$\frac{d}{dx} \int_0^x \frac{z^2 M(z)}{\sqrt{x^2 - z^2}}\, dz = x \int_0^x \frac{1}{\sqrt{x^2 - z^2}}\, d\big(zM(z)\big). \tag{3.35}$$

Substituting Eq. (3.35) into Eq. (3.26) yields

$$P^*(x) = 2x \int_0^x \frac{d\big(zM(z)\big)}{\sqrt{x^2 - z^2}}. \tag{3.36}$$

Since $P^*(x)$ must be solved at each values of x, i.e., $x = x_j$, Eq. (3.36) can be written as

$$P^*(x_j) = 2x_j \int_0^{x_j} \frac{d(zM(z))}{\sqrt{x_j^2 - z^2}}. \tag{3.37}$$

Comparing Eqs. (3.29) and (3.30) with Eq. (3.37) and again employing method of cursors, $P^*(x_j)$ can be estimated. Defining $A_s(\cdot) \triangleq zM(z)$ and $h(\cdot) \triangleq \frac{1}{\sqrt{x_j^2 - z^2}}$, the $P^*(x_j)$ estimation is

$$P^*(x_j) \cong 2x_j \frac{A_\theta}{\eta} \sum_{i=1}^{\eta} h(z_i)\,. \tag{3.38}$$

Equation (3.38) is similarly solved for all values of x_j in the range of the amplitude of the input signal.

3.4.3 Numerical Solution for $P(x)$

Equation (3.28) can be written as

$$P(x) = \frac{-\pi}{2}\left[2xS(x) + x^2 \frac{dS(x)}{dx}\right]. \tag{3.39}$$

Using a first-order forward difference approximation for the derivative term in Eq. (3.39) gives

$$\left.\frac{dS(x)}{dx}\right|_{x=x_j} = \frac{S(x_{j+1}) - S(x_j)}{x_{j+1} - x_j}. \tag{3.40}$$

Substituting Eq. (3.40) into Eq. (3.39) for $x = x_j$, yeilds

$$P(x_j) = \frac{-\pi}{2}\left[2x_j S(x_j) + x_j^2\left(\frac{S(x_{j+1}) - S(x_j)}{x_{j+1} - x_j}\right)\right]. \tag{3.41}$$

Equation (3.41) is solved for all values of x_j in the range of the amplitude of the input signal.

3.4.4 Recovering the Nonlinear Function

In solving Eq. (3.22), there are three equations and four unknowns, therefore setting $q_1(x) = q_2(x)$ in Eq. (3.22) produces

$$q_1(x) = q_2(x) = \frac{Q(x)}{2}, \tag{3.42}$$

$$p_1(x) = \frac{P^*(x) + P(x)}{2}, \tag{3.43}$$

and

$$p_2(x) = \frac{P^*(x) - P(x)}{2}. \tag{3.44}$$

Substituting Eqs. (3.42) to (3.44) into Eq. (3.14) and using Eq. (3.6), the nonlinear function can be recovered as

$$y(x) = \begin{cases} \dfrac{Q(x) + P^*(x) + P(x)}{2} & \delta x < 0 \\ \dfrac{Q(x) + P^*(x) - P(x)}{2} & \delta x > 0 \end{cases}. \tag{3.45}$$

Equation (3.45) can be simplified if the nonlinearity is odd. For an odd function $M(A) = 0$ in see Eq. (3.8) and consequently $P^*(x) = 0$ in Eq. (3.26). Therefore, Eq. (3.45) reduces to

$$y(x) = \begin{cases} \dfrac{Q(x) + P(x)}{2} & \delta x < 0 \\ \dfrac{Q(x) - P(x)}{2} & \delta x > 0 \end{cases}. \tag{3.46}$$

3.4.5 Computational Issues

To estimate the nonlinear function, $n(x)$, from its gain and phase distortions, a computational code must be developed that solves Eqs. (3.34), (3.38) and (3.41) independently and then uses Eq. (3.45) to recover the non-parametric model of the nonlinearity. For this following issues must be considered.

3.4.5.1. Resampling the Input Signal Amplitude Vector

Eqs. (3.34), (3.38) and (3.41) have to be solved for the whole range of input signal amplitudes. Given a discrete set of gain and phase distortions, $M(A)$, $C(A)$ and $S(A)$, functions $P^*(x)$,$Q(x)$ and $P(x)$ have to be obtained for all values of x, between A_{min} and A_{max}, the lowest and highest values of input signal amplitude. Therefore, input signal amplitude vector, A, must be evenly resampled from A_{min} to A_{max} to include all values of x in this range. The resampled input signal amplitude vector, A_r, is defined as

$$A_r = \{A_{min} : \Delta : A_{max}\}, \tag{3.47}$$

where Δ is the discretization in A_r. A measure for choosing the value of Δ is the lowest increment in the original vector A. Additionally, to make the size of all vectors compatible, $M(A), C(A)$ and $S(A)$, must also be resampled based on A_r. The resampled vectors, i.e., $M_r(A_r)$,$C_r(A_r)$ and $S_r(A_r)$ will be used for calculations of $P^*(x_j)$, $Q(x_j)$ and $P(x_j)$.

3.4.5.2. Discretization in the Method of Cursors

Another factor to consider is a measure for selecting η in Eq. (3.30). In general, by increasing η the output solution will have higher resolution. One possible value for η is at least ten times of the dimension of A_r, l, defined as

$$l = \left\lfloor \frac{A_{max} - A_{min}}{\Delta} \right\rfloor + 1, \tag{3.48}$$

where $\lfloor . \rfloor$ is the *floor* function, the largest integer less than or equal to $\left(\frac{A_{max}-A_{min}}{\Delta}\right)$.

3.5 Case Studies

In this section, three case studies are presented to validate the proposed numerical solution. First, the proposed inverse SIDF algorithm is used to recover a hysteresis nonlinearity from its gain and phase distortions. In the second example, three piecewise continuous functions are recovered from the gain distortions of a nonlinear PID controller. The third case study investigates the application of the proposed inverse SIDF algorithm in estimation of asymmetric hysteresis nonlinearities.

3.5.1 Case Study 1: Double-valued Nonlinearity

For the first example, identification of a common nonlinear function with memory is used. The schematic of this nonlinear function is shown in Figure 3-4.

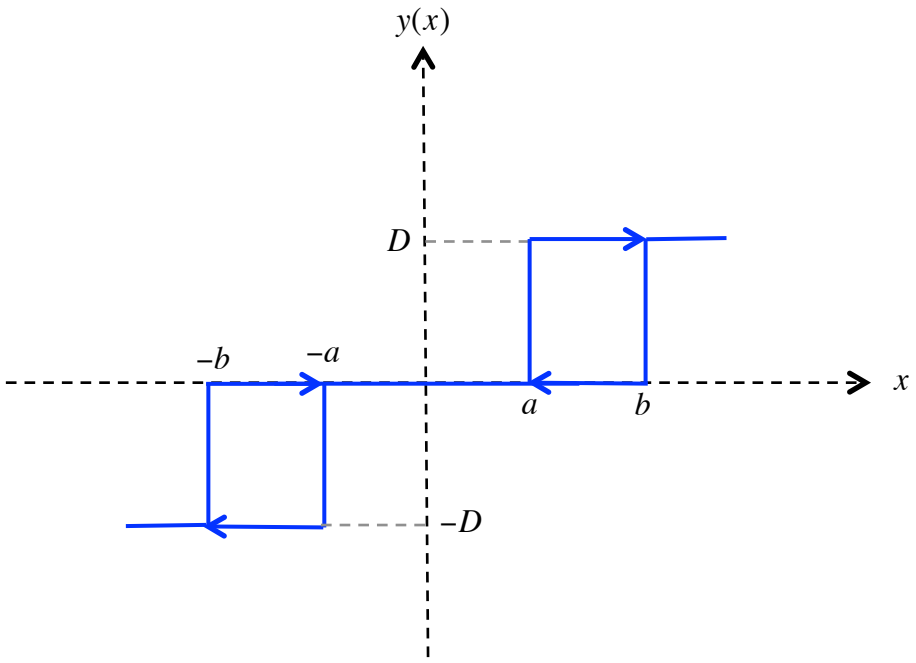

Figure 3-4 Schematics of the Hysteresis Nonlinearity.

The analytical formulation for SIDF of this nonlinearity given in [44] is

$$C(A) = \begin{cases} 0 & |A| \le a \\ \dfrac{2D}{\pi A^2}\sqrt{A^2 - a^2} & a < |A| < b \\ \dfrac{2D}{\pi A^2}\left(\sqrt{A^2 - a^2} + \sqrt{A^2 - b^2}\right) & b \le |A| \end{cases} \tag{3.49}$$

and

$$S(A) = \begin{cases} 0 & |A| \le a \\ \frac{2D}{\pi A^2}(A-a) & a < |A| < b \\ \frac{2D}{\pi A^2}(b-a) & b \le |A| \end{cases}, \tag{3.50}$$

where $M(A) = 0$, and a, b, and D are the parameters illustrated in Figure 3-4. By arbitrarily choosing $a = 2$, $b = 5$, and $D = 2$, the gain and phase distortions have been generated for the input amplitude range $0 < A \le 8$.

The gain and phase distortions are then used in the proposed numerical solution for different values of Δ and η, such that $\Delta_1 = 0.01 < \Delta_2 = 0.05$ and $\eta_1 = 100\, l > \eta_2 = 10\, l$. The output solutions are illustrated in Figure 3-5 and Figure 3-6.

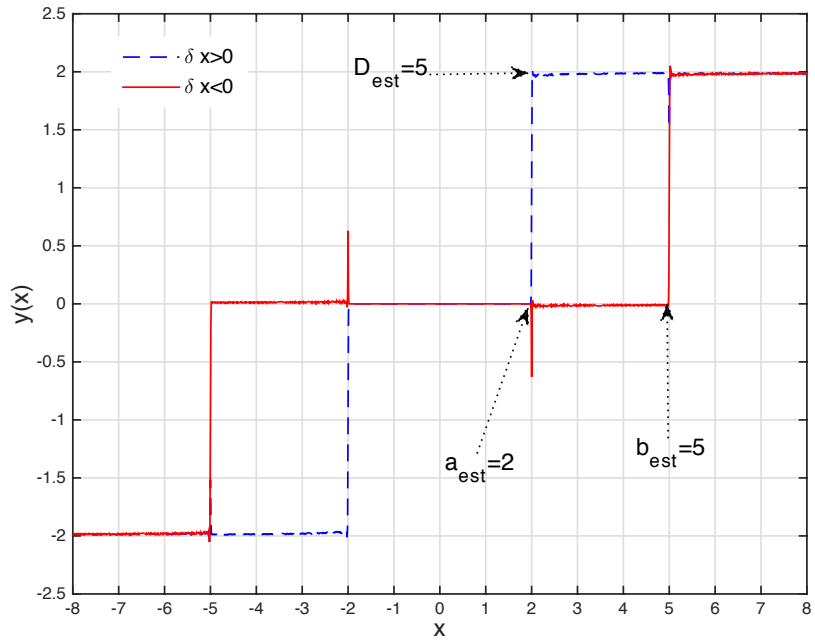

Figure 3-5 Non-parametric Output Solution: 1st Selection of the Discretization Parameters.

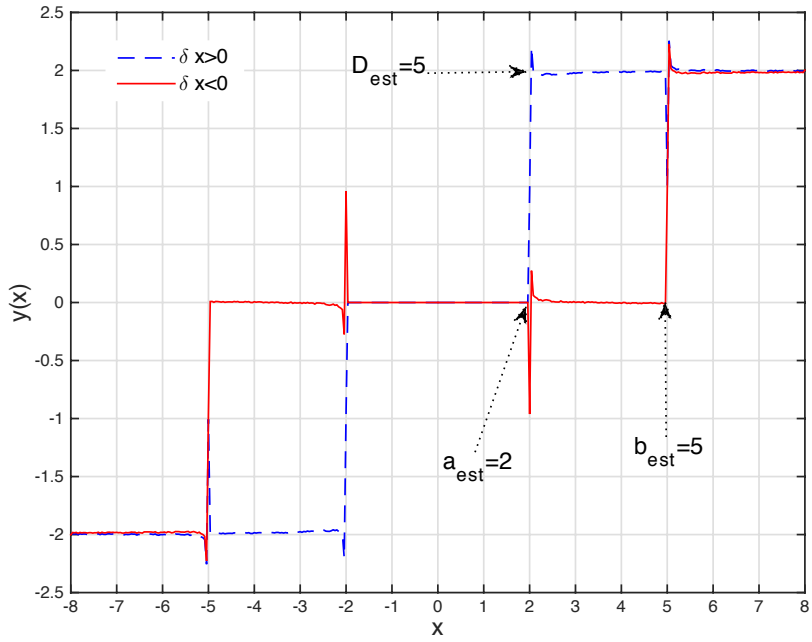

Figure 3-6 Non-parametric Output Solution: 2nd Selection of the Discretization Parameters.

From Figure 3-5 and Figure 3-6, the numerical solution has identified the nonlinearity correctly. The parameters associated with this nonlinearity (a, b, and D) can also be measured from the non-parametric models. The estimated values for each of these parameters, as illustrated in Figure 3-5 and Figure 3-6 are $a_{est} = 2$, $b_{est} = 5$, and $D_{est} = 2$, which are consistent what was used in the analytical formula in Eqs. (3.49) and (3.50). It is to be noted that the peaks in Figure 3-5 and Figure 3-6 at $x = \pm a = \pm 2$ and $x = \pm b = \pm 5$ are due to the discontinuities in the numerical solutions for different segments of input signal amplitude defined in Eqs. (3.49) and (3.50).

Moreover, comparing Figure 3-5 to Figure 3-6, the effect of the values of Δ and η on the resolution of the identified nonlinearity can be observed. In general, regardless of the values of Δ and η, the proposed numerical solution can identify the nonlinearity,

however, the resolution of the output model from the numerical solution and accuracy of the estimated parameters of the nonlinearity can be improved by proper adjustments in the values of Δ and η. By decreasing Δ and/or increasing η, the resolution of the output solution will improve.

3.5.2 Case Study 2: Single-valued Nonlinearity

The SIDF gain and phase distortions used for the second example is based on the results in [16]. In [16], the goal was to design a nonlinear PID controller for a nonlinear system. The nonlinearities in the plant consist of motor saturation and stiction. The controller synthesis parallels the procedure proposed in the [13-15]. The gain distortions for different gains of the nonlinear PID controller obtained in [16] are listed in Table 3. 1.

Table 3. 1. SIDF Gain Distortions Information, from Ref. [16].

e_i	K_P	K_I	K_D
0.0628	5.97	37.4	0.043
0.0804	5.13	36.0	0.045
0.1005	4.71	36.0	0.050
0.1608	4.38	39.5	0.069
0.3215	6.81	55.9	0.129
0.6430	8.89	64.0	0.167
1.2811	9.84	67.7	0.193
2.5621	10.5	68.5	0.206

To identify the nonlinearity in [16] associated with each of these nonlinear PID gains, it is assumed that all three nonlinear PID gains can be represented by a piecewise

continuous nonlinear function. An initial estimate for the parameters of such functions for each gain are determined, and based on this, the estimated gain distortions are developed. Next, the cost function defined as the squared error between the estimated gain distortions and the true values is minimized to obtain the actual values of the parameters of the nonlinear function. These parameters are listed in Table 3. 2 to Table 3. 4.

To validate the proposed numerical solution, the information in Table 3. 1 is used to identify the nonlinearity of these PID gains. The SIDF distortions show no phase distortion, therefore $S(A) = 0$. Each gain represents one distinct nonlinearity, i.e., $[A, C_1(A)] = \{e_i, K_P\}, [A, C_2(A)] = \{e_i, K_I\}$ and $[A, C_3(A)] = \{e_i, K_D\}$. The data from Table 3. 1 are used in the developed inverse SIDF algorithm with the following results for the parametric models

$$K_P(x) = \begin{cases} 4.5147\,x & x \le 0.19 \\ 11.1676\,x - 1.2641 & x > 0.19 \end{cases}, \tag{3.51}$$

$$K_I(x) = \begin{cases} 35.92\,x & x \le 0.125 \\ 70.32\,x - 4.3 & x > 0.125 \end{cases}, \tag{3.52}$$

and

$$K_D(x) = \begin{cases} 0.0449\,x & x \le 0.13 \\ 0.2171\,x - 0.0224 & x > 0.13 \end{cases}. \tag{3.53}$$

The parametric models in Eqs. (3.51) to (3.53) are obtained from the non-parametric models from the output solutions. The non-parametric models for K_P, K_I, and K_D gains are shown in Figure 3-7 to Figure 3-9. The solid-lines represent the output solutions from the developed algorithm, from which it can be concluded that each gain in the nonlinear

PID controller has the characteristics of a piecewise continuous function. This identified model for the nonlinearity is consistent with what was assumed in [16]. In this work, however, the structure of the nonlinear function is an output of the proposed numerical algorithm. Therefore, no prior information or assumption was needed to initiate the estimation process.

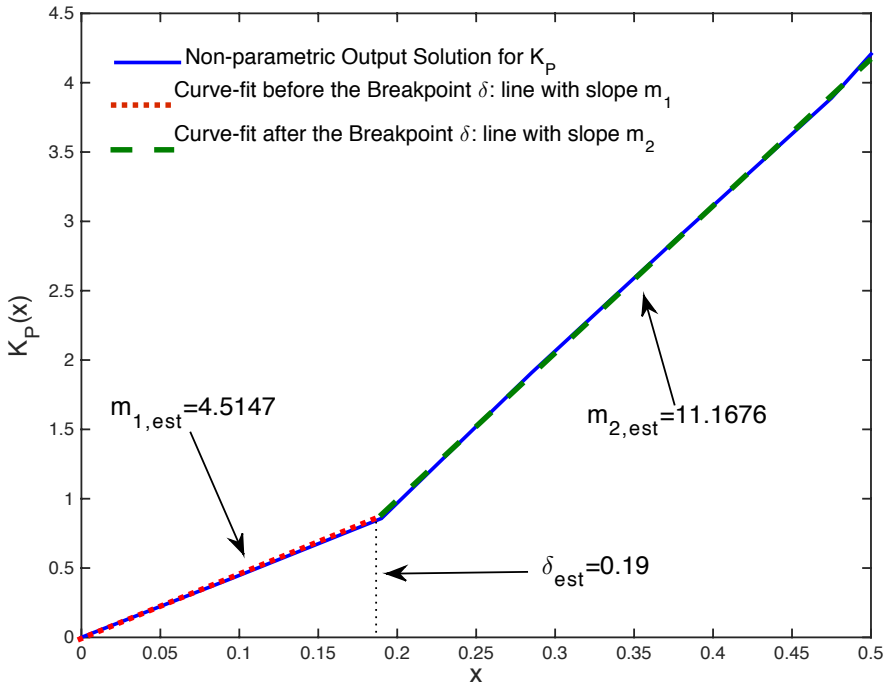

Figure 3-7 Nonlinear Controller Gain from Proposed Numerical Solution, K_P.

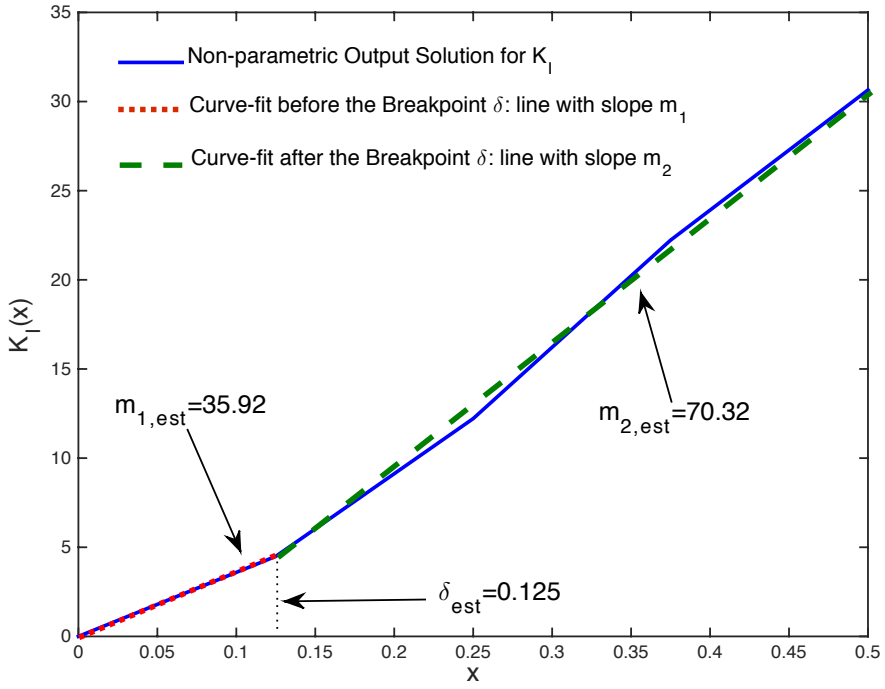

Figure 3-8 Nonlinear Controller Gain from Proposed Numerical Solution, K_I.

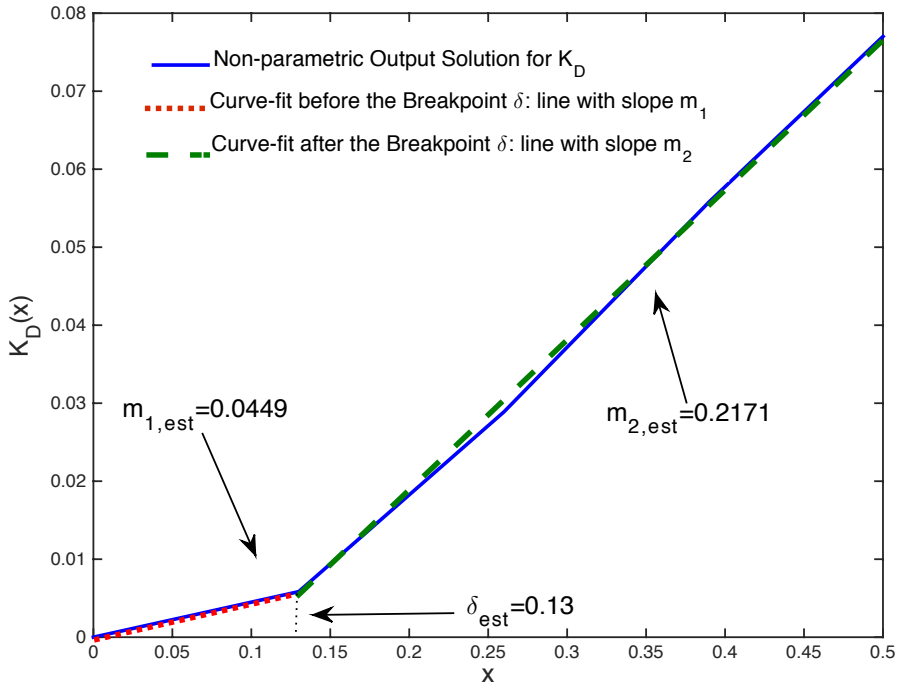

Figure 3-9 Nonlinear Controller Gain from Proposed Numerical Solution, K_D.

Employing a LSE method on the solid-line in Figure 3-7, Eq. (3.51) can be obtained. The dotted-line with the estimated slope, $m_{1,est} = 4.5147$ is the segment of Eq. (3.51) before the estimated breakpoint, $\delta_{est} = 0.19$. Similarly, the dashed-line with the estimated slope, $m_{2,est} = 11.1676$ is the segment of Eq. (3.51) after the estimated breakpoint.

Similarly, the parameters of K_I and K_D are estimated, as depicted in Figure 3-8 and Figure 3-9. The resulting information is listed in Table 3. 2 to Table 3. 4, where each parameter has been compared against its corresponding value obtained in [16] and their percentage differences are also listed. From the data in Table 3. 2 to Table 3. 4, the values for each parameter of each gain obtained from the proposed numerical solution match their corresponding values that were proposed in [16]. A comparison for frequency domain and time domain representations of K_P, K_I, and K_D gain are shown in Figure 3-10 to Figure 3-12.

Table 3. 2. Comparison for Breakpoint.

	Breakpoint value: δ		
	This work	From [16]	% Difference
K_P	0.19	0.189	0.5277
K_I	0.125	0.126	0.7968
K_D	0.13	0.132	1.5267

Table 3. 3. Comparison for Slope Before Breakpoint.

	Slope Before Breakpoint: m_1		
	This work	From [16]	% Difference
K_P	4.5147	5.10	12.18
K_I	35.92	36.77	2.3387
K_D	0.0449	0.047	4.5702

Table 3. 4. Comparison for Slope After Breakpoint.

	Slope After Breakpoint: m_2		
	This work	From [16]	% Difference
K_P	11.1676	11.16	0.0681
K_I	70.32	72.81	3.4794
K_D	0.2171	0.215	0.972

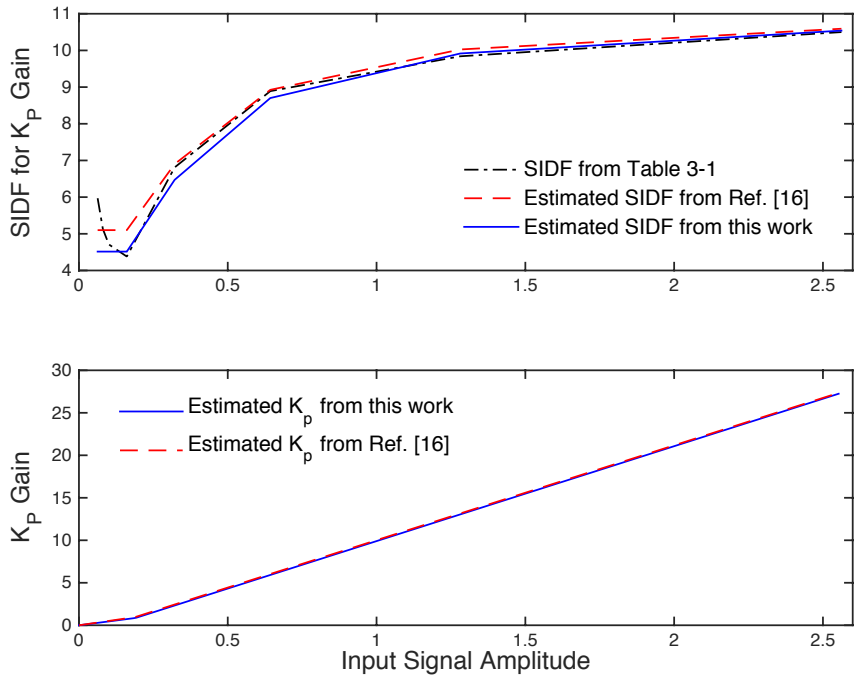

Figure 3-10 Comparison for Estimation of K_P Gain: Ref. [16] vs. this work.

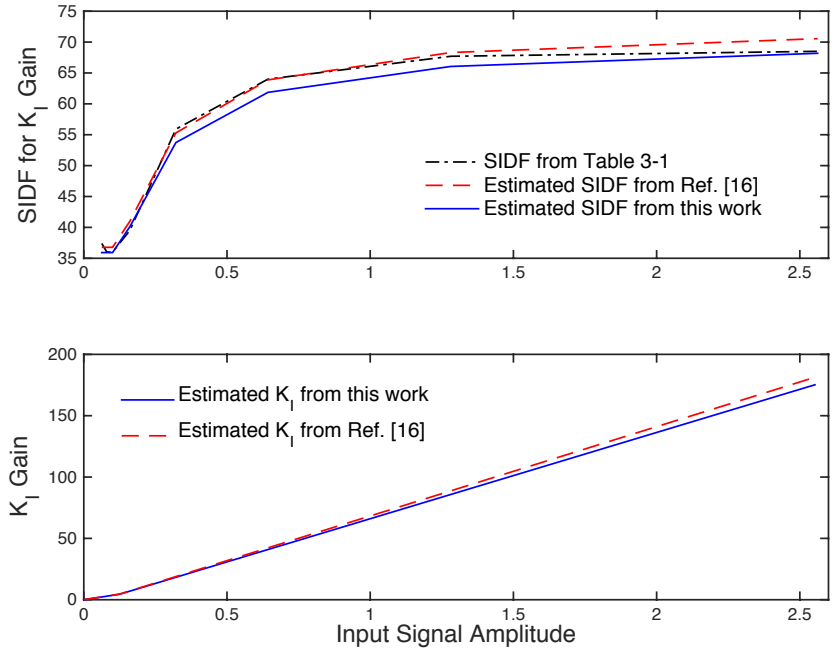

Figure 3-11 Comparison for Estimation of K_I Gain: Ref. [16] vs. this work.

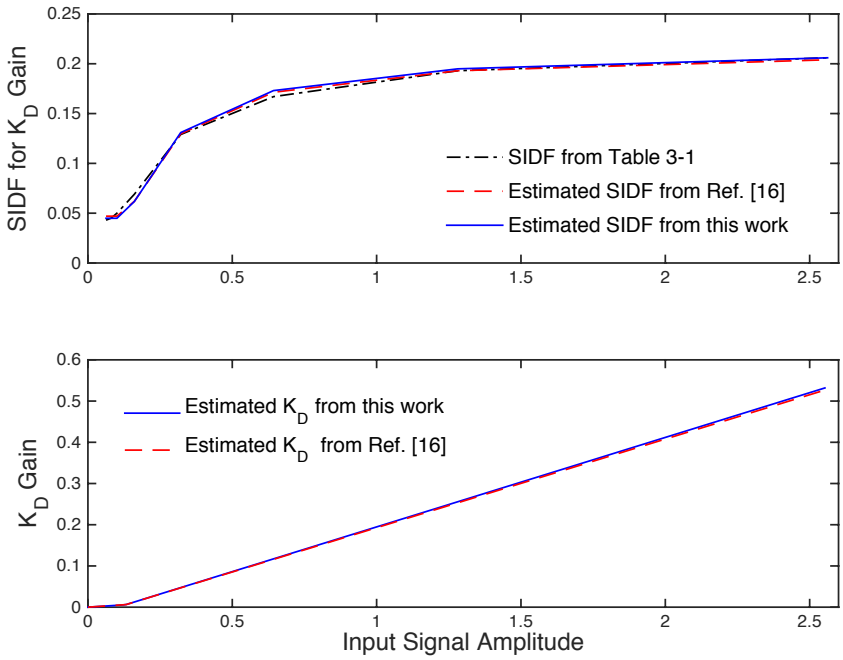

Figure 3-12 Comparison for Estimation of K_D Gain: Ref. [16] vs. this work.

3.5.3 Case Study 3: Limitations of the Algorithm

In this case study, identification of asymmetric double-valued nonlinearities is investigated. Applications of SIDF for asymmetric nonlinearities are more complicated compared to symmetrical nonlinearities, owing to one or both of the followings:

(i.) There is a bias term present in the nonlinearity output. The output bias term is not included in the formulation of SIDF [9]. In the case of a biased single-valued nonlinearity, the bias term issue can be resolved by a curve-fit in the gain distortions in the vicinity of $A \cong 0$ [9]. However, this is not applicable to the double-valued nonlinearities. If the asymmetric double-valued nonlinearity was known, it could be shifted along its input-output axis to the point at which the harmonic input results in an unbiased output [9]. However, in the application of the inverse SIDF, the nonlinearity is not known. Moreover, the solution of inverse SIDF is not unique, owing to the approximate nature of SIDF method. Therefore, the output solutions from the numerical inverse SIDF algorithm are expected to be an incomplete representation of an asymmetric double-valued nonlinearity with the bias term.

(ii.) Nonlinearity output is defined in an asymmetric range of operation of the input signal. In this case $n_1(x)$ and $n_2(x)$ in Eq. (3.6), are not defined over the same range of input signal amplitude. Therefore, while recovering the nonlinearity from inverse SIDF solution, Eq. (3.45) must be modified to account for the unsymmetrical ranges of operation of $n_1(x)$ and $n_2(x)$.

To illustrate these cases, consider two asymmetric hysteresis nonlinearities shown in Figure 3-13. The diagram shown in Figure 3-13L is asymmetric due to the bias term in the output nonlinearity. For the diagram shown in Figure 3-13R the nonlinearity is asymmetric, besides the presence of the output bias term, $n_1(x)$ (for $\delta x < 0$) and $n_2(x)$ (for $\delta x > 0$) in Eq. (3.6) are not defined in the same range of input signal amplitude.

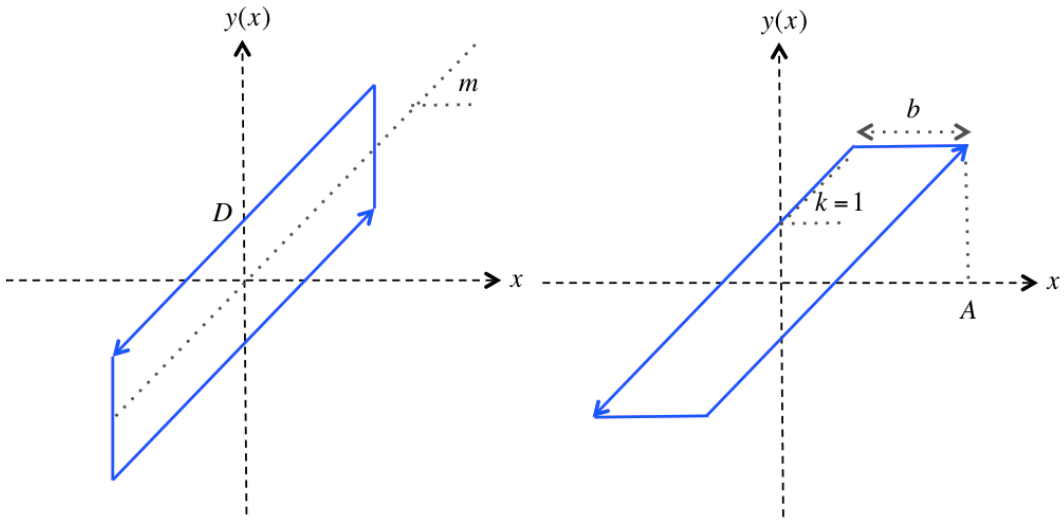

Figure 3-13 Schematics of Asymmetric Double-Valued Nonlinearities: (L) with Biased Output, and (R) with both Asymmetric Range of Input Amplitude and Biased Output.

To show the output models from the proposed numerical inverse SIDF for these two nonlinearities, consider their SIDF analytical formulation given in [9]. For the static nonlinearity shown in Figure 3-13L,

$$C(A) = m, \;\; S(A) = \frac{-4D}{\pi A}, \tag{3.54}$$

where m and D are the parameters illustrated in Figure 3-13L. Additionally, for the system shown in Figure 3-13R,

$$\text{for } A > \frac{b}{2}: \;\; C(A) = \frac{1}{2}\left[1 + f\left(1 - \frac{b}{A}\right)\right], S(A) = \frac{-1}{\pi}\left[\frac{2b}{A} - \left(\frac{b}{A}\right)^2\right], \tag{3.55}$$

where $f(\cdot)$ is the saturation function, and b is the parameter illustrated in Figure 3-13R.

Note that $M(A)$ that is related to the output bias term is not accounted for in Eqs. (3.54) and (3.55) and is considered to be zero in both. By arbitrarily choosing $m = 1$, $D = 4$ in Eq. (3.54) the gain and phase distortions have been generated for the input amplitude range $0 < A \leq 10$. Additionally, by selecting $b = 4$ in Eq. (3.55) the gain and phase distortions have been generated for the input amplitude range $\frac{b}{2} < 2.5 \leq A \leq 10$. The generated gain and phase distortions are then used in the proposed numerical solution. The output solutions are shown in Figure 3-14 and Figure 3-15.

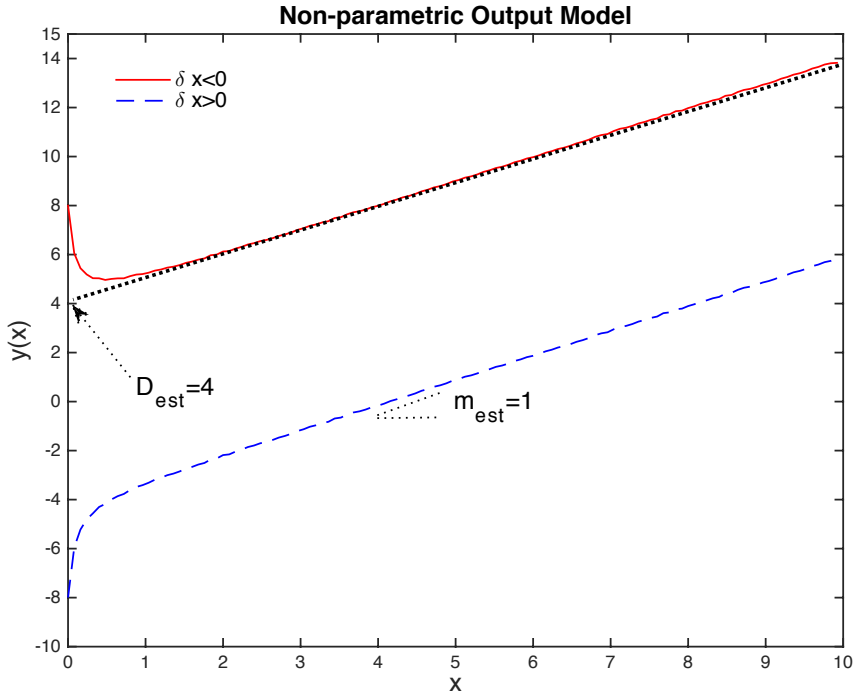

Figure 3-14 Non-parametric Output Solution for the 1st Asymmetric Hysteresis Nonlinearity.

From Figure 3-14, the numerical solution has partially identified the hysteresis loop for the first asymmetric double-valued nonlinearity. From this non-parametric output model, the parameters associated with the nonlinearity (D and m) can be estimated. The estimated values for each of these parameters, as illustrated in Figure 3-14, are $D_{est} = 4$ and $m_{est} = 1$, which are consistent with what was used in the analytical formula in Eq. (3.54). The second part of the hysteresis loop can be estimated by extrapolation of the output model in Figure 3-14. It is to be noted that the values of $y(x)$ shown in Figure 3-14 around $x \cong 0$ are due to the singularity of the analytical SIDF in Eq. (3.54) around $A \cong 0$.

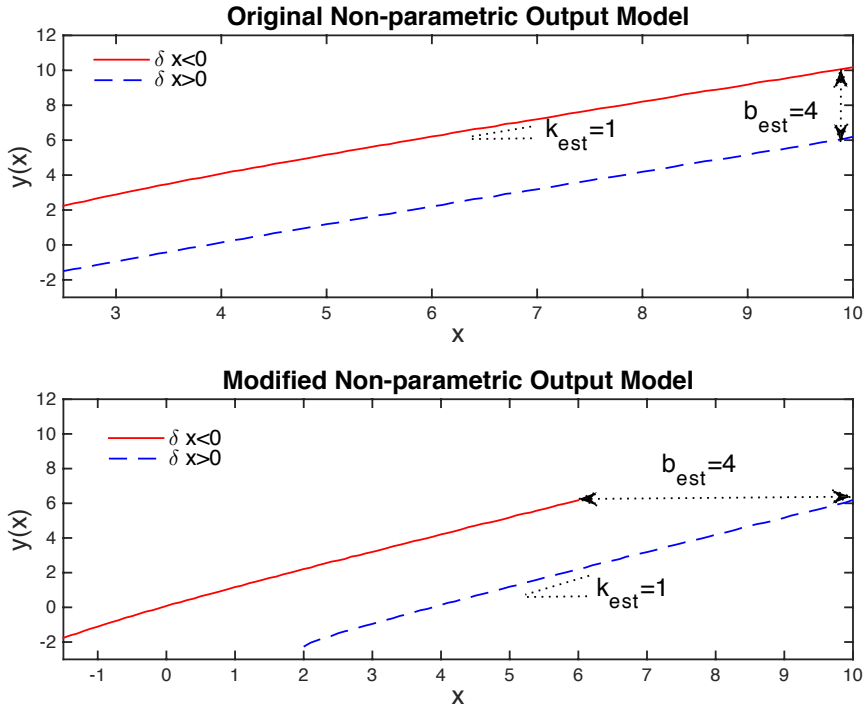

Figure 3-15 Non-parametric Output Solution for the 2nd Asymmetric Hysteresis Nonlinearity.

Shown in the top plot of Figure 3-15, is the output solution from the numerical inverse SIDF algorithm for the second asymmetric hysteresis nonlinearity considered in Eq. (3.55). From this, the identified non-parametric model is not consistent with Figure 3-15R. This inconsistency is due to the asymmetric range of the input signal amplitude for different segments of this nonlinearity that is not accounted for in the proposed inverse SIDF solution. From Figure 3-13R, the range of input signal amplitude for $n_1(x)$ (for $\delta x < 0$) and $n_2(x)$ (for $\delta x > 0$) are different by the value of b. Considering this asymmetric range for x, Eq. (3.45) can be modified to recover the nonlinearity. The result of employing this modification is shown in the bottom plot of Figure 3-15, from which the parameters associated with the nonlinearity (b and k) can be estimated. The estimated values for each of these parameters, as illustrated in Figure 3-15, are $b_{est} = 4$ and $k_{est} = 1$, which are consistent with what was used in the analytical formula in Eq. (3.55). Additionally, the second part of the hysteresis loop can be estimated by extrapolation of the modified output model in the bottom plot of Figure 3-15.

It is to be noted that the original output solution (shown in the top plot of Figure 3-15) is similar to the schematics shown in Figure 3-13L. Therefore, one possibility is to interpret the output solution in terms of Eq. (3.54). This is one example on the non-uniqueness of the inverse SIDF solution. In other words, although Eqs. (3.54) and (3.55) are different, the interpretation of the inverse SIDF shown in the top plot of Figure 3-15 can be either in terms of Eq. (3.54) shown in Figure 3-13L or by using above-mentioned modifications in terms of Eq. (3.55) shown in Figure 3-13R.

3.5.4 Section Summary

As illustrated in these examples, the proposed numerical solution estimates a non-parametric model for explicit nonlinear functions based on the gain and phase distortions information. Moreover, by employing LSE method, the parameters of the non-parametric model can be numerically identified from the output of the numerical solution; and therefore, one can defines the nonlinear function associated with the gain and phase distortions. The limitation of the proposed numerical solution is also discussed. This limitation is related to the identification of asymmetric double-valued nonlinearities, in which the inverse SIDF solutions is an incomplete representation of the nonlinearity.

3.6 Chapter Summary

A method for numerically solving the inverse SIDF problem is developed. The method is based on an analytical solution of the inverse SIDF problem. The proposed numerical solution can identify a broad class of static (explicit) nonlinearities with or without memory based merely on their gain and phase distortions. More specifically, numerical solutions are developed that extend the solution of inverse SIDF to the double-valued and not necessarily odd nonlinear functions. The algorithm is computationally programmed and identifies a non-parametric model of the nonlinearity, from which a parametric model can be recovered by employing LSE method. Selection of the discretization parameters (Δ, η) in the algorithm and their effect on the resolution of the solution has been investigated. The proposed numerical solution has been utilized to identify nonlinearities in three illustrative examples. From these examples, the

effectiveness and limitations of the algorithm are discussed. A major advantage of the proposed numerical solution over previous methods in the area of inverse SIDF problem is that, the numerical solution developed in this work does not require *a priori* knowledge or information of the structure of the nonlinearity to initiate the identification process.

Chapter 4. Frequency Based Linear Controller Design for Regulating Systems

Presented in this chapter is the methodology of designing linear controllers for linear regulating systems subject to time domain constraints. The controller design procedure is executed in the frequency domain; hence the time domain performance constraints are translated in to the frequency domain tolerances. These frequency domain tolerances will be utilized in Chapter 5 to formulate a nonlinear controller design methodology for the same class of systems. The basis of the methods presented in Chapter 4 and Chapter 5 is the loop shaping approach that is an extension of the Quantitative Feedback Theory (QFT) methodology [49-53].

4.1 Overview of Quantitative Feedback Theory

Quantitative Feedback Theory (QFT) is a well-known classical robust control methodology and analysis framework. QFT is formulated in the frequency domain and was originally developed for Single Input Single Output (SISO) and Linear Time Invariant (LTI) systems [54-57]. The applications of QFT has since been extended to systematic feedback controller design approaches for systems subject to (i.) uncertainties, (ii.) time delays, (iii.) restricted controller bandwidth, (iv.) sensor noise, (v.) disturbances, (vi.) rate and magnitude saturation of the actuator, and, (vii.) system nonlinearities. The

first six items have been extensively studied [58-64]. Integration of the nonlinearities in the QFT formulation is still an open research area, which is the focus of Chapter 5.

In QFT, the time domain performance constraints are translated to the frequency domain characteristic that can be directly imposed on the frequency response of the open loop to ensure closed loop performance requirements. Some of these basic translations are presented in Chapter 1. Other constraints on the closed loop performance of a feedback system subject to a disturbance can also be directly enforced on the closed loop frequency response [65]. The enforcement of these performance specifications can also be extended to include rate and output actuator saturation [66]. The details on this will be discussed later in the following sections.

The design process in QFT is transparent that results in a clear understanding of the trade-offs that are necessary to maintain certain level of closed loop performance. Owing to the frequency-by-frequency basis of the controller design process in QFT, a loop shaping approach for controller design can be developed [57]. This loop shaping process is done on the Nichols chart and is based on analyzing the gain and phase properties of the open loop transfer function.

The advantage of using Nichols charts is that the desired closed loop properties of the system can be directly mapped to the open loop properties of the system. This allows a direct design of the closed loop properties (such as output constraints) while specifying properties of the controller (such as controller order or bandwidth). Frequency domain controller design makes the analysis of the non-minimum phase and delayed systems easier. Other implementation issues, such as sensor noise amplification, can be easily

addressed in the frequency domain by adjusting the bandwidth of the open loop transfer function.

4.1.1 Nichols Chart

Nichols chart makes a connection between open loop and the closed loop transfer functions. In the Nichols chart, the properties of the closed loop transfer function can be directly obtained from the open loop frequency response. The controller design in QFT is performed on the open loop transfer function, therefore; the closed loop information can be interpreted from the Nichols chart [2].

Let $L(s)$ be the open loop transfer function. Hence, the closed loop transfer function can be expressed as

$$T(s) = \frac{L(s)}{1 + Ls)}. \tag{4.1}$$

The open loop information for a constant closed loop magnitude can be obtained by evaluating the magnitude of Eq. (4.1), as

$$|T(j\omega)| = \left|\frac{X + jY}{1 + X + jY}\right| = M, \tag{4.2}$$

where M is a constant, and X, Y are defined as

$$|L(j\omega)| = \sqrt{X^2 + Y^2} \tag{4.3}$$

and

$$\measuredangle L(j\omega) = \tan^{-1}\frac{Y}{X}. \tag{4.4}$$

Using Eqs. (4.3) and (4.4), Eq. (4.2) can be reduced to

$$\left[X + \frac{M^2}{M^2 - 1}\right]^2 + Y^2 = \frac{M^2}{(M^2 - 1)^2}. \tag{4.5}$$

Additionally, the constant closed loop phase is defined as

$$\measuredangle T(j\omega) = N = \measuredangle L(j\omega) - \measuredangle[1 + L(j\omega)] = \tan^{-1}\frac{Y}{X} - \tan^{-1}\frac{Y}{1 + X}, \tag{4.6}$$

where N is a constant.

Using Eqs. (4.3) and (4.4), Eq. (4.6) can be reduced to

$$\left[X + \frac{1}{2}\right]^2 + \left[Y - \frac{1}{2\tan N}\right]^2 = \frac{\tan^2 N + 1}{4\tan^2 N}. \tag{4.7}$$

Constant closed loop magnitude of Eq. (4.5) and constant closed loop phase of Eq. (4.7) are equations of circles whose centers and radii are function of constants M and N. These circles develop constant closed loop gain and phase contours in the open loop gain/ phase plane. This creates the Nichols chart, which provides a direct translation between open loop and closed loop frequency domain properties. This means, for a given closed loop magnitude of M or a given closed loop phase of N, the gain and phase of the open loop transfer function can be directly calculated from the Nicholas chart. The standard units for gain and phase on the Nichols chart are decibel (dB) and degree (°), respectively.

4.2 Problem Statement

Consider the SISO linear regulating systems shown in Figure 4-1.

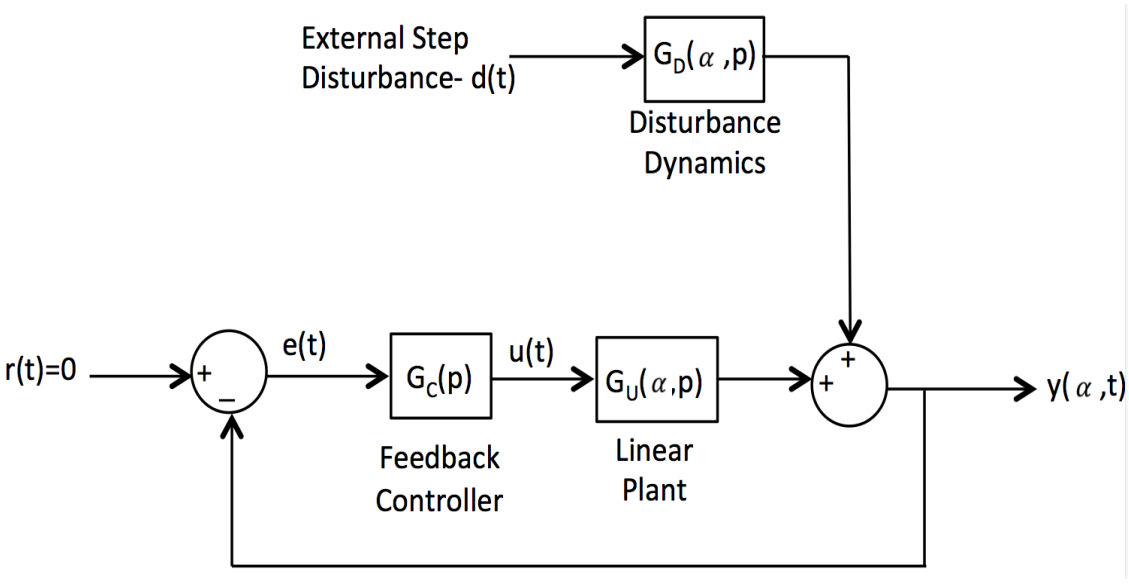

Figure 4-1 Block Diagram of a Regulating System.

In Figure 4-1, p denotes the derivative operator, α is a compact set representing uncertainty in the system that belongs to the parameter space for the plant uncertainty Ω, $y(\alpha, t)$ denotes the output variation about a desired set point, $u(t)$ is the controlled output, and $d(t)$ is the external step disturbance of size γ. Plant and disturbance dynamics, $G_U(\alpha, p)$ and $G_D(\alpha, p)$, are LTI, minimum phase, and $\mathbf{RH_2}$ (class of strictly proper and stable transfer functions with real valued coefficients).

To ensure finite gains for the controller, performance constraints for system must be defined. The output performance specification is defined as an allowable tolerance about a desired operating point $z_0(t)$ as

$$|z(t) - z_0(t)| = |y(\alpha, t)| \leq \beta \quad \forall t > 0. \tag{4.8}$$

Additionally, the actuator saturation constraint is defined as an allowable tolerance about the nominal control effort $g_0(t)$ as

$$|g(t) - g_0(t)| = |u(t)| \leq \Gamma \quad \forall t > 0. \tag{4.9}$$

The closed loop transfer functions for the system shown in Figure 4-1 are

$$T_y(s, \alpha) = \frac{G_D(s, \alpha)}{1 + G_C(s) G_U(s, \alpha)} \tag{4.10}$$

and

$$T_u(s, \alpha) = \frac{-G_D(s, \alpha) G_C(s)}{1 + G_C(s) G_U(s, \alpha)}. \tag{4.11}$$

The objective is to design a linear controller in the frequency domain, for the class of systems shown in Figure 4-1 such that the closed loop system represented in Eqs. (4.10) and (4.11) maintains system performance requirements in Eqs. (4.8) and (4.9) for a predicted level of the disturbance step size.

4.3 Performance Based Linear Controller Design

The performance specifications in Eqs. (4.8) and (4.9) can be enforced through frequency domain amplitude inequalities. These inequalities develop upper and lower amplitude bounds on the open loop plant, $L(s, \alpha) = G_C(s) G_U(s, \alpha)$. To formulate these bounds, consider the following theorem and lemma.

Theorem: The step response of a stable, minimum phase transfer function, whose impulse response is non-negative, is monotonic [67].

Proof: Let the impulse response of a stable, minimum phase transfer function be denoted as $h(t)$. Then the corresponding step response $y(t)$ with zero initial conditions can be written as [67]

$$y(t) = \int_0^t h(t-\tau)d\tau. \tag{4.12}$$

Since $h(t) \geq 0$, then

$$y(t_1) \geq y(t_2) \text{ for } t_1 \geq t_2. \tag{4.13}$$

Equation (4.13) implies that $y(t)$ monotonically increases until it reaches its steady state value, i.e., y_∞. Therefore the following can be concluded,

$$y(t) \leq y_\infty \ \forall t > 0. \tag{4.14}$$

Q.E.D.

Additionally, the following lemma can be directly inferred from this theorem.

Lemma: Consider a signal $y(t)$ whose Laplace transform is defined as [68]

$$Y(s) = H(s)\frac{\gamma}{s}, \tag{4.15}$$

where $H(s) \in \mathbf{RH_2}$ and $H(s)$ has a finite bandwidth. If the impulse response of $H(s)$ is of one sign and the initial conditions are zero, then

$$|y(t)| \leq \gamma \Lambda \|H(j\omega)\|_\infty \quad \forall t > 0, \tag{4.16}$$

where $\|.\|_\infty$ is the frequency domain H_∞ norm and Λ is a scaling constant justifying the time to frequency domain transformation and is a function of the closed loop transfer function.

In the following sections, this lemma will be used to translate the time domain performance specifications in Eqs. (4.8) and (4.9) to the frequency domain amplitude inequalities.

4.3.1 Developing Upper Bounds from the Constraints on the Actuator Effort

The upper amplitude bounds will be obtained from the actuator effort constraints. To develop the upper amplitude bounds, consider the transfer function in Eq. (4.11). To use the Theorem in previous section, $T_u(s, \alpha)$ must have an impulse response of one sign. Since $G_u(s, \alpha)$ and $G_D(s, \alpha)$ are minimum phase and stable, this impulse response condition is valid. Using the Lemma in previous section, the following can be concluded [65, 68]

$$|u(t)| \leq \gamma \Lambda_u \|T_u(j\omega)\|_\infty, \tag{4.17}$$

where Λ_u is a scaling constant justifying the time to frequency domain transformation and is a function of the closed loop transfer function $T_u(s)$, and $\|T_u(j\omega)\|_\infty$ is the frequency domain H_∞ norm of $T_u(s)$,

$$\|T_u(j\omega)\|_\infty = \left\| \frac{G_D(j\omega,\alpha)G_C(j\omega)}{1+G_C(sj\omega)G_U(j\omega,\alpha)} \right\|_\infty . \tag{4.18}$$

Next step, if the following inequality holds,

$$\gamma \left| \frac{G_D(j\omega,\alpha)G_C(j\omega)}{1+G_C(j\omega)G_U(j\omega,\alpha)} \right| \leq \Gamma \quad \forall\omega \ \& \alpha \in \Omega, \tag{4.19}$$

then Eq. (4.9) is satisfied. Consider the rearrangement in Eq. (4.19) as

$$\left| \frac{L(j\omega,\alpha)}{1+L(j\omega,\alpha)} \right| \leq |M(j\omega,\alpha)| \quad \forall\omega \ \& \alpha \in \Omega, \tag{4.20}$$

where $L(j\omega,\alpha) = G_C(j\omega)G_U(j\omega,\alpha)$, and

$$|M(j\omega,\alpha)| = \left| \frac{\Gamma\, G_U(j\omega,\alpha)}{\gamma\Lambda_u\, G_D(j\omega,\alpha)} \right|. \tag{4.21}$$

The inequality in Eq. (4.20) defines an "upper" bound on the closed loop transfer function magnitude, i.e., $\left|\frac{L(j\omega,\alpha)}{1+L(j\omega,\alpha)}\right|$, for any given frequency. This upper amplitude bound corresponds to an M-circle on the Nichols chart with magnitude of $|M(j\omega_k,\alpha_i)|$. Therefore, inequality in Eq. (4.20) can be satisfied when $|L(j\omega_k,\alpha_i)|$ is not contained within the M-circle with magnitude of $|M(j\omega_k,\alpha_i)|$. Based on the Eq. (4.21), these upper bounds are function of different parameters such as frequency, disturbance size, and system parameter α_i.

It is to be noted that since Λ_u is a function of the closed loop transfer function, i.e., $T_u(s)$, it cannot be determined prior to the controller design. For the sake of the design

process, Λ_u will be embedded in to γ and it can be set to be equal to one (i.e., $\Lambda_u = 1$ in Eq. (4.21)).

Shown in Figure 4-2 is an example of the upper bound at a given $\omega = \omega_k$ and $\alpha = \alpha_i$. If $|L(j\omega_k, \alpha_i)|$ falls in the area below the upper bound (shown with down-ward arrows in Figure 4-2), then the actuator effort constraint, in Eq. (4.9) is satisfied for $\omega = \omega_k$ and $\alpha = \alpha_i$.

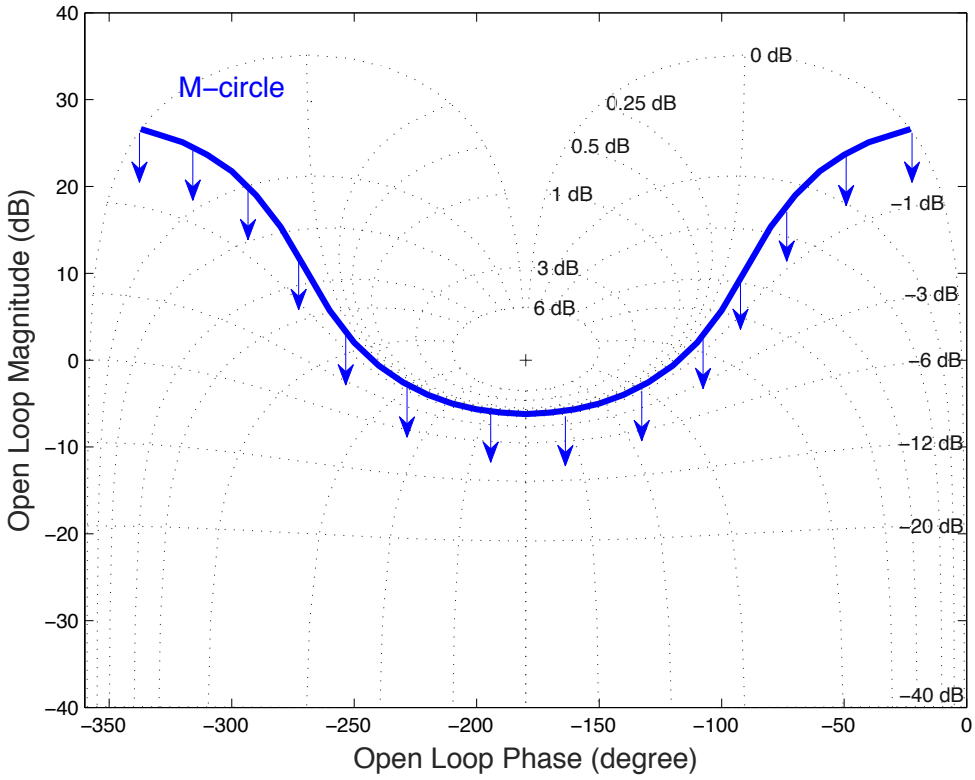

Figure 4-2 Example of an Upper Amplitude Bound.

4.3.2 Developing Lower Bounds from the Constraints on the Output Performance

With the similar approach, the lower amplitude bounds can be obtained from the output performance constraints. To develop the lower amplitude bounds, consider the

transfer function in Eq. (4.10). Similar to $T_u(s,\alpha)$, since $G_u(s,\alpha)$ and $G_D(s,\alpha)$ are minimum phase and stable, impulse response condition for $T_y(s,\alpha)$ is valid and therefore the Theorem in previous section is applicable. Using the Lemma in previous section, the following can be concluded [65, 68]

$$|y(t)| \leq \gamma \Lambda_y \left\| T_y(j\omega) \right\|_\infty, \tag{4.22}$$

where Λ_y is a scaling constant justifying the time to frequency domain transformation and is a function of the closed loop transfer function $T_y(s)$, and $\left\| T_y(j\omega) \right\|_\infty$ is the frequency domain H_∞ norm of $T_y(s)$,

$$\left\| T_y(j\omega) \right\|_\infty = \left\| \frac{G_D(j\omega,\alpha)}{1 + G_C(sj\omega) G_U(j\omega,\alpha)} \right\|_\infty . \tag{4.23}$$

Next step, if the following inequality holds,

$$\gamma \left| \frac{G_D(j\omega,\alpha)}{1 + G_C(j\omega) G_U(j\omega,\alpha)} \right| \leq \beta \quad \forall\omega \ \& \alpha \in \Omega, \tag{4.24}$$

then Eq. (4.8) is satisfied. Consider the rearrangement in Eq. (4.24) as

$$|1 + L(j\omega,\alpha)| \geq |m(j\omega,\alpha)| \quad \forall\omega \ \& \alpha \in \Omega, \tag{4.25}$$

where

$$|m(j\omega,\alpha)| = \left| \frac{\gamma \Lambda_y \, G_D(j\omega,\alpha)}{\beta} \right|. \tag{4.26}$$

An alternative form of Eq. (4.25) is

$$\left|\frac{l(j\omega,\alpha)}{1+l(j\omega,\alpha)}\right| \leq \frac{1}{|m(j\omega,\alpha)|} \quad \forall\omega \ \& \ \alpha \in \Omega, \tag{4.27}$$

where $l(j\omega,\alpha) = \frac{1}{L(j\omega,\alpha)}$.

The inequality in Eq. (4.27) defines an upper bound on the inverted closed loop transfer function magnitude, i.e., $\left|\frac{l(j\omega,\alpha)}{1+l(j\omega,\alpha)}\right|$, for any given frequency. This upper amplitude bound corresponds to an M-circle on the Nichols chart with magnitude of $\frac{1}{|m(j\omega_k,\alpha_i)|}$. Since $l(j\omega,\alpha) = \frac{1}{L(j\omega,\alpha)}$, inverting this M-circle on the Nichols chart creates a "lower" bound on the closed loop transfer function magnitude, i.e., $\left|\frac{L(j\omega,\alpha)}{1+L(j\omega,\alpha)}\right|$, for any given frequency. Therefore, inequality in Eq. (4.27) can be satisfied when $|L(j\omega_k,\alpha_i)|$ is not contained within the *inverted* M-circle of magnitude $\frac{1}{|m(j\omega_k,\alpha_i)|}$. Based on the Eq. (4.26), these lower bounds are function of different parameters such as frequency, disturbance size, and system parameter α_i.

It is to be noted that since Λ_y is a function of the closed loop transfer function, i.e., $T_y(s)$, it cannot be determined prior to the controller design. For the sake of the design process, Λ_y will be embedded in to γ and it can be set to be equal to one (i.e., $\Lambda_y = 1$ in Eq. (4.26)).

Shown in Figure 4-3 is an example of the lower bound at a given $\omega = \omega_k$ and $\alpha = \alpha_i$. If $|L(j\omega_k,\alpha_i)|$ falls in the area above the lower bound (shown with upward arrows in

Figure 4-3), then the output performance constraint, as in Eq. (4.8) is satisfied for $\omega = \omega_k$ and $\alpha = \alpha_i$.

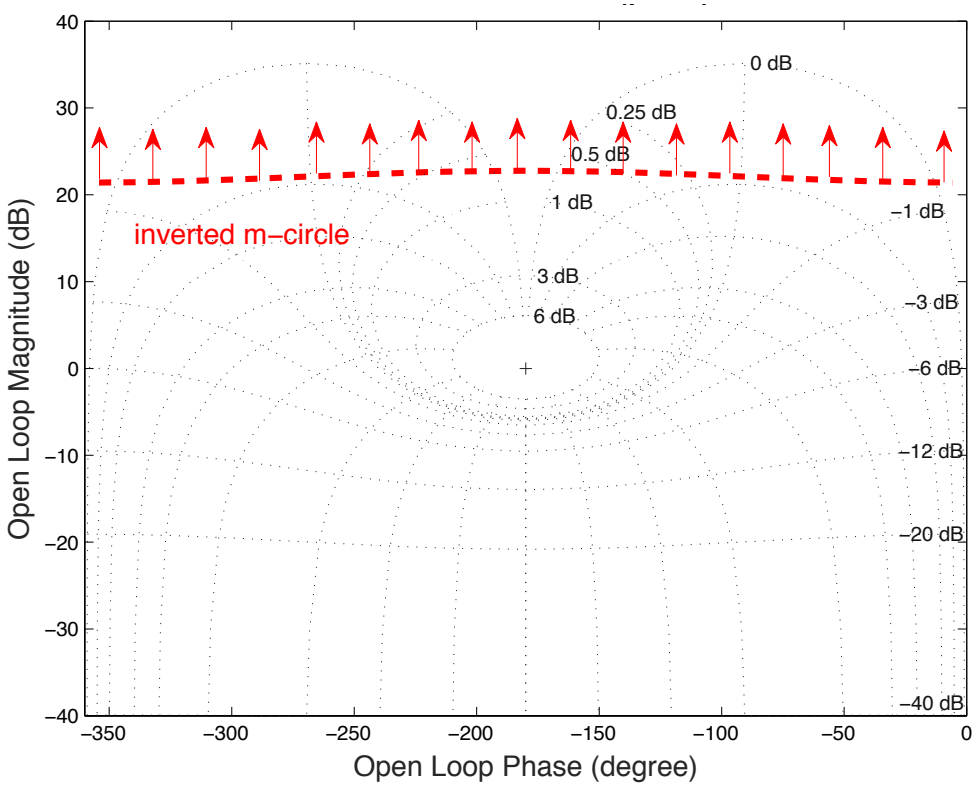

Figure 4-3 Example of a Lower Amplitude Bound.

4.3.3 Developing Acceptable Design Regions

The upper and lower amplitude bounds defined is Eqs. (4.21) and (4.26) develop an acceptable design region for the frequency response of the open loop transfer function. This acceptable design region can be obtained by considering the intersection of areas shown in Figure 4-2 and Figure 4-3, as shown with the hatched areas in Figure 4-4.

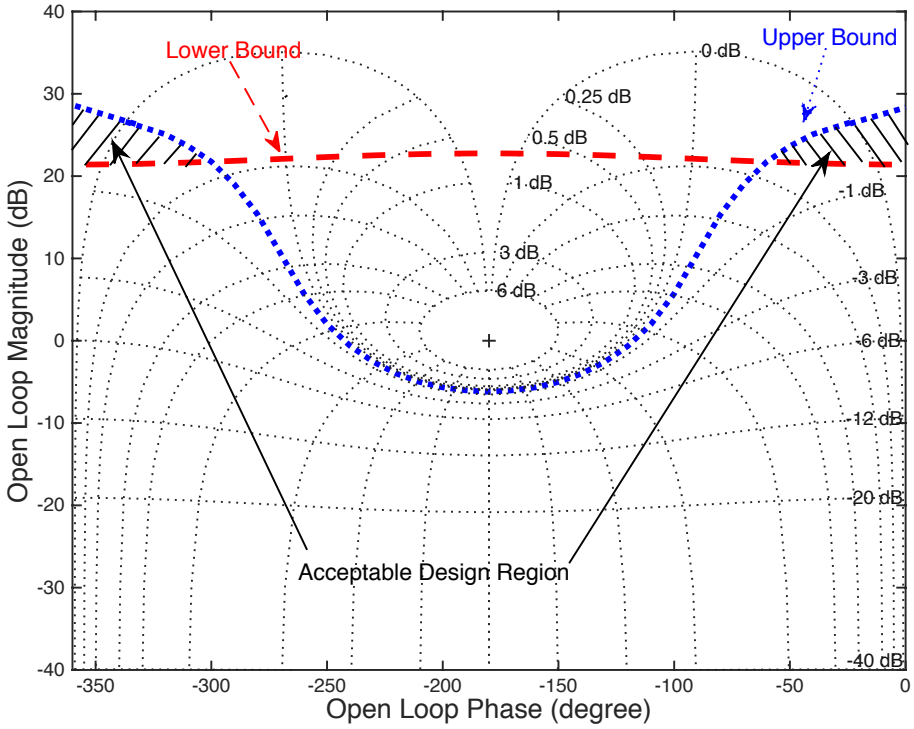

Figure 4-4 Example of the Acceptable Design Region.

Through the controller design process, to meet the performance requirements in Eqs. (4.8) and (4.9), the frequency response of $L(s)$ must be contained in this "safe" design region. The gain and phase characteristics of the open loop transfer function in this design region are confined by Eqs. (4.20) and (4.25).

Remark: In the case on an uncertain system, the upper and lower amplitude bounds must be determined $\forall \alpha \in \Omega$, at each particular frequency, i.e., $\omega = \omega_k$. These amplitude bounds are used to form "composite" upper and lower amplitude bounds on the nominal transfer function, $L_0(j\omega_k) = G_C(j\omega_k)G_{U_0}(j\omega_k)$, where $G_{U_0}(j\omega_k)$ is the nominal plant transfer function, i.e., $G_{U_0}(j\omega_k) = G_U(j\omega_k, \alpha = \alpha_0)$. The acceptable design region at each frequency will also be developed based on the composite bounds. To satisfy the

performance requirements in Eqs. (4.8) and (4.9), the frequency response of $L_0(s)$ must be contained in the composite acceptable design region [68].

4.3.4 Performance Level Prediction

To obtain the acceptable design region for $L(s)$, as described in the previous section, Eqs. (4.21) and (4.26) must be used for $\omega = [0, \infty)$. For a given system dynamics, i.e., known $G_U(s)$ and $G_D(s)$, to fully define the lower and upper amplitude bounds, the size of the step disturbance, γ must be determined prior to controller design. In this section, a method is presented that allows the designer to predict the allowable size of the step disturbance prior to the linear controller design.

For any given frequency, an increase in the size of the step disturbance yields to a smaller acceptable design region. The inverse relationship between disturbance size and the size of the design region can be utilized to predict the allowable size of the step disturbance. For this, a value for the phase angle of the point at which the upper and lower bounds intersect will be chosen [68, 69]. This choice imposes special gain and phase conditions on the open loop transfer function such that a linear controller is achievable.

In [69], it is assumed that the phase is $\varphi = 0°$ at the intersection point of the lower and upper amplitude bounds. This leads to a very difficult gain and phase conditions that usually cannot be met by a linear controller. Therefore, the predicted allowable disturbance size will not be achievable by a linear controller. In [68], on the other hand, the phase at the intersection point is chosen as $\varphi = -90°$, that results in a $-20\,\frac{dB}{dec}$ rate of

change for the amplitude of the open loop transfer function at the intersection. Given $\varphi = -90°$ for the phase at the intersection point and using Eqs. (4.21) and (4.26), the allowable disturbance step size can be determined. It is to be noted that the predicted level of disturbance step size, γ^* is a function of frequency, thereby defined as

$$\gamma^* = \min\{\gamma\} \quad \forall\omega \in [0, \infty) \,\&\, \alpha \in \Omega. \tag{4.28}$$

The phasor representation of the open loop transfer function is

$$L(j\omega) = |L(j\omega)|e^{j\measuredangle L(j\omega)}. \tag{4.29}$$

For $\varphi = -90°$ and using Euler's formula in Eq. (4.29), at the intersection point the following can be written

$$L(j\omega) = -j|L(j\omega)|. \tag{4.30}$$

Substituting Eq. (4.30) into Eqs. (4.20) and (4.25) yields

$$\frac{|L(j\omega)|^2}{1 + |L(j\omega)|^2} \leq |M(j\omega)|^2 \tag{4.31}$$

and

$$|L(j\omega)|^2 \geq |m(j\omega)|^2 - 1. \tag{4.32}$$

Using Eqs. (4.21) and (4.26) and after math simplifications, Eqs. (4.31) and (4.32) can be written as

$$|L(j\omega)|^2 \leq \frac{\Gamma^2|G_U(j\omega)|^2}{\gamma^2|G_D(j\omega)|^2 - \Gamma^2|G_U(j\omega)|^2} \tag{4.33}$$

and

$$|L(j\omega)|^2 \geq \frac{\gamma^2|G_D(j\omega)|^2 - \beta^2}{\beta^2}. \tag{4.34}$$

Considering the magnitude of the open loop transfer function at the intersection point in Eqs. (4.33) and (4.34), equating the right hand side of the inequalities in Eqs. (4.33) and (4.34) yields

$$\gamma = \frac{\sqrt{\Gamma^2|G_U(j\omega)|^2 + \beta^2}}{|G_D(j\omega)|}. \tag{4.35}$$

Therefore, the predicted level of the disturbance step size that can be achieved via a linear controller, i.e., γ^*, can be obtained from Eq. (4.28) and using Eq. (4.35).

4.4. Synthesis of Linear Regulating Controllers

To design a linear controller through the H_∞controller design approach for the system shown in Figure 4-1, consider the performance constraint defined by

$$\left\| W_1(j\omega)\frac{1}{1 + L(j\omega)} \right\|_\infty < 1, \tag{4.36}$$

and the robust stability constraint defined by

$$\left\| W_2(j\omega) \frac{L(j\omega)}{1 + L(j\omega)} \right\|_\infty < 1, \tag{4.37}$$

where $W_1(s)$ and $W_2(s)$ are the performance weights, $\|.\|_\infty$ is the frequency domain H_∞ norm, and $L(s)$ is the open loop transfer function, i.e., $L(s) = G_C(s)G_U(s)$ [65, 70].

Equations (4.36) and (4.37) collectively construct the mixed sensitivity H_∞ optimization problem. In other words, the necessary and sufficient condition for the robust performance of the regulating system shown in Figure 4-1 can be formulated as [71]

$$\left\| \left| W_1(j\omega) \frac{1}{1 + L(j\omega)} \right| + \left| W_2(j\omega) \frac{L(j\omega)}{1 + L(j\omega)} \right| \right\|_\infty < 1. \tag{4.38}$$

There are different methods for defining the performance weights, $W_1(s)$ and $W_2(s)$ [71]. In [65], a method for selection of these performance weights is proposed that ensures enforcing Eqs. (4.8) and (4.9) by a H_∞controller synthesis for a system shown in Figure 4-1. For a system without uncertainty, these performance weights are [65]

$$W_1(s) = \frac{\gamma\, G_D(s)}{\beta} \tag{4.39}$$

and

$$W_2(s) = \frac{\gamma\, G_D(s)}{\Gamma\, G_U(s)}. \tag{4.40}$$

Comparing Eqs. (4.39) and (4.40) with Eqs. (4.26) and (4.21), respectively, these performance weights functions can be represented by the upper and lower magnitude bounds developed in earlier sections, i.e., $W_1(s) = m$ and $W_2(s) = \frac{1}{M}$.

Using Eqs. (4.39) and (4.40), a linear controller can be designed by minimizing Eq. (4.38) through a H_∞controller synthesis. The resulting controller, $G_{C1}(s)$, maintains the closed loop system performance requirements in Eqs. (4.8) and (4.9) for the predicted level of disturbance step size $\gamma = \gamma^*$.

4.4.1 Maximizing the Disturbance Size

To improve the closed loop performance beyond the predicted level of disturbance step size, γ^*, the problem of the maximization of the allowable step disturbance via a linear controller through the H_∞controller synthesis is considered. For this, the trade-off between the performance constraints and the largest allowable disturbance step size must be defined. To formulates this trade-off, the inequality in Eq. (4.38) can be modified as

$$\left\| \left| k_1 W_1(j\omega) \frac{1}{1 + L(j\omega)} \right| + \left| k_2 \, W_2(j\omega) \frac{L(j\omega)}{1 + L(j\omega)} \right| \right\|_\infty < 1, \tag{4.41}$$

where k_1 and k_2 are positive scalars.

To minimize Eq. (4.41), first, convex design sets must be defined for k_1 and k_2. Then, using Eqs. (4.39) and (4.40) and by selecting values of k_1 and k_2, time domain tolerances in Eqs. (4.8) and (4.9) can be enforced in the frequency domain via a controller. For the case of a linear controller, the actual allowable disturbance step size,

γ_a, for the given values of k_1 and k_2 can be obtained by scaling the closed loop responses due to a unit step disturbance, as [65]

$$\gamma_a = \min\left\{\frac{\beta}{\|y_1(t)\|_\infty}, \frac{\Gamma}{\|u_1(t)\|_\infty}\right\}, \tag{4.42}$$

where $y_1(t)$ and $u_1(t)$ are the system output and controlled output due to a unit disturbance step size.

Next, to find the maximum allowable disturbance step size via a linear controller, $\widetilde{\gamma^*}$, Eq. (4.41) must be minimized by globally searching over all possible values of k_1 and k_2. In other words, for each pair of k_1 and k_2, a linear controller will be designed through a H_∞controller synthesis by minimizing Eq. (4.41). Then, γ_a will be obtained from Eq. (4.42), and finally $\widetilde{\gamma^*}$ will be defined as

$$\widetilde{\gamma^*} = \max\{\gamma_a\} \quad \forall k_1, k_2. \tag{4.43}$$

It is to be noted that an initial guess for the disturbance step size for starting the optimization of Eq. (4.41) is needed. The predicted level of the disturbance step size, γ^*, obtained using Eqs. (4.28) and (4.35) can serve for this initial guess. In fact, γ^* is considered as the lower bound for the allowable disturbance step size via a linear controller, i.e., $\gamma \geq \gamma^*$.

Let the linear controller for $\widetilde{\gamma^*}$ be $G_{C2}(s)$, that is designed through H_∞ controller synthesis approach. Also, let the values of k_1 and k_2 corresponding to $\widetilde{\gamma^*}$ be denoted by $\widetilde{k_1}$ and $\widetilde{k_2}$. By implementing $G_{C2}(s)$ in the feedback loop, the closed loop is able to

maintain system performance constraints in Eqs. (4.8) and (4.9) for the disturbance step size of $\widetilde{\gamma^*}$.

For a known dynamic system, $\widetilde{k_1}$ and $\widetilde{k_2}$ will be found in an iterative process. This means, there is no analytical formulation to estimate $\widetilde{k_1}$ and $\widetilde{k_2}$ prior to the controller design, and they must be obtained in a case-by-case basis. In general, the local maximum values of γ_a can happen in multiple directions of the gradients of k_1 and k_2. In fact, in some cases, the solutions of $\widetilde{k_1}$ and $\widetilde{k_2}$ for a $\widetilde{\gamma^*}$ are not unique. Consequently, $\widetilde{\gamma^*}$ must also be obtained in a case-by-case basis by an iterative process.

4.5. Case Study

In this section, an illustrative example is utilized to demonstrate the procedure of designing linear controllers for a regulating system based on the formulation presented in this chapter. The objectives are (i.) to predict the allowable disturbance step size prior to controller design and (ii.) design a linear controller for the predicted level of disturbance size. For this, the idle speed control of a V-6 fuel injected engine is considered. The block diagram of the system can be considered as shown Figure 4-1. The plant and disturbance dynamics are described by [72]

$$G_U(s) = \frac{15.9(s+3)}{s^2 + 2.2s + 5.62} \tag{4.44}$$

and

$$G_D(s) = \frac{19.1(s+3)}{s^2 + 2.2s + 5.62}. \tag{4.45}$$

The system is subject to a step external disturbance torque with the magnitude of $|d(t)| = \gamma\ N.m$ delivered by onboard accessories, an output tolerance of $|y(t)| \leq 20\ rpm$, and a control effort constraint of $|u(t)| \leq 20°$ of spark advance.

4.5.1 Synthesizing a Linear Controller for $\gamma = \gamma^*$

For this example problem the performance constraints described in Eqs. (4.8) and (4.9) are $\Gamma = 20°$ and $\beta = 20\ rpm$. To obtain the predicted level of disturbance size achievable via a linear controller, the solution of Eq. (4.28) using Eq. (4.35) is considered. The graphical representation of Eq. (4.35) for this case study is shown in Figure 4-5.

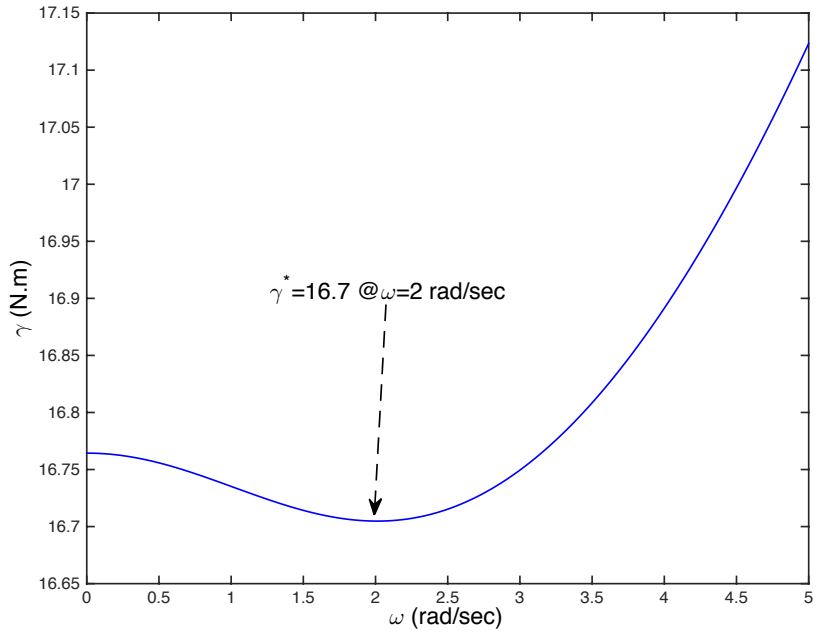

Figure 4-5 Prediction of the Level of Regulating Performance.

From Figure 4-5, the predicted level of disturbance size achievable via a linear controller is identified as $\gamma^* = 16.7\ N.m$, which is the minimum of γ for all frequencies. This predicted level of disturbance size guarantees the existence of a linear controller that can maintain the system performance constrains of $|y(t)| \leq 20\ rpm$ and $|u(t)| \leq 20°$. This level of step disturbance is in the vicinity of $\omega = 2\,\frac{rad}{sec}$. This yields in tightest acceptable design region for $\omega = 2\,\frac{rad}{sec}$ and it surrounding frequencies.

Next step is to design a linear controller for $\gamma = \gamma^*$. Using Eqs. (4.44) and (4.45) in Eqs. (4.39) and (4.40), the performance weights for H_∞ controller design for $\gamma = \gamma^*$ are

$$\mathrm{W}_1(s) = \left(\frac{16.7\times19.1}{20}\right)\frac{s+3}{\mathrm{s}^2 + 2.2s + 5.62} \tag{4.46}$$

and

$$\mathrm{W}_2(s) = \frac{16.7\times19.1}{20\times15.9}. \tag{4.47}$$

Due to the similar dynamics of plant and disturbance, the upper bound from Eq. (4.21) and $W_2(s)$ from Eq. (4.40) remain the same as frequency changes. However, the lower bound from Eq. (4.26) and $W_2(s)$ from Eq. (4.39) change by frequency.

Using the performance weights in Eqs. (4.46) and (4.47), a linear controller is designed for $\gamma = \gamma^*$ through H_∞ controller synthesis method. The resulting linear controller is [65]

$$G_{C1}(s) = \frac{0.9223(\frac{s}{1.334}+1)}{\left(\frac{s}{3}+1\right)\left(\frac{s}{500}+1\right)^2}. \tag{4.48}$$

With the controller in Eq. (4.48), the feedback system is capable of maintaining the performance specifications of $|y(t)| \leq 20\,rpm$ and $|u(t)| \leq 20°$ for the predicted level of step disturbance $\gamma^* = 16.7\,Nm$. Shown in Figure 4-6 is the closed loop output response and actuator effort. In this example problem, the time domain performance specifications are directly enforced in the frequency domain by use of the proposed performance weights through H_∞ controller synthesis.

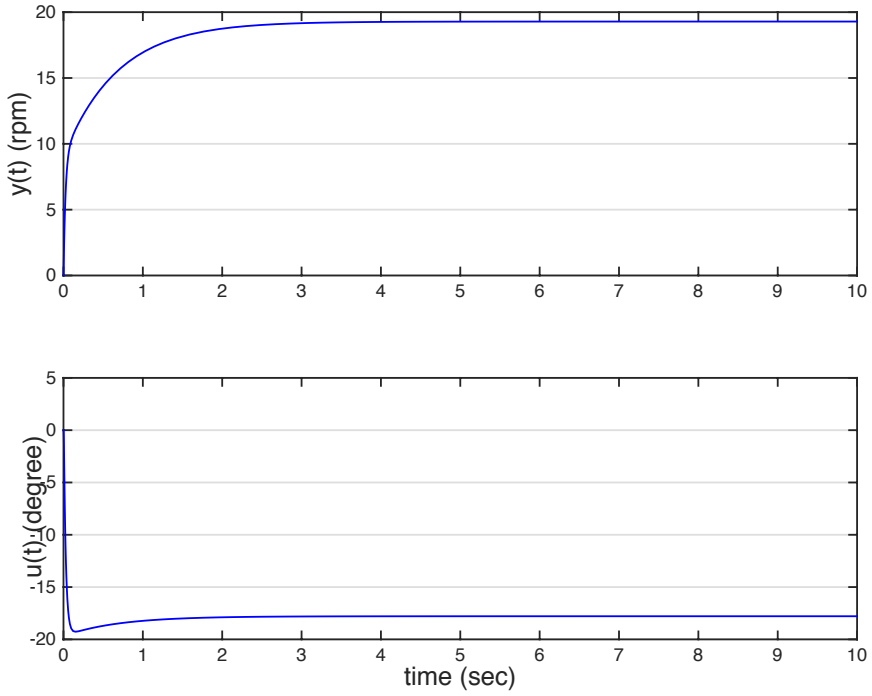

Figure 4-6 Closed Loop Responses for $\gamma = 16.7$.

4.5.2 Synthesizing a Linear Controller for $\gamma = \widetilde{\gamma^*}$

The minimization of the inequality in Eq. (4.41) is considered for the case study to obtain the maximum allowable disturbance step size via a linear controller, $\widetilde{\gamma^*}$, and design a linear controller, $G_{C2}(s)$, for this level of step disturbance. The performance weights obtained in Eqs. (4.46) and (4.47) are used in Eq. (4.41), that yields

$$\left\| \left| k_1 \frac{19.1\gamma\,(j\omega+3)}{20((j\omega)^2+2.2j\omega+5.62)} \frac{1}{1+L(j\omega)} \right| + \left| k_2 \frac{19.1\gamma}{15.9\times 20} \frac{L(j\omega)}{1+L(j\omega)} \right| \right\|_\infty < 1. \quad (4.49)$$

To start minimization of Eq. (4.49), $\gamma^* = 16.7\ N.m$ obtained in the previous section is considered as the initial guess. Convex design spaces for k_1 and k_2 are considered as $0 < k_1 \leq 1$ and $0 < k_2 \leq 10$. The selection of these design sets is based on the existence of a stabilizing linear controller. For this example, it was found that no stabilizing linear controller exists for $k_2 \geq 1.05$ and all value of k_1.

For each selected pair of k_1 and k_2, by minimizing Eq. (4.41), a linear controller is designed using H_∞ controller synthesis approach. Then, the corresponding value of γ_a is obtained using Eq. (4.42). Finally, using Eq. (4.43) $\widetilde{\gamma^*}$ is found. The resulting values from this iterative process are $\widetilde{\gamma^*} = 17.4\ N.m$, $\widetilde{k_1} = 0.5$, and $\widetilde{k_2} = 0.969$. Additionally, the designed linear controller from H_∞ synthesis is

$$G_{C2}(s) = \frac{0.9278\left(\frac{s}{1.66}+1\right)}{\left(\frac{s}{3.03}+1\right)\left(\frac{s}{1.53\,10^7}+1\right)}. \quad (4.50)$$

With the controller in Eq. (4.50), the feedback system is capable of maintaining the performance specifications of $|y(t)| \leq 20\,rpm$ and $|u(t)| \leq 20°$ the maximum allowable disturbance step size via a linear controller $\widetilde{\gamma^*} = 17.4\,N.m$. Shown in Figure 4-7 is the closed loop output response and actuator effort.

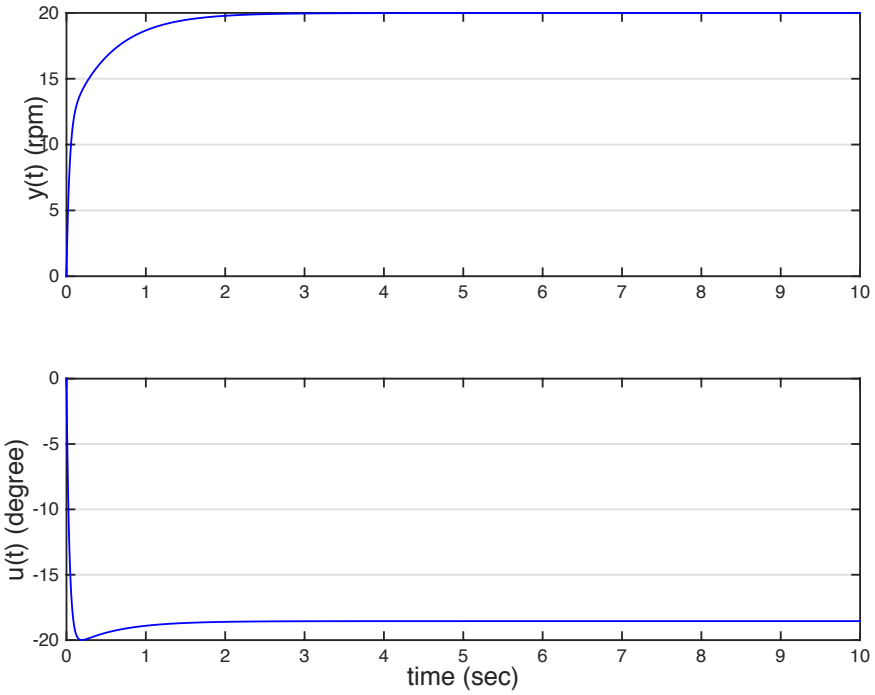

Figure 4-7 Closed Loop Responses for $\gamma = 17.4$.

4.6 Chapter Summary

Presented in this chapter is the formulation for the performance bounds development to create the acceptable design region for the linear control of linear regulating systems subject to time domain performance constraints. It is shown that the time domain specifications can be formulated as the frequency domain amplitude constraints on the open loop transfer function. A method for predicting the level of disturbance step size

achievable by a linear controller, γ^*, prior to the controller design is also presented. The method presented in this chapter, guarantees the existence of a linear controller for the predicted level of disturbance step size through H_∞ controller synthesis.

Additionally, a method of maximizing the disturbance size achievable by a linear controller is proposed. This is done by scaling the performance weights in the H_∞ controller synthesis. The maximum disturbance size achievable by a linear controller, $\widetilde{\gamma^*}$, will be obtained in an iterative process and the resulting linear controller will be synthesize via H_∞ controller design approach.

To illustrate the linear controller design techniques, the idle speed control of a V-6 fuel injected engine model subject to an external torque load disturbance is considered. For this case study, the predicted level of disturbance step size, γ^*, and the maximum disturbance size achievable by a linear controller, $\widetilde{\gamma^*}$, are found and the linear controllers are designed through H_∞ controller synthesis that maintains system performance specifications.

Chapter 5. Nonlinear Controller Synthesis for Regulating Systems using Inverse SIDF Approach

Presented in this chapter is a methodology to incorporate the nonlinearities in the formulation of QFT and thereby extend its application. More specifically, a nonlinear controller design methodology is developed that improves the closed loop performance of linear regulating systems subject to time domain constraints beyond what is achievable by a linear controller. The proposed nonlinear controllers are synthesized around a linear controller. The proposed methodology translates an increase (from what is achievable by the linear controller) in the disturbance step size to the frequency domain distortions and imposes required gain and phase distortions on the frequency response of the linear open loop transfer function. The performance bounds developed in Chapter 4 are used to define the gain and phase distortions (in the sense of SIDF) due to the nonlinearity, and the inverse SIDF algorithm developed in Chapter 3 is utilized to design an isolated explicit nonlinear controller that the imposed gain and phase distortions are representing.

5.1 Motivation for Nonlinear Control

From the developed acceptable design regions in Chapter 4, the gain and phase characteristics of the open loop transfer functions are restricted within the acceptable design regions. The size of the acceptable design regions is depended on frequency, ω and disturbance step size, γ. In particular, as the disturbance step size, γ, increases, the

allowable design region contracts. This inverse relationship is shown for an illustrative example in the gain/ phase plane in Figure 5-1 and the complex plane in Figure 5-2. Therefore, the corresponding allowable gain and phase characteristics of the open loop transfer function are further restricted as γ increases.

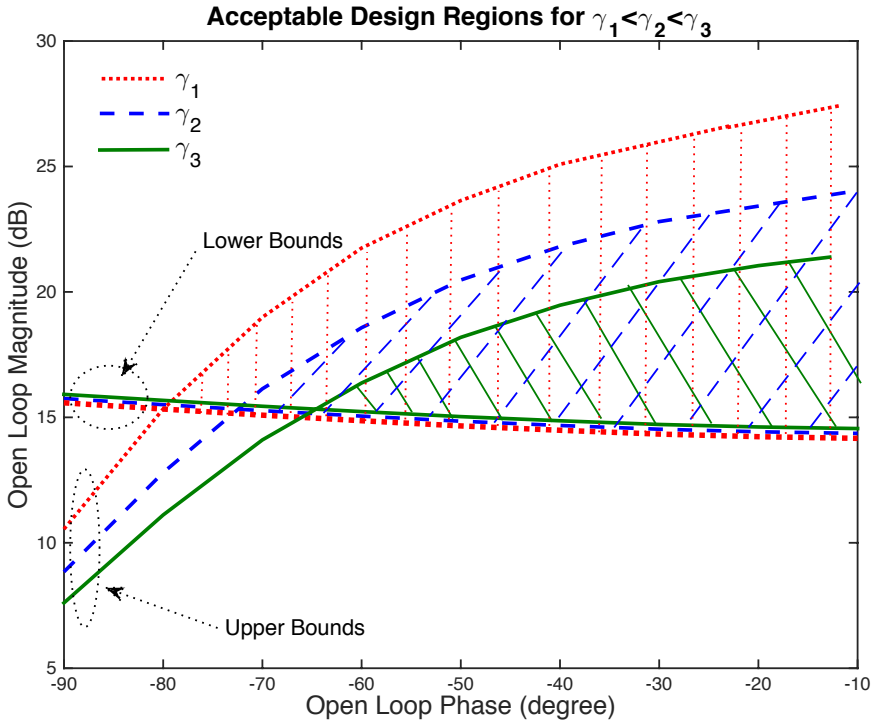

Figure 5-1 Acceptable Design Region Size vs. Disturbance Size: Gain/ Phase Plane.

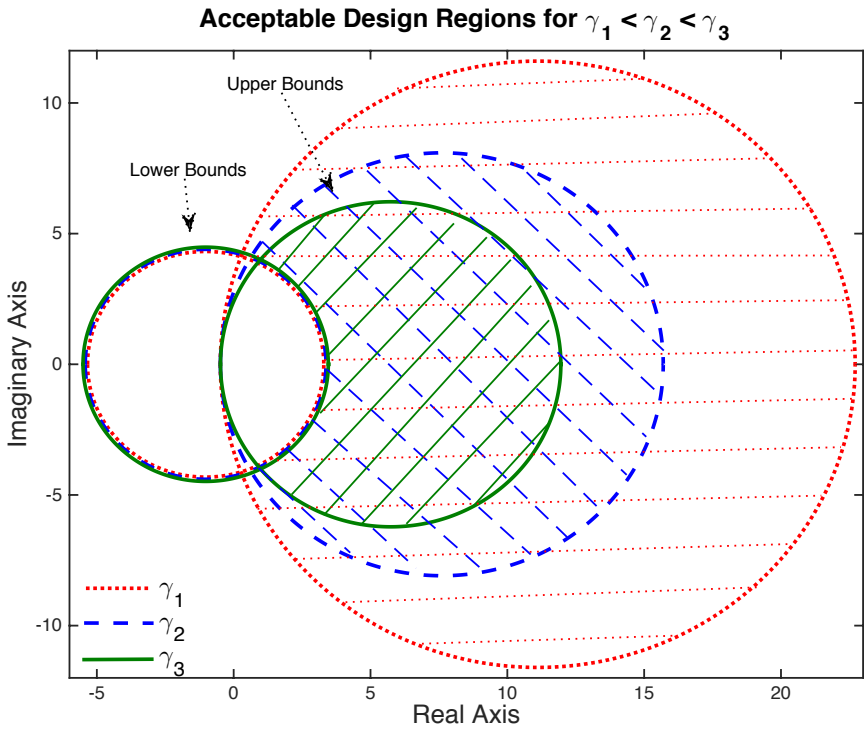

Figure 5-2 Acceptable Design Region Size vs. Disturbance Size: Complex Plane.

On the other hand, the gain and phase characteristics of a linear transfer function are confined by the so-called Bode gain/phase relationship. For a linear stable, minimum phase system, this relationship can be written as [73]

$$\measuredangle L(j\omega_i) = \frac{1}{\pi}\int_{-\infty}^{\infty} \frac{d(\ln|L(j\omega)|)}{d\left(\ln\frac{\omega}{\omega_i}\right)} \coth\left(\frac{\left|\ln\frac{\omega}{\omega_i}\right|}{2}\right) d\left(\ln\frac{\omega}{\omega_i}\right), \tag{5.1a}$$

or for a constant slope, it can be approximated as

$$\measuredangle L(j\omega_i) \cong 90° \times \frac{1}{20}\frac{d|L(j\omega_i)|}{d\omega}. \tag{5.1b}$$

Equation (5.1) implies that the phase characteristics of linear systems cannot be independently specified from their gain characteristics.

The coupling between the gain and phase characteristics of a linear system due to Bode gain/phase relationship and the inverse relationship between the acceptable design region size and γ, directly impose a limitation of the maximum allowable disturbance step size, γ, for linear control systems. In general, increasing the allowable disturbance step size imposes frequency characteristics that are often very difficult or even impossible to meet with linear controller. In particular, an increase in the disturbance step size, while holding time domain performance constraints constant, requires a phase lead while simultaneously requiring a decrease in gain. A linear controller comprised of complex poles and zeros can achieve these frequency characteristics. However, these gain and phase modifications occur over a very narrow frequency band. Consequently, the design region at surrounding frequencies may require additional compensation, which results in increasing controller order [1].

There are many cases in which the frequency domain specifications imposed by the time domain performance requirements violate the Bode gain/phase relationship. In these cases, a linear controller does not exist and nonlinear controllers are desirable.

5.2 Background

Nonlinear controllers, in essence, are not confined by the Bode gain/phase relationship. This results in more flexibility in designing controllers for higher closed loop performance requirements. Presented in this chapter is a new methodology to design

nonlinear controllers for linear regulating systems to improve their closed loop performance by utilizing inverse SIDF algorithm. First, a brief review of the previous developed methodologies is presented.

Different methods of designing nonlinear controllers for linear regulating systems to improve their closed loop performance have been previously proposed. In [19], a controller design technique is proposed that utilizes actuator saturation to meet output performance specification for linear regulating systems. The proposed nonlinear controller saturates for large disturbances while it operates linearly for smaller disturbance sizes. In that case, the gain distortions (in the sense of SIDF) of the nonlinear element are obtained by using analytical SIDF formulation of the nonlinear element. This could be done since the structure of the nonlinearity (saturation element) was preconceived.

A Volterra series representation is used in [1, 8, 17, 18] to design a nonlinear controller in the frequency domain for regulating systems subject to time domain constraints. The use of Volterra series limits the class of nonlinear controllers to the continuous functions. Their proposed strategy involves two steps: (i.) designing a linear controller that balances the trade-off between output performance and required actuation, and (ii.) augmenting the linear controller with an odd cubic polynomial. For that, the SIDF calculation is automated by the use of Volterra series. This enables imposing necessary gain and phase distortions to the linear system to assure that time domain constraints are satisfied. The coefficients of the nonlinear term are calibrated such that the gain and phase distortions meet the frequency domain tolerances.

Developed in this chapter is a novel nonlinear controller design methodology. The controller design is conducted in frequency domain. The unique aspect of this work is that the structure of the nonlinear controller is not known *a priori* and will be identified using the inverse SIDF algorithm developed in Chapter 3. Another advantage of this methodology is that the nonlinear controller is not necessarily continuous or single valued. This extends the utility of the proposed methodology by including the applications of hysteresis nonlinear controllers in the feedback systems. The required gain and phase distortions due to the nonlinearity will be obtained by utilizing the performance bounds developed in Chapter 4 to impose required gain and phase distortions on the linear open loop frequency response to assure that the frequency domain constraints are satisfied.

5.3 Synthesis of Nonlinear Controllers

Consider the linear regulating system shown in Figure 5-3, with the closed loop performance constraints as

$$|y(t)| \leq \beta \text{ and } |u(t)| \leq \Gamma \quad \forall t > 0. \tag{5.2}$$

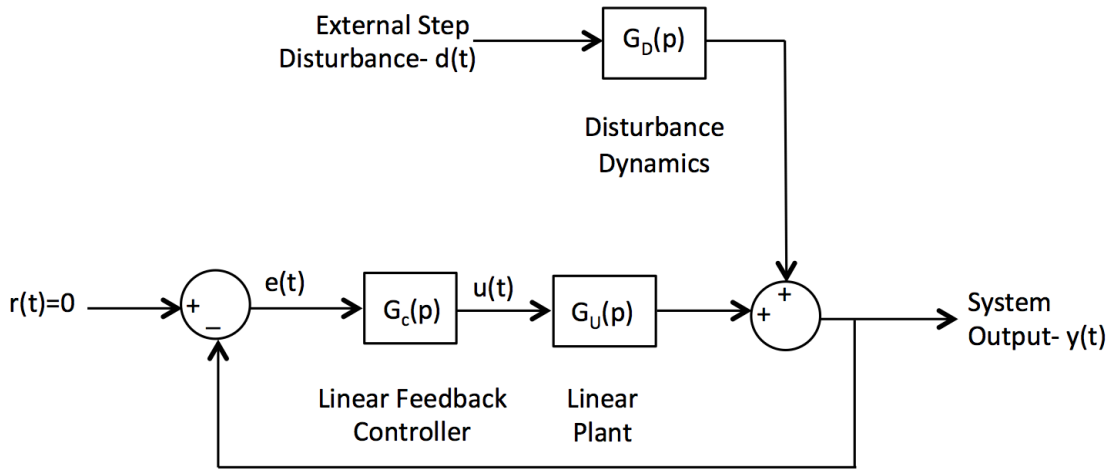

Figure 5-3 Block Diagram of a Regulating System.

In Chapter 4, it was shown that the time domain constraints in Eq. (5.2) can be translated to the frequency domain characteristics of the open loop transfer function as

$$\left|\frac{L(j\omega)}{1+L(j\omega)}\right| \leq \left|\frac{\Gamma\, G_U(j\omega)}{\gamma\, G_D(j\omega)}\right| \quad \forall\omega \tag{5.3}$$

and

$$|1+L(j\omega)| \geq \left|\frac{\gamma\, G_D(j\omega)}{\beta}\right| \quad \forall\omega. \tag{5.4}$$

Let assume that for the system shown in Figure 5-3, a linear controller, $G_C(s)$, is designed through H_∞ controller synthesis approach in Chapter 4, for a given level of disturbance step size γ_1. Therefore, the closed loop system maintains the time domain constraints in Eq. (5.2) for the level of step disturbance of γ_1. The resulting linear open loop transfer function is $L(s) = G_C(s)G_U(s)$. In other words, the frequency response of the open loop transfer function will be inside the acceptable design regions for γ_1.

Now, consider an increase in the disturbance step size from γ_1 to $\gamma > \gamma_1$. For this increased level of disturbance step size the frequency response of $L(s)$ falls outside the acceptable design regions of the increased level of γ for some discrete sets of frequencies. Consequently, the time domain constraints in Eq. (5.2) will be violated at these discrete sets of frequencies. This means that the linear controller $G_C(s)$ is not able to maintain the performance constraints for $\gamma > \gamma_1$. A methodology is proposed that synthesize a nonlinear controller that imposes required gain and phase distortions to the frequency response of $L(s)$ at the discrete sets of frequencies to move them inside their corresponding acceptable design regions. The linear controller, $G_C(s)$ designed for γ_1 will be augmented by the designed nonlinear controller and the resulting nonlinear feedback system will maintain the system performance requirements in Eq. (5.2) for $\gamma > \gamma_1$.

5.3.1 Defining the Discrete Sets of Frequencies

Using the inequality in Eq. (5.3), the set of frequencies in which the frequency response of the open loop transfer function violates the upper bound constraint for $\gamma > \gamma_1$ is defined as

$$\Psi = \left\{ \omega \left| \left| \frac{L(j\omega)}{1 + L(j\omega)} \right| > \left| \frac{\Gamma\, G_U(j\omega)}{\gamma\, G_D(j\omega)} \right| \right. \right\}. \tag{5.5}$$

The number of elements in Ψ is κ. Similarly, using the inequality in Eq. (5.4), the set of frequencies in which the frequency response of the open loop transfer function violates the lower bound constraint for $\gamma > \gamma_1$ is defined as

$$\Theta = \left\{ \omega \;\middle|\; |1 + L(j\omega)| < \left| \frac{\gamma\, G_D(j\omega)}{\beta} \right| \right\}. \tag{5.6}$$

The number of elements in Θ is ζ. The nonlinear control law will be defined for the frequency sets defined in inequalities in Eqs. (5.5) and (5.6).

5.3.2 Defining Nonlinear Control Laws

The proposed nonlinear controller synthesis methodology augments the linear controller, $G_C(s)$, with a nonlinear controller, $\mathcal{N}$, such that the frequency response of the modified open loop transfer function is contained in the acceptable design regions for $\gamma > \gamma_1$. Therefore, the modified open loop system can be defined as

$$\hat{L}(A, j\omega) = N(A) G_C(j\omega) G_U(j\omega), \tag{5.7}$$

where $N(A)$ is the gain and phase distortions due to the explicit nonlinear controller in the sense of SIDF, i.e., $N(A) = \rho_N e^{j\theta_N}$, and A is the amplitude of the input signal to the nonlinearity in the feedback loop. In other words, the nonlinear controller move the out of bound points (i.e., $\omega \in \Psi \cup \Theta$) into their corresponding acceptable design regions, and operates linearly when ω does not belong to Ψ or Θ. This can be formulated as

$$\text{for } \omega \in \Psi\text{: } \mathrm{K_i} = \left\{ N(A) \;\middle|\; \left| \frac{\hat{L}(A, j\omega_i)}{1 + \hat{L}(jA, \omega_i)} \right| = \left| \frac{\Gamma\, G_U(j\omega_i)}{\gamma\, G_D(j\omega_i)} \right| \right\}, \tag{5.8}$$

where $i = 1{:}\,\kappa$, and

$$\text{for } \omega \in \Theta\text{: } \mathrm{Z_i} = \left\{ N(A) \left| \left|1 + \hat{L}(A, j\omega_i)\right| = \left|\frac{\gamma\, G_D(j\omega_i)}{\beta}\right| \right.\right\}, \tag{5.9}$$

where $i = 1{:}\,\zeta$.

Since the gain and phase distortions of the nonlinear controller (in the sense of SIDF) are dependent on the amplitude of the input signal to the nonlinearity in the feedback loop, they cannot be directly obtained from gain/phase or complex planes information related to $L(j\omega)$. In other words, by considering the effect of the amplitude of the input signal to the nonlinearity on the SIDF gain and phase distortions, from Eqs. (5.8) and (5.9), first $\hat{L}(A, j\omega)$ must be obtained from the frequency response of $L(j\omega)$ and then $N(A)$ must be extracted from $\hat{L}(A, j\omega)$. In General, there are three options to impose required gain and phase distortions on $L(j\omega)$ to obtain $\hat{L}(A, j\omega)$. In the following, these options are discussed.

5.3.2.1 Option 1: Imposing Both Gain and Phase Distortions

The first option to consider is imposing both gain and phase distortions to bring the out of bound points in to their acceptable design regions. This can be better explained in the gain/phase plane. For this, consider an arbitrary example shown in Figure 5-4. In this example the frequency response of the open loop transfer function (shown as a point labeled by 0) is outside the acceptable design region. Defining control law for the first option means to impose enough gain and phase distortions to relocate the point shown in Figure 5-4 from location labeled as 0 (for $L(j\omega)$) to the location labeled as 1 (for $\hat{L}(A, j\omega)$).

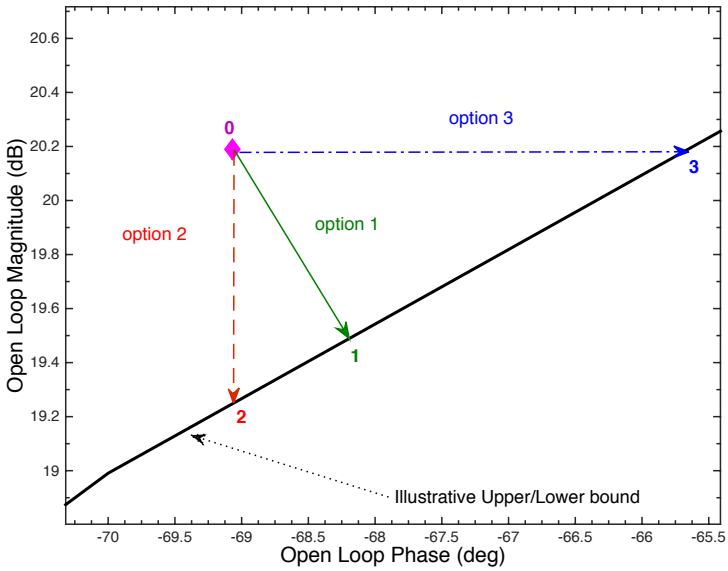

Figure 5-4 Illustration of Different Options to Define Nonlinear Controller Law.

5.3.2.2 Option 2: Imposing Only Gain Distortions

The second option is imposing only gain distortions (i.e., holding the phase characteristics constant) to bring the out of bound points in to the acceptable design regions. Defining control law for the second option means to impose enough gain distortions to relocate the point shown in Figure 5-4 from location labeled as 0 (for $L(j\omega)$) to the location labeled as 2 (for $\hat{L}(A, j\omega)$).

5.3.2.3 Option 3: Imposing Only Phase Distortions

The third option is imposing only phase distortions (i.e., holding the gain characteristics constant) to bring the out of bound points in to the acceptable design regions. Defining control law for the third option means to impose enough phase

distortions to relocate the point shown in Figure 5-4 from location labeled as 0 (for $L(j\omega)$) to the location labeled as 3 (for $\hat{L}(A, j\omega)$).

5.3.2.4 Discussion on Different Options

Comparing these three different options shown in Figure 5-4, in this specific illustrative example, the first option results in the minimum control action and the third option results in the largest control action among all three options, which is not desirable. In general implementing nonlinear control laws described in the second option are easier, because they are associated with achieving only gain distortions (i.e., single-valued nonlinearities). On the other hand, there are cases in which defining the control law in one or more of the options described above are not possible. One example is shown in Figure 5-5.

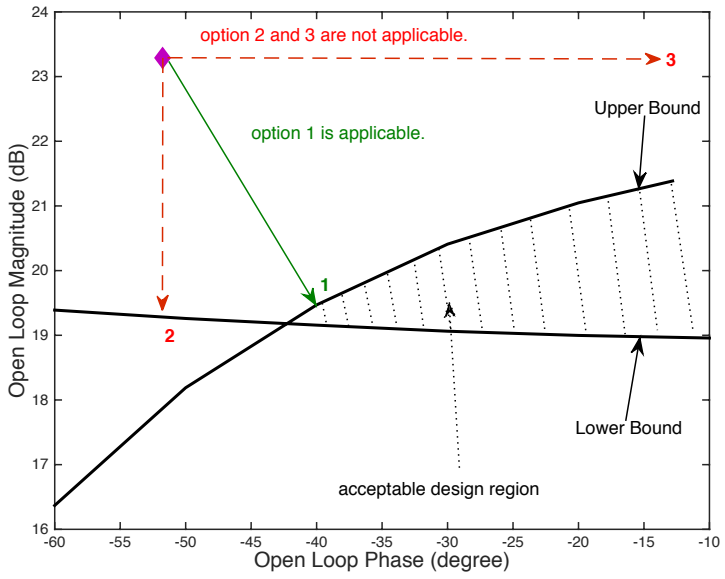

Figure 5-5 Special Case for Designing Nonlinear Control Law.

In this example the frequency response of the open loop transfer function is out of bound by violating the upper amplitude bound constraint. From Figure 5-5, the out of bound point cannot be relocated into the acceptable design region by the second or third options. This means, the first option is the only way to define the nonlinear control law. Therefore, the selection between these three options must be done in a case-by-case basis.

The basis for the method proposed in this chapter is the classical QFT and loop shaping methodologies that allows frequency-by-frequency controller synthesis. Therefore, in the proposed nonlinear controller synthesis methodology, the control action choice can change from one frequency range to another.

5.3.3 Isolation of the Nonlinearity

Next step is to isolate the gain and phase distortions due to the nonlinearity, i.e., $N(A)$, from the obtained gain and phase distortions for $\hat{L}(A, j\omega)$. This must be done in the feedback loop to account for the dependency of the amplitude of the input signal to the nonlinearity, A, and SIDF gain and phase distortions of the nonlinear controller, $N(A)$. For this, a method of calculating A in the feedback loop is proposed that is outlined in the following section.

5.3.3.1 Calculations of the Amplitude of the Input Signal to the Nonlinearity in the Feedback Loop

One important challenge is to calculate the amplitude of the input signal to the nonlinearity in the feedback loop. As discussed in Chapter 2, the gain and phase distortions of a nonlinear function (in the notion of the SIDF) is dependent on the input

signal amplitude. If the structure of the nonlinear element was known, the input signal amplitude could be determined by relating it to the characteristics of the nonlinear element via its SIDF analytical representation [19]. In the current application, however, the structure of the nonlinearity is not known and will be determined by utilizing the inverse SIDF algorithm developed in Chapter 3. Proposed in this section, is the method of calculating the input signal amplitude that is employed in the proposed methodology.

The formulation presented in this section, is for a general block diagram shown in Figure 5-6. This derivation parallels the derivation of the amplitude of the input signal to a nonlinear element in the closed loop system in [9].

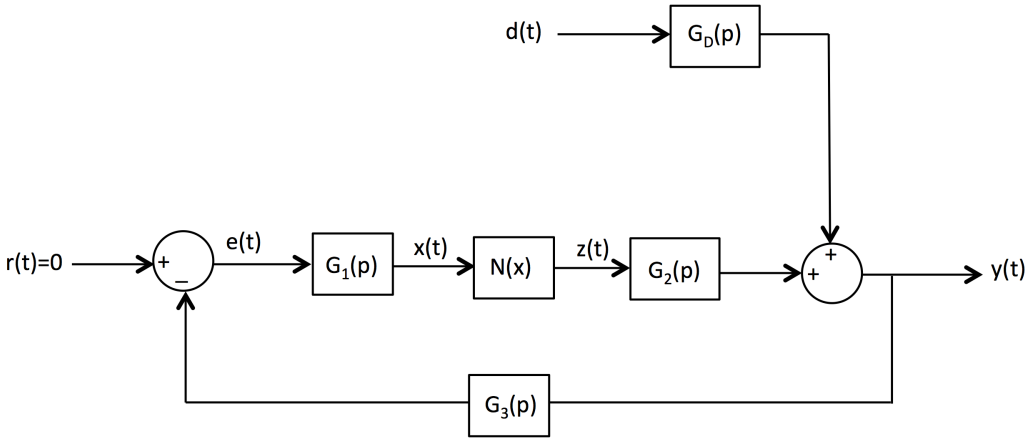

Figure 5-6 Block Diagram of the General Nonlinear Control Regulating Feedback System.

To justify the use of the inverse SIDF algorithm developed in Chapter 3, let $d(t)$ in Figure 5-6 be a simple harmonic excitation,

$$d(t) = M_d \sin \omega t. \tag{5.10}$$

Assuming the input to the nonlinear element ($N(x)$ in Figure 5-6) is also a sinusoid wave with amplitude A and frequency ω ($x(t) = A\sin(\omega t)$), and because of the presence of the nonlinearity in the loop, all the transfer functions relating different signals to one another, are function of A and ω. To find A, consider the transfer function relating $d(t)$ to $x(t)$ as

$$\frac{X}{D}(j\omega, A) = \frac{-G_1(j\omega)G_3(j\omega)G_D(j\omega)}{1 + G_1(j\omega)G_2(j\omega)G_3(j\omega)N(A,\omega)}. \tag{5.11}$$

The absolute magnitude of the transfer function in Eq. (5.11) is written as

$$\left|\frac{X}{D}(j\omega, A)\right| = \frac{A}{M_d}. \tag{5.12}$$

Consider the following definitions for components of the feedback loop in Figure 5-6

$$\begin{gathered} G_1(j\omega) = \rho_1 e^{j\theta_1}, G_2(j\omega) = \rho_2 e^{j\theta_2}, G_3(j\omega) = \rho_3 e^{j\theta_3}, \\ G_D(j\omega) = \rho_D e^{j\theta_D}, \text{and } N(A,\omega) = \rho_N e^{j\theta_N}, \end{gathered} \tag{5.13}$$

where $\rho_1, \rho_2, \rho_3, \rho_D$ and $\theta_1, \theta_2, \theta_3, \theta_D$ are functions of ω, while ρ_N and θ_N are functions of both A and ω. Using definitions provided in Eq. (5.13) in Eq. (5.11) yields

$$\left|\frac{X}{D}(j\omega, A)\right| = \left|\frac{\rho_1\rho_3\rho_D e^{j(\theta_1+\theta_3+\theta_D)}}{1 + \rho_1\rho_2\rho_3\rho_N e^{j(\theta_1+\theta_2+\theta_3+\theta_N)}}\right|. \tag{5.14}$$

Using Eq. (5.14) in Eq. (5.12) yields

$$\frac{A}{M_d} = \left| \frac{\rho_1 \rho_3 \rho_D e^{j(\theta_1+\theta_3+\theta_D)}}{1 + \rho_1 \rho_2 \rho_3 \rho_N e^{j(\theta_1+\theta_2+\theta_3+\theta_N)}} \right|. \tag{5.15}$$

Defining $\tilde{\rho} \triangleq \rho_1 \rho_3 \rho_D$, $\rho \triangleq \rho_1 \rho_2 \rho_3$, and $\theta \triangleq \theta_1 + \theta_2 + \theta_3$, and using Euler's formula, Eq. (5.15) is simplified to

$$\frac{A}{M_d} = \frac{\tilde{\rho}}{\sqrt{(1 + \rho \rho_N \cos(\theta + \theta_N))^2 + \rho^2 \rho_N^2 \sin^2(\theta + \theta_N)}}. \tag{5.16}$$

Applying math simplifications on Eq. (5.16) produces

$$\frac{A}{M_d} = \frac{\tilde{\rho}}{\sqrt{1 + \rho^2 \rho_N^2 + 2\rho \rho_N \cos(\theta + \theta_N)}}. \tag{5.17}$$

An alternative representation of Eq. (5.17) is

$$A\rho_N = -\frac{A}{\rho}\cos(\theta + \theta_N) \pm \frac{1}{\rho}\sqrt{\tilde{\rho}^2 M_d^2 - A^2 \sin^2(\theta + \theta_N)}. \tag{5.18}$$

The left hand side of Eq. (5.18) is the amplitude of the nonlinearity output fundamental. Eq. (5.18) can be used to obtain a numerical solution of A. In other words, at a particular frequency, each side of Eq. (5.18) is only dependent on A. Therefore, by changing A iteratively, one can find the value at which left and right hand sides of Eq. (5.18) intersect. This will be considered as the solution for A.

It is to be noted that in the development of Eq. (5.18), a general form of feedback loop is considered. In the case of using a different feedback system such as one that is

shown in Figure 5-3, appropriate modifications must be applied. It means, since in the system in Figure 5-3 $G_3(s) = 1$, then in Eqs. (5.13) through (5.18) $\rho_3 = 1, \theta_3 = 0$.

5.3.3.2 Transforming Data to the Gain and Phase Distortions of the Nonlinearity

To illustrate how Eq. (5.18) is utilized to extract $N(A)$ from $\hat{L}(A, j\omega)$, consider the block diagram shown in Figure 5-7. The blocks inside the box labeled with 1 represent the linear open loop system, in which the linear controller G_C is designed for γ_1. This linear open loop transfer function can maintain system performance requirements in Eq. (5.2) for the disturbance step size of γ_1.

The blocks inside the dashed-line box labeled with 2 represent the nonlinear open loop system (i.e., $\hat{L}(A, j\omega)$), in which the linear controller G_C in tandem with the nonlinear controller $\mathcal{N}$ (to be determined) is capable of maintaining system performance requirements for a given disturbance step size $\gamma > \gamma_1$.

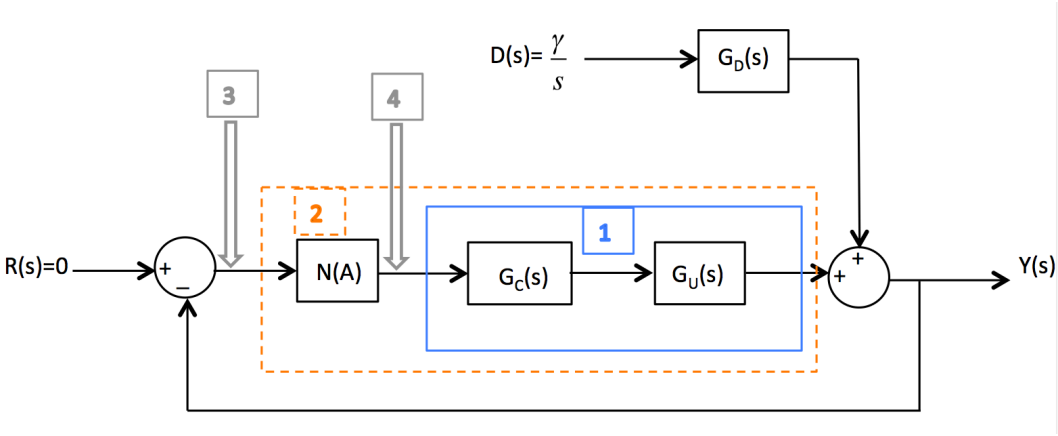

Figure 5-7 Converting the Obtained Data to the Gain and Phase Distortions of the Nonlinearity.

To extract the gain and phase distortions of the nonlinearity from the modified open loop frequency response, the frequency response of the nonlinearity must be isolated. In essence, the SIDF can be written as the ratio of the phasor representation of output signal (the signal shown with the arrow labeled with 4 in in Figure 5-7) to the phasor representation of input signal (the signal shown with the arrow labeled with 3 in Figure 5-7) [9].

If the input signal amplitude of $L(j\omega)$ and $\hat{L}\left(\hat{A}_{\hat{L}}, j\omega\right)$ are denoted by A_L and $\hat{A}_{\hat{L}}$, respectively, then the SIDF gain and phase distortions due to the nonlinearity can be obtained by

$$N(A) = \frac{\hat{L}(\hat{A}_{\hat{L}}, j\omega)\hat{A}_{\hat{L}}}{L(j\omega)A_L}, \tag{5.19}$$

where A_L and $\hat{A}_{\hat{L}}$ are obtained with the repeated use of Eq. (5.18).

5.3.4 Identification of the Nonlinear Controller

The phasor representation of the SIDF gain and phase distortions obtained from Eq. (5.19), $N(A)$, can be written as

$$N(A) = \rho_N e^{j\theta_N} = C(A) + jS(A), \tag{5.20}$$

where $C(A) = \rho_N \cos\theta_N$, $S(A) = \rho_N \sin\theta_N$, and A is obtained from Eq. (5.18).

Considering SIDF representation in Eq. (5.20), the inverse SIDF algorithm developed in Chapter 3 can be utilized to recover an isolated static (explicit) nonlinearity that the obtained gains and phase distortions are corresponded to. The outcome of this step is a

non-parametric representation of the nonlinearity. The characteristics of the nonlinearity can be identified from the non-parametric solution by Least Square Estimation (LSE) method. This identified nonlinear function can be implemented in the feedback loop in tandem with G_C. Doing so, the system is capable of maintaining performance requirements in Eq. (5.2) for the considered disturbance step size $\gamma > \gamma_1$.

5.4 Case Study

In this section, the same example that was studied in Chapter 4 is considered. The linear controller, $G_{C1}(s)$, designed through H_∞ controller synthesis approach for the predicted value of the disturbance step size, i.e., $\gamma_1 = \gamma^*$ based on the methodology in Chapter 4 is considered as the starting points. From Chapter 4, the obtained value of $\gamma^* = 16.7\ N.m$ and the resulting linear controller is

$$G_{C1}(s) = \frac{0.9223(\frac{s}{1.334} + 1)}{\left(\frac{s}{3} + 1\right)\left(\frac{s}{500} + 1\right)^2}. \tag{5.21}$$

Next, a four percent increase in the step size disturbance from its predicted value for the designed linear controller is considered, i.e., $\gamma = 1.04\,\gamma^*$. At this level, both performance constraints in Eq. (5.2) are violated.

The objective in this section is to append the linear controller in Eq. (5.21) with a nonlinear controller, designed based on the proposed methodology, such that the modified nonlinear feedback loop can maintain the performance constraints of the system for $\gamma = 1.04\,\gamma^*$.

5.4.1 Defining the Discrete Sets of Frequencies

To define Ψ and Θ sets, first, the upper and lower amplitude bounds and their corresponding acceptable design regions at different frequencies for $\gamma = 1.04\,\gamma^*$ must be obtained. Shown in Figure 5-8 and Figure 5-9 are the acceptable design regions in the gain/phase and complex planes, respectively. The unit of frequency is $\frac{rad}{sec}$.

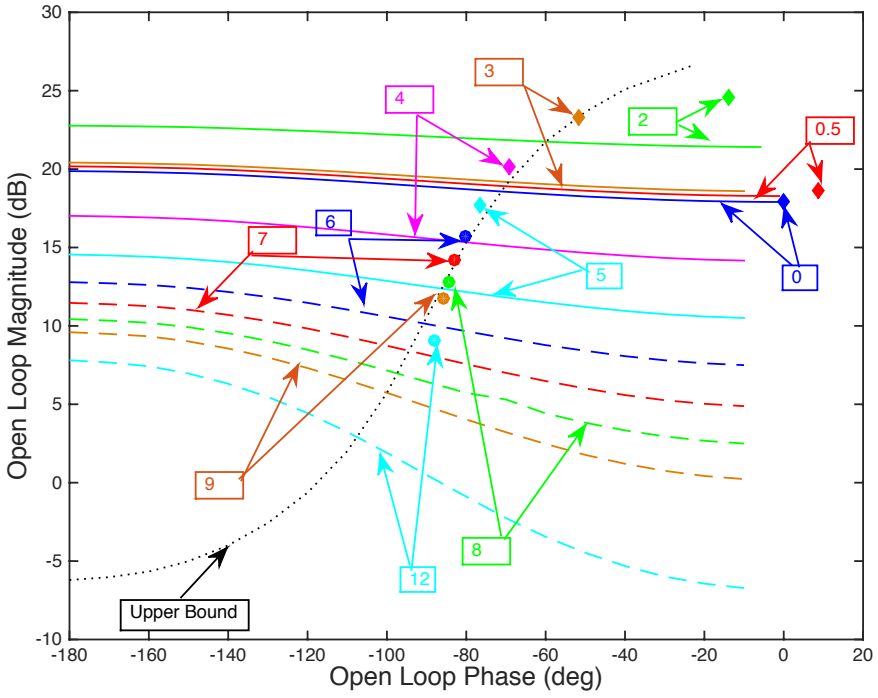

Figure 5-8 Selection of Discrete Frequency Sets in the Gain/phase Plane.

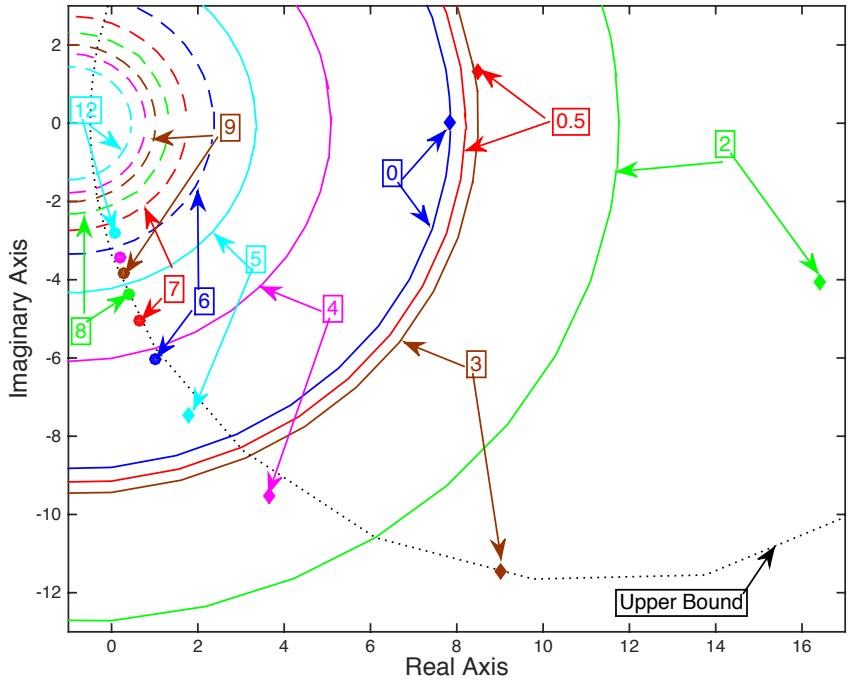

Figure 5-9 Selection of Discrete Frequency Sets in the Complex Plane.

In these figure, solid-lines and dashed-lines are the representations of lower bounds for $\gamma = 1.04\,\gamma^*$. Additionally, the dotted-line is the representation of upper bound for $\gamma = 1.04\,\gamma^*$. As explained in Chapter 4, the dynamics of the disturbance are canceled by the dynamics of the linear plant, and therefore, the upper bound does not change as frequency changes. The acceptable design region is the area between the upper bound and lower bound, at each frequency. It is worth mentioning that, the tightest acceptable design region in Figure 5-8 and Figure 5-9 is at $\omega = 2\frac{rad}{sec}$, which is consistent with what was concluded in Chapter 4 for obtaining the predicted value of the disturbance step size for this example problem.

Additionally, shown with points in Figure 5-8 and Figure 5-9 are the frequency response of the linear transfer function $L(s) = G_{C1}(s)G_U(s)$. If $L(j\omega_i)$ is not contained in the acceptable design region at $\omega = \omega_i$, then $\omega_i \in \Psi$ if Eq. (5.5) is satisfied, and $\omega_i \in \Theta$ if Eq. (5.6) is satisfied. For this case study, from Figure 5-8 Ψ and Θ sets are defined as

$$\Psi = \left\{\omega | 0 \ \frac{rad}{sec} \leq \omega < 0.5 \frac{rad}{sec}\right\} \tag{5.22}$$

and

$$\Theta = \left\{\omega | 3 \frac{rad}{sec} \leq \omega < 8 \frac{rad}{sec}\right\}. \tag{5.23}$$

The nonlinear control law will be defined for the frequency ranges defined in Eqs. (5.22) and (5.23).

5.4.2 Defining Nonlinear Control Laws

In this step based on Eqs. (5.8) and (5.9) the nonlinear control law will be defined. For this, as mentioned, three options are available. For the example studied here, it is found that for the frequencies defined in Eq. (5.22) first and third options are not helpful. In other words, for these points, imposing phase distortions does not move them toward their corresponding acceptable design regions. Therefore, for Eq. (5.22) the nonlinear control law is defined based on the second option, i.e., imposing only gain distortions. For the frequencies defined in Eq. (5.23), however, all three options are applicable. Here, first and second options are considered to define two nonlinear control laws for the frequencies defined in Eq. (5.23).

Hence, in the following, two nonlinear control laws are defined: (i.) Case 1 considers imposing only gain distortions on both Ψ and Θ defined in Eqs. (5.22) and (5.23), and (ii.) Case 2 imposes gain distortions on Ψ defined in Eq. (5.22) and both gain and phase distortions on Θ defined in Eq. (5.23).

5.4.2.1 Nonlinear Control Law for Case 1

The nonlinear controller for Case 1 will be designed to be in tandem with and before the linear controller, i.e., $G_{C1}(s)$, in the feedback loop. For this, to define K based on Eq. (5.8), for frequency range defined in Eq. (5.22), there must be an increase in the gain characteristics of $L(j\omega)$ to obtain $\hat{L}(A, j\omega)$. Additionally, to define Z based on Eq. (5.9) for frequency range defined in Eq. (5.23), the gain characteristics of $L(j\omega)$ must decrease to obtain $\hat{L}(A, j\omega)$.The results are listed in Table C. 1 in Appendix C.

5.4.2.2 Nonlinear Control Law for Case 2

The nonlinear controller for Case 2 will be designed to be in tandem with and after the linear controller, i.e., $G_{C1}(s)$, in the feedback loop. In this case, K is defined in the same way that was defined for Case 1. To define Z based on Eq. (5.9) for frequency range defined in Eq. (5.23), there should be a decrease in the gain characteristics of $L(j\omega)$ and an increase in the phase characteristics of $L(j\omega)$ to obtain $\hat{L}(A, j\omega)$. The results are listed in Table C. 2 in Appendix C.

5.4.3 Isolation of the Nonlinearity

By utilizing Eqs. (5.18) and (5.19) in this step, the gain and phase distortions of the nonlinear controllers for Case 1 and Case 2 are extracted from the obtained data in Table C. 1 and Table C. 2, for $\hat{L}(A, j\omega)$. The sorted SIDF gain and phase distortions for both Case 1 and Case 2 are listed in Table C. 3 and Table C. 4 in Appendix C. Additionally, SIDF gain and phase distortions of the nonlinear controllers for Case 1 and Case 2 are shown in Figure 5-10 and Figure 5-11.

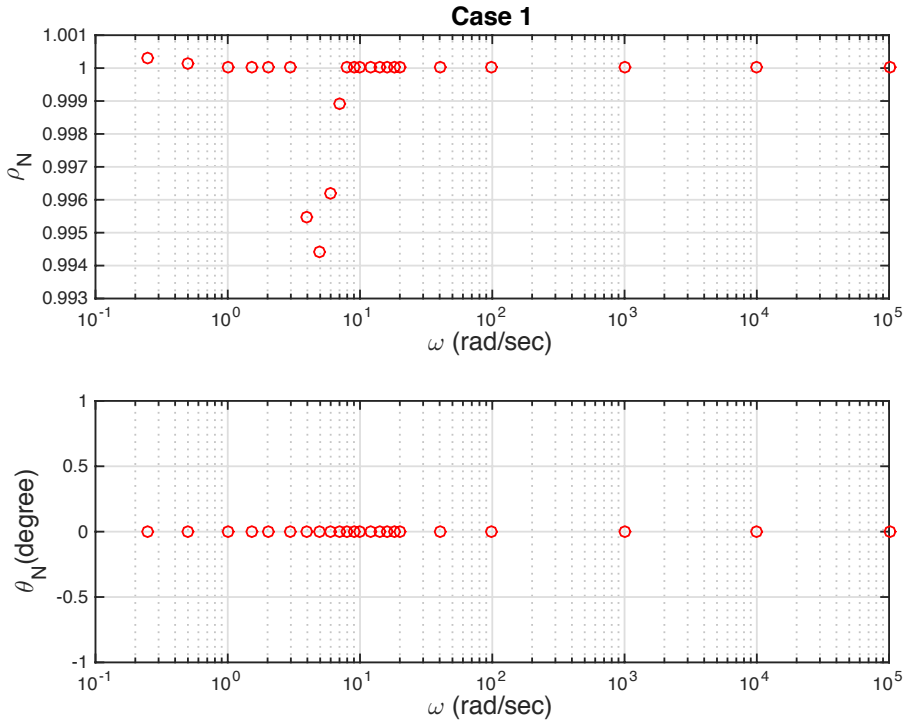

Figure 5-10 SIDF Gain and Phase Distortions of Nonlinear Controller in Case 1.

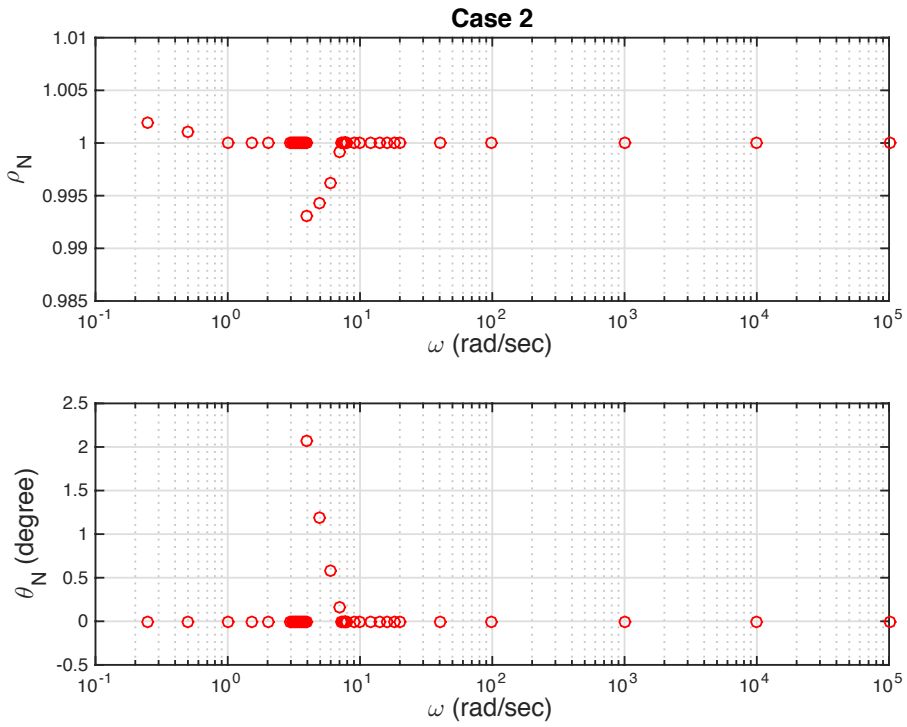

Figure 5-11 SIDF Gain and Phase Distortions of Nonlinear Controller in Case 2.

5.4.4 Identification of the Nonlinear Controller

The SIDF gain and phase distortions obtained in Table C. 3 and Table C. 4, are used in the developed inverse SIDF algorithm in Chapter 3, and the nonlinear controllers that these SIDF gain and phase distortions are corresponded to are identified for both cases. Shown in Figure 5-12 and Figure 5-13, are the non-parametric output solutions from the numerical inverse SIDF solution presented in Chapter 3 for the nonlinear controllers designed in Case 1 and Case 2, respectively.

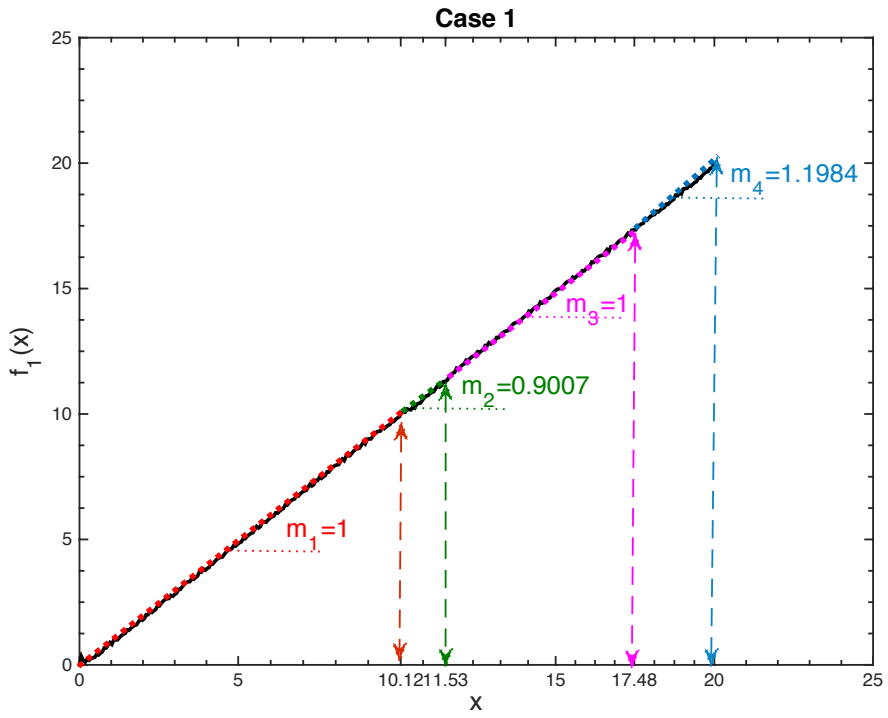

Figure 5-12 Isolated Explicit Nonlinear Controller from Inverse SIDF Algorithm for Case 1.

The nonlinear control law for Case 1 was defined such that the resultant nonlinearity imposes only gain distortions on the linear open loop frequency response. Therefore, the identified nonlinearity is single-valued. From Figure 5-12, the identified nonlinearity (shown with the solid-line) has the characteristics of a piecewise continuous gain changing function. The parameters of this nonlinear function can also be identified from the non-parametric solution using LSE method, as shown by the dotted-lines for different segments in Figure 5-12. The identified parametric solution of the nonlinear controller obtained in Case 1 is

$$f_1(x) = \begin{cases} x & x \leq 10.12 \\ 0.9007x + 1.0049 & 10.12 < x \leq 11.53 \\ x - 0.14 & 11.53 < x \leq 17.48 \\ 1.1984x - 3.608 & 17.48 < x \end{cases} \quad (5.24)$$

The properties of the identified parameters in Figure 5-12 are consistent with the definition of the nonlinear control law in Table C. 1. For example, for the frequencies defined in Eq. (5.22), an increase in the gain characteristics of the linear open loop transfer function was desired. This frequency range corresponds to the last section of the nonlinearity shown in Figure 5-12. In this section, the slope is $m_4 = 1.1984$, which causes an increase in the gain characteristics.

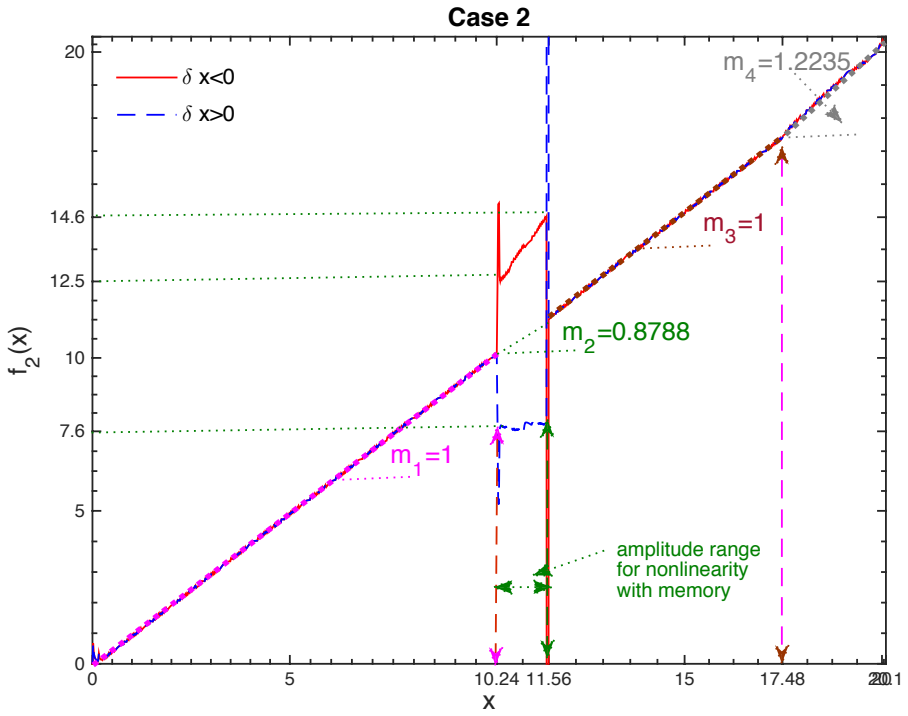

Figure 5-13 Isolated Explicit Nonlinear Controller from Inverse SIDF Algorithm for Case 2.

The control law for Case 2 was defined such that the resultant nonlinearity imposes only gain distortions for the discrete set of frequencies defined in Eq. (5.22) and imposes both gain and phase distortions for the discrete set of frequencies defined in Eq. (5.23). Therefore, the overall identified nonlinearity is double-valued. Shown with solid-line and dashed-line in Figure 5-13, is the non-parametric output solution of the inverse SIDF that the nonlinear control law in Case 2 corresponds to. The parameters of this isolated explicit nonlinear function can be identified from the non-parametric solution using LSE method, as shown by the dotted-lines for different segments in Figure 5-13. The identified parametric solution of the nonlinear controller obtained in Case 2 is

$$f_2(x) = \begin{cases} x & x \leq 10.24 \\ \begin{cases} 1.5909x - 3.790 & \text{for } \delta x < 0 \\ 7.6 & \text{for } \delta x \geq 0 \end{cases} & 10.24 < x \leq 11.56 \\ x - 0.16 & 11.56 < x \leq 17.48 \\ 1.2235x - 4.0668 & 17.48 < x \end{cases}. \tag{5.25}$$

5.4.5 Implementation Results

The closed loop responses for the nonlinear controllers designed are presented in this section. G_{C1} in Eq. (5.21) is appended with the nonlinear controllers obtained in Eqs. (5.24) and (5.35) for Case 1 (before G_{C1}) and Case 2 (after G_{C1}), respectively. Then the controller effort and system output responses of the closed loop system are obtained for $\gamma = 1.04\,\gamma^*$. The results are shown in Figure 5-14 to Figure 5-17.

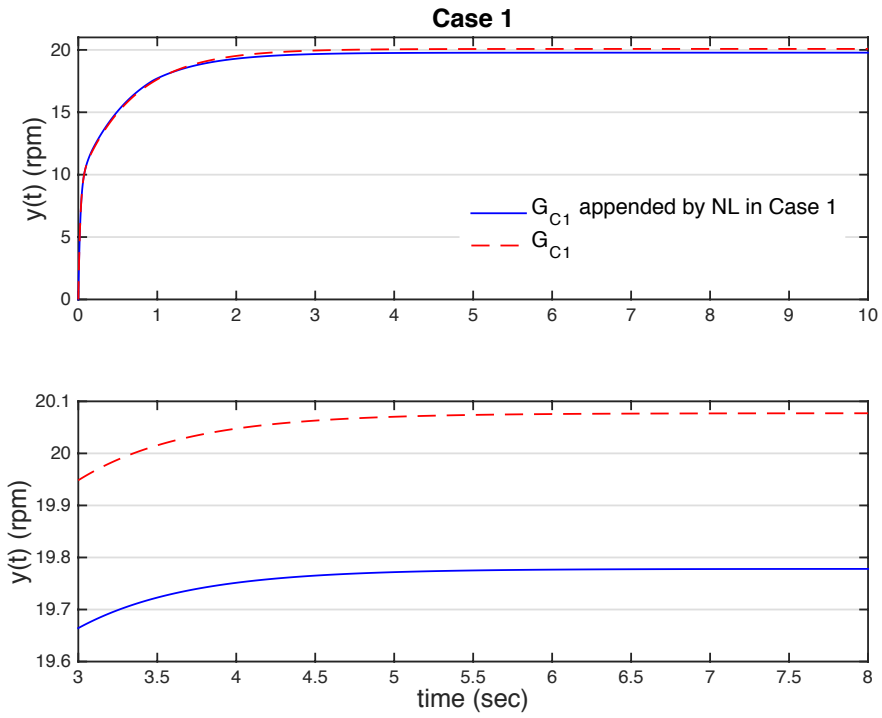

Figure 5-14 Output Performance for Case 1.

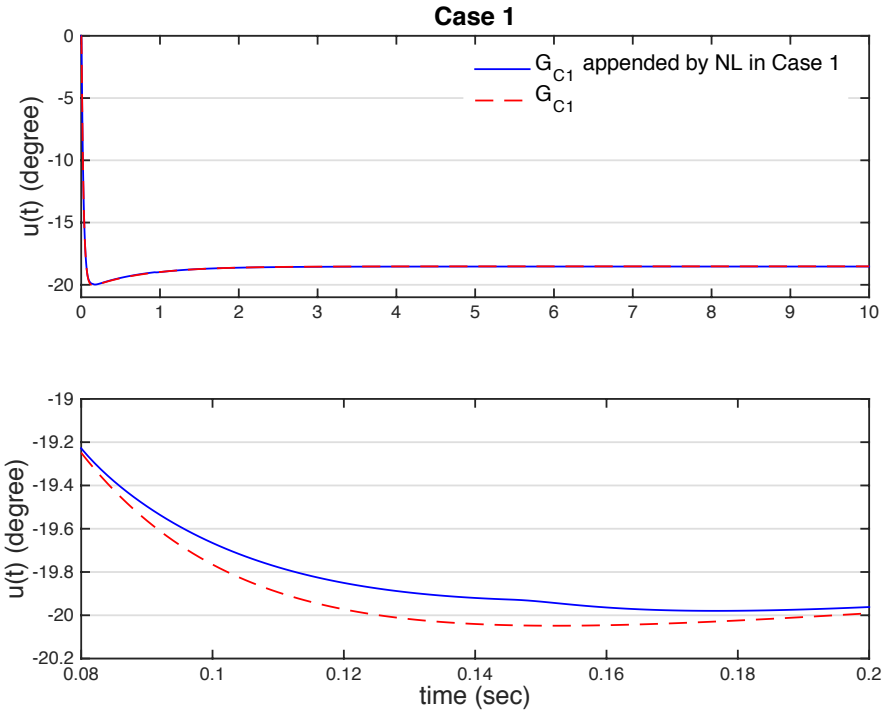

Figure 5-15 Actuator Effort for Case 1.

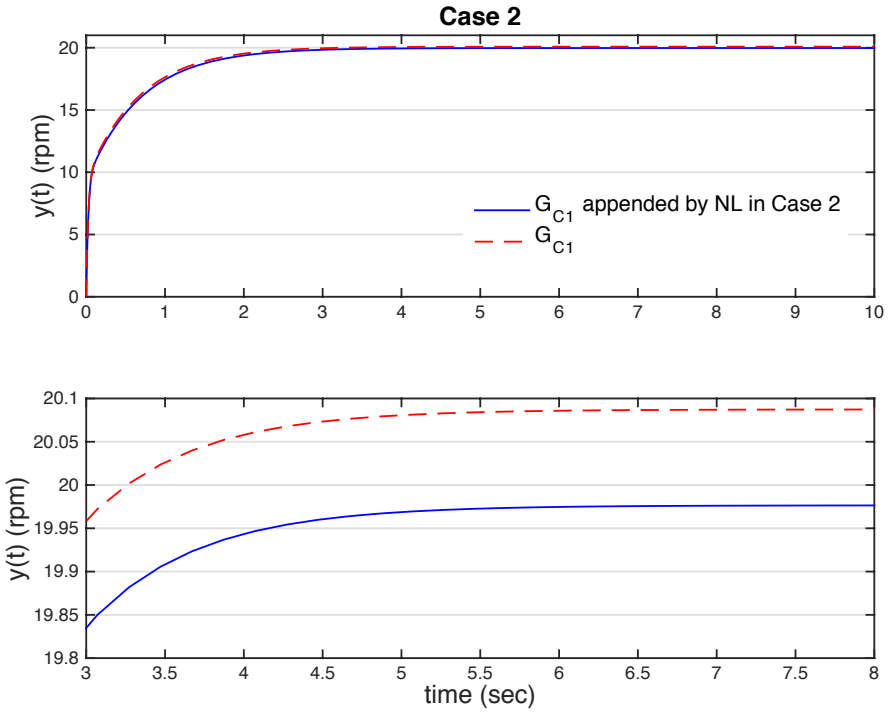

Figure 5-16 Output Performance for Case 2.

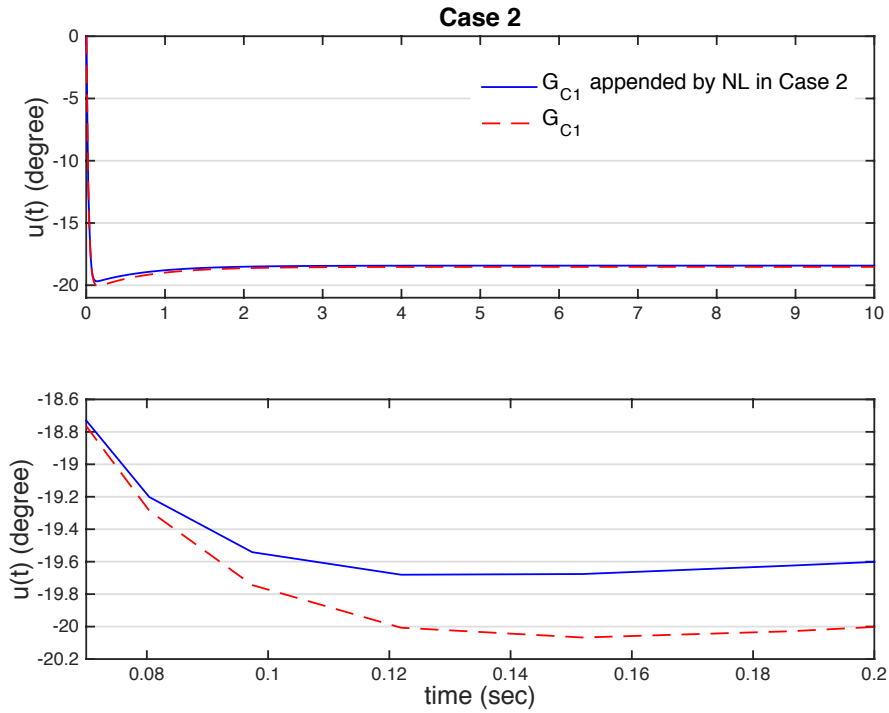

Figure 5-17 Actuator Effort for Case 2

From these figures, adding the nonlinear controllers to the linear system has improved the performance of the system, such that it can maintain the performance requirements for a larger value of the disturbance step size (i.e., $\gamma_1 = 1.04\gamma^* > \gamma^*$).

5.4.6 Discussion on the Results

The maximum allowable disturbance step size via a linear controller, i.e., $\widetilde{\gamma^*}$, obtained in Chapter 4 is equivalent with almost four percent increase in the disturbance step size from the predicted value also obtained in Chapter 4, i.e., $\widetilde{\gamma^*} \cong \gamma_1 = 1.04\gamma^*$. Therefore, the comparison of the closed loop responses obtained from G_{C1} in tandem with the nonlinear controllers for Case 1 and Case 2 with those obtained from G_{C2} is considered in this section. In other words, the closed loop responses shown in Figure 5-14 to Figure 5-17 are compared against using G_{C2} obtained in Chapter 4 for $\gamma = \widetilde{\gamma^*}$ in the feedback loop. The results are shown in Figure 5-18 to Figure 5-21.

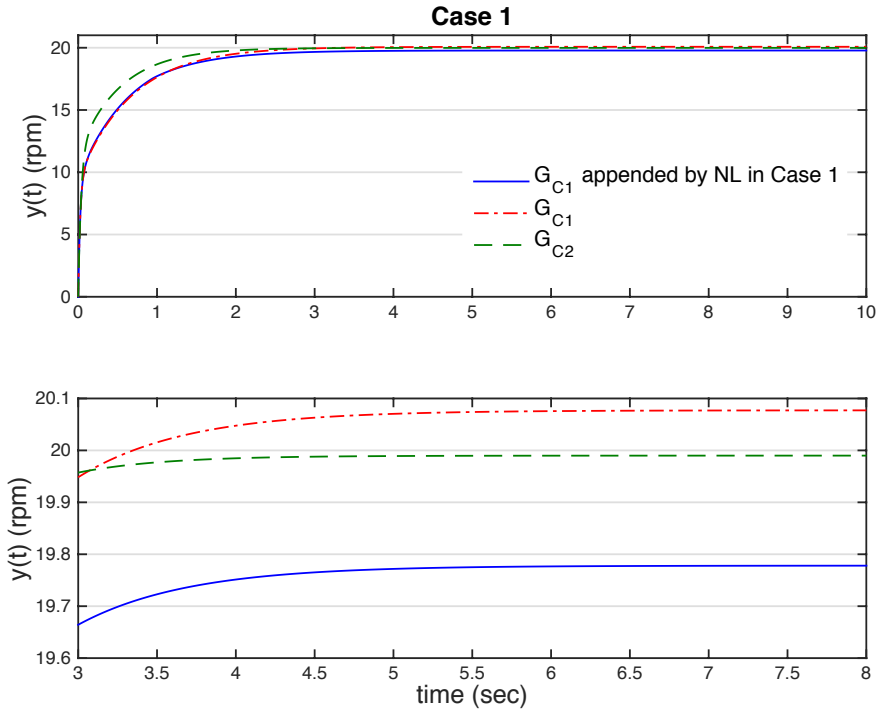

Figure 5-18 Output Performance Comparison for Case 1 and G_{C2}.

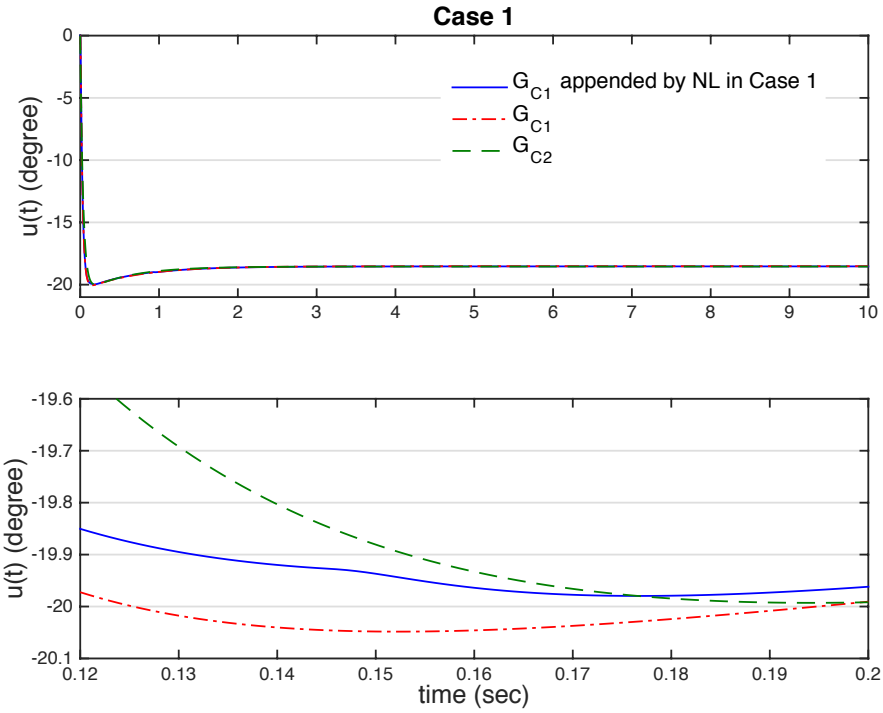

Figure 5-19 Actuator Effort Comparison for Case 1 and G_{C2}.

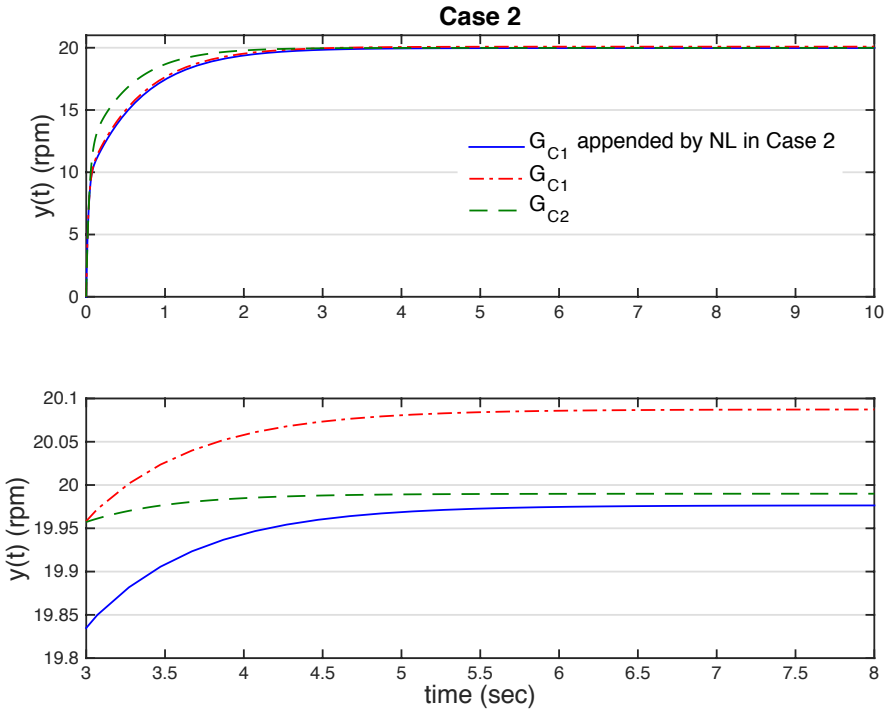

Figure 5-20 Output Performance Comparison for Case 2 and G_{C2}.

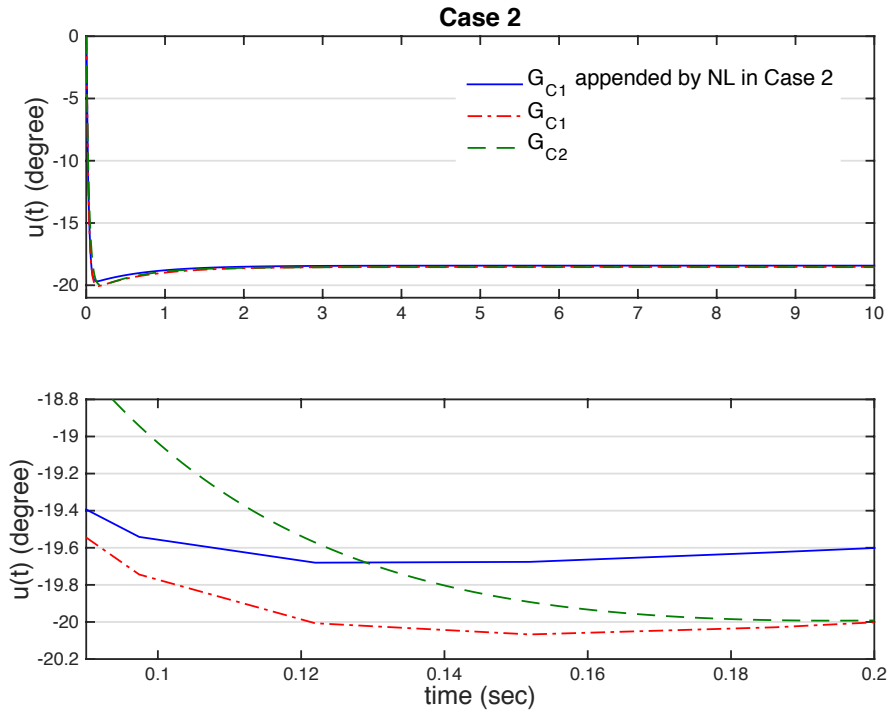

Figure 5-21 Actuator Effort Comparison for Case 2 and G_{C2}.

From these figures, relatively better closed loop performances are obtained by adding the nonlinear controllers in the feedback loop comparing to using G_{C2}. The performance is considered in terms of the maximum output and actuator effort responses. In other words, $\|y(t)\|_\infty$ and $\|u(t)\|_\infty$ are smaller in the case of using G_{C1} augmented by the nonlinear controllers than the case of using G_{C2}. Additionally, as mentioned in Chapter 4, the procedure of designing G_{C2} is an iterative process. Synthesizing the nonlinear controllers, on the other hand, is through an automated process that results in a more systematic approach of the controller design.

Comparing Figure 5-18 to Figure 5-21 suggest that if the nonlinear controllers were built around G_{C2} instead of G_{C1}, higher closed loop performances would have been achieved. For this, the actual impact of time domain parameters $\widetilde{k_1}$ and $\widetilde{k_2}$ in the frequency domain (i.e., upper and lower bounds and more specifically Λ_u and Λ_y defined in Eqs. (4.17) and (4. 22)) must be determined. Unfortunately, there is no direct translation of $\widetilde{k_1}$ and $\widetilde{k_2}$ in the frequency domain due to the intrinsic incompatibilities between time and frequency domains. This can be an interesting subject for future research.

Additionally, Figure 5-1 and/or Figure 5-2 suggests that for some level of γ, eventually there will be no acceptable design regions for some restraining frequencies. This will be considered as the absolute maximum of disturbance step size, γ_{max}, regardless of the type of the controller in the feedback loop.

The restraining frequency for the particular example studied here, is $\omega = 2\frac{rad}{sec}$ that has the tightest acceptable design region for all values of γ, as shown in Figure 5-8 and Figure 5-9. The corresponding absolute maximum of γ for this example problem is found to be $\gamma_{max} \cong 1.08\gamma^*$, at which there will be no acceptable design region for $\omega = 2\frac{rad}{sec}$ and its surrounding frequencies.

A bang-bang controller can be designed for this level of γ_{max} [19, 68]. For this specific case study and using the proposed method, it is found that a nonlinear controller can be designed for up to around six percent increase in γ^*.

This limitation is due to the couple of factors. (i.) Approximations in the SIDF method as well as approximations in the formulations of amplitude of the input signal to the nonlinearity in the feedback loop: because of these approximations, a rigorous justification of using Eq. (5.18) for calculating the amplitude of the input signal to the nonlinearity in the case of a regulating system subject to a step disturbance cannot be developed. Moreover, the actual impact of the pseudo-linearization of the nonlinear element (that is determined from inverse SIDF algorithm) in the time domain is not known. Instead, applications of this technique will be used to test the proposed hypothesis on a case-by-case basis [19]. (ii.) Excluding the dynamics nonlinearities in the formulation of the inverse SIDF: the SIDF of dynamic (implicit) nonlinearities is a function of both amplitude and frequency of the input signal. In the computational method developed in Chapter 3 for the inverse SIDF, the dependency of the SIDF to the frequency of the input signal wave is not considered. Therefore, the method can only

identify static (explicit) nonlinearities. By formulating a more accurate approach for the calculation of the amplitude of the input signal to the nonlinearity as well as including dynamic (implicit) nonlinearities in the inverse SIDF algorithm, increase in the disturbance step size beyond six percent and up to γ_{max} would be achievable. This is also an interesting subject for future research.

Nevertheless, the advantage of using the proposed methodology over a bang-bang controller is that, in the method presented here, the actuator response is proportional to the disturbance size. In the case of using a bang-bang controller, however, it will always lead to saturation, regardless of the value of step disturbance.

5.5 Chapter Summary

A nonlinear controller design methodology is developed for a class of SISO linear regulating systems subject to time domain constraints. The proposed design method is conducted in the frequency domain and improves the closed loop performance of the system by allowing for larger values of the disturbance step size. The proposed method imposes required gain and phase distortions on the frequency response of the linear open loop to ensure that system performance requirements are met. The obtained gain and phase distortions are used in the inverse SIDF algorithm developed in Chapter 3 to estimate an isolated static (explicit) nonlinear controller. An illustrative example is used to demonstrate the application of the proposed nonlinear controller design method. For this, a linear controller designed for the predicted level of disturbance step size, γ^* is appended by two nonlinear controllers designed based on the proposed methodology by

considering four percent increase in γ^*. The nonlinear feedback systems are capable of maintaining the time domain constraints for the increased level of disturbance step size.

Chapter 6. Stability Analysis of the Nonlinear Feedback Control Systems in the Frequency Domain

The final step for the validation of any feedback control system is its stability assessment. The focus of this chapter is to outline a stability assessment tool for nonlinear feedback systems subject to external inputs. The presented method is based on the functional analysis. The stability of the nonlinear feedback systems designed in Chapter 5 is discussed based on the presented method in this chapter.

6.1 Introduction

The stability analysis of nonlinear feedback systems has been of a great interest in the literature and different methods have been formulated [10, 74-76]. Unlike linear systems, the methods developed for evaluating the stability of nonlinear feedback systems often provide sufficient (and not necessary) conditions. These methods usually are formulated for very general conditions and very few assumptions on the open loop elements are made, therefore they often produce conservative results. The aim of this section is to provide a brief introduction of the most useful methods for stability analysis of the nonlinear feedback system.

The traditional approach to stability assessment involves the Lyapunov method [77]. This method is very valuable, since it can provide stability conditions for many practical nonlinear systems. Moreover, the Lyapunov method is the basis for obtaining most of the

frequency domain stability analysis methods, including the original contribution by Popov [78].

Lyapunov method is formulated in the time-domain and is based on the state space representation of the system, i.e., $\dot{x} = f(x)$, where x is the space vector and $f(x)$ is a nonlinear function of states. The method involves of finding a candidate Lyapunov function, $V(x)$ such that $V(x) \geq 0$ and $V(0) = 0$ [74, 77]. The Lyapunov function can be considered as the energy representation of the system. Unfortunately, there is no general approach for finding the Lyapunov function for nonlinear systems, due to the fact that the behavior of the nonlinear systems around their singular points changes very rapidly and unpredictably. Several methods are proposed for the selection of this function, such as the variable gradient method and Lur'e method [74]. Given a Lyapunov function, the stability can be assessed by examining the negativity of the derivative of the Lyapunov function, $\dot{V}(x) = \frac{dV(x)}{dt}$. In other words, if $V(x)$ is considered as the energy representation of the system, the stability can be concluded if $\dot{V}(x)$ is negative.

Several methods have also been suggested for the stability analysis of the nonlinear feedback systems in the frequency domain. The original contribution in this regard is the Generalized Theorem of Popov [10, 74, 78], which is a very important and fundamental theorem, because it is the basis for other frequency domain methods. The Generalized Theorem of Popov is formulated for a basic system as shown in Figure 6-1, in which p is the derivative operator [10, 74, 78].

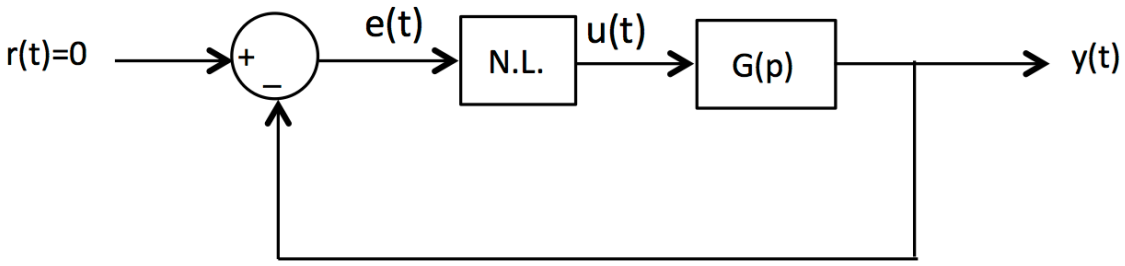

Figure 6-1 Basic Nonlinear Feedback Control System.

The Generalized Theorem of Popov: Let the linear element in Figure 6-1 to be output stable, and the nonlinear element to lie in the sector $\{0, K\}$. In order for the closed loop system to be both absolutely control and output asymptotic, it is sufficient that a real number q exists such that for all $\omega \geq 0$ and an arbitrarily small $\nu > 0$, $G(j\omega)$ satisfies

$$Re\{(1 + j\omega q)G(j\omega)\} + \frac{1}{K} \geq \nu > 0. \tag{6.1}$$

Depending on the nature of the nonlinearity, there are some restrictions on q and K:

(i.) If the nonlinearity is memoryless and time-invariant,

(i-a.) if $0 < K < \infty$, then $-\infty < q < \infty$, and

(i-b) if $K = \infty$, then $0 \leq q < \infty$,

(ii.) If the nonlinearity is passive hysteresis, then $0 < K < \infty$, and $-\infty < q \leq 0$,

(iii.) If the nonlinearity is active hysteresis, then $0 < K \leq \infty$, and $0 \leq q < \infty$,

(iv.) For a general nonlinearity (time-varying, and possibly with hysteresis), $0 < K \leq \infty$, and $q = 0$.

Proof: See reference [74, 78].

The Generalized Theorem of Popov provides sufficient conditions for the closed loop stability by imposing certain requirements on the linear element of the feedback loop depending on the nature of the nonlinearity. Wide range of nonlinear elements, i.e., time-varying and double-valued nonlinearities, are included in this theorem. However, based on this theorem, there is a trade-off between the requirements on the frequency response of the linear element and the nature of the nonlinearity.

The generalized Popov theorem can be extended to different applications. For example, to evaluate the stability of feedback systems with unstable or non-asymptotically stable linear plants, the pole-shifting method is formulated [10, 74]. In this method the original feedback system will be transformed by means of

$$u'(t) = u(t) - a\, e(t), \tag{6.2}$$

where $u(t)$ are $e(t)$ are depicted in Figure 6-1, and a is a constant. If the original nonlinearity lies in sector $\{K_1, K_2\}$, Eq. (6.2) causes the transformed nonlinearity to lie in $\{K_1 - a, K_2 - a\}$. It can be shown that the linear plant will also be transformed to [10, 74]

$$G_a(p) = \frac{G(p)}{1 + aG(p)}. \tag{6.3}$$

From Eqs. (6.2) and (6.3), a sector can be found for the transformed nonlinearity such that the Popov theorem can be applicable for the transformed system. This can be used to treat the unstable or non-asymptotically stable linear plants.

An alternative approach for pole-shifting method is formulated as the Generalized Circle Theorem [10, 74]. In this method, for the system shown in Figure 6-1, it is assumed that the linear element will be output stable by applying a negative feedback through a constant feedback gain a. In order for the original feedback system to be absolutely control and output asymptotic for the nonlinearity that lies in sector $\{a, b\}$, with $a < b$, it is sufficient that there exists a real number q such that for all $\omega \geq 0$ and an arbitrarily small ν, $G(j\omega)$ satisfies [10, 74]

$$\left|G(j\omega) + \frac{b + a - j\omega q(b - a)}{2ab}\right|^2 - \left(\frac{b - a}{2ab}\right)^2 (1 + q^2\omega^2) \geq \nu > 0 \quad \text{for} \frac{1}{a} > \frac{1}{b} \qquad (6.4)$$

and

$$\left|G(j\omega) + \frac{b + a - j\omega q(b - a)}{2ab}\right|^2 - \left(\frac{b - a}{2ab}\right)^2 (1 + q^2\omega^2) \leq -\nu < 0 \quad \text{for} \frac{1}{a} < \frac{1}{b}. \qquad (6.5)$$

The restrictions on the ranges of q and $b - a$ are similar to those for the Generalized Popov theorem for q and K, respectively. For the case of a stable linear plant, i.e., $a = 0$, it can be shown that Eq. (6.1) and Eq. (6.4) / Eq. (6.5) are equivalent, if $K = b$.

Additionally, the zero-shifting method is introduced in an attempt to partially relax the trade-off between the restrictions on the linear element and those on the nonlinear element in the feedback loop [10, 74]. In this method the sector that the nonlinearity lies in will be manipulated such that the basic stability properties (e.g., poles location) of the linear element are not changed. In this method, for a nonlinearity that lies in the sector $\{K_1, K_2\}$, a transformation is defined as

$$e'(t) = e(t) + c\,u(t). \tag{6.6}$$

The transformation in Eq. (6.6) causes the transformed nonlinearity to lie in $\left\{\frac{K_1}{K_1+c}, \frac{K_2}{2+c}\right\}$. Moreover the linear plant will be transformed to

$$G_c(p) = G(p) - c. \tag{6.7}$$

From Eq. (6.7), it can be concluded that although the basic stability properties of the linear plant are preserved, the transformed linear plant is not necessarily output stable. Therefore, using zero-shifting method, the output stability condition of the linear element in the Generalize Popov theorem can be waived [10, 74].

All of the methods presented above, are for nonlinear feedback systems without external input (in Figure 6-1 $r(t) = 0$). However, to evaluate the stability of nonlinear feedback systems designed in Chapter 5, stability analysis tools for nonlinear feedback system subject to non-zero external inputs are desirable. In the following section, this topic is discussed.

6.2 Stability Formulation for the Nonlinear Feedback Systems Subject to Non-zero External Inputs

The stability discussion presented in this section is based on the assessment of the input-output relationship. For a system to behave properly, the input-output must have two properties: (i.) Bounded inputs must produce bounded outputs (i.e., the stability in

the sense of Bounded Input Bounded Output: BIBO), and (ii.) Outputs must not be critically sensitive to small changes in inputs (e.g., changes caused by noise) [75, 76].

These two properties are the basis for stability criterion presented in this section. In other words, it is desirable to find conditions on the open loop relations that result in the closed loop stability. In particular, conditions are sought for the closed loop stability of the feedback systems with both linear and nonlinear elements, such as those designed in Chapter 5.

6.2.1 Preliminaries

Before presenting the main results needed for the stability analysis of the feedback systems designed in Chapter 5, several primary definitions are needed. This section presents these prerequisites [75, 76].

Truncated Function: Let x be any function mapping T (time interval) into V (range of input or output values), i.e., $x: T \to V$. Let t be any point in T. Then the symbol x_t denotes the truncated function, $x_t: T \to V$, which assumes the values $x_t(t_0) = x(t_0)$ if $t_0 < t$ and $x_t(t_0) = 0$ elsewhere.

Normed Space: L_p, where $p = 1,2,3 \ldots$ is the space consisting of those real and non-negative x for which $\int_0^\infty |x(t)|^p dt$ is finite. In addition, for the case $p = 2$, L_2 is an inner-product space, where inner-product is defined as

$$\langle x, y \rangle = \int_0^\infty x(t)y(t)dt. \tag{6.8}$$

Extended Normed Linear Space: Assume X is a normed linear space. The extension of X, denoted by X_e, is defined as the space consisting of those functions whose truncations lie in X, that is

$$X_e = \{x | x: T \to V, \text{and } x_t \in X \ \ \forall t \in T\}. \tag{6.9}$$

X_e is also a linear space. An extended norm, $\|x\|_e$, is assigned to each $x \in X_e$, such that $\|x\|_e = \|x\|$ if $x \in X$, and $\|x\|_e = \infty$, elsewhere.

Relation: An operator L is said to be a relation on X_e if : (i.) the domain of L is equal to X_e, and (ii.) L is one-to-one.

$\mathcal{R}_0$ Class: $\mathcal{R}_0$ is a class of relations on L_{2e}, which holds the property of zero element (i.e., zero element belongs to the domain of the relation and its image is also zero).

Gain and Incremental Gain: The gain of a relation L in $\mathcal{R}_0$, denoted by $g(L)$, is

$$g(L) = \sup \frac{\|(Lx)_t\|}{\|x_t\|}, \tag{6.10}$$

where the supremum is taken over all possible input-output pairs, and over all possible truncations. These gains have the properties of norms. Additionally, the incremental gain of any L in $\mathcal{R}_0$, denoted by $\tilde{g}(L)$, is

$$\tilde{g}(L) = \sup \frac{\|(Lx)_t - (Ly)_t\|}{\|x_t - y_t\|}. \tag{6.11}$$

$\mathcal{L}$ Class: $\mathcal{L}$ is the class of operators on L_{2e}, satisfying

$$Lx(t) = h_\infty x(t) + \int_0^t h(t-t')x(t')dt', \tag{6.12}$$

where h_∞ is a real constant, and the impulse response h is a function in L_1 (normed space) with the property that, for some $\sigma_0 < 0$, $h(t)\exp(-\sigma_0 t)$ is also in L_1. Operators in $\mathcal{L}$ are linear and time-invariant.

Definitions Related to the Concept of Conicity: A relation L in $\mathcal{R}_0$ is interior conic if there are real constants $r \geq 0$ and c for which satisfy

$$\|(Lx)_t - cx_t\| \leq r\|x_t\| \quad \forall x \in \mathrm{Do}(L)\ \&\ \forall t \in T. \tag{6.13}$$

Additionally, L is exterior conic if the sign in inequality in Eq. (6.13) is reversed. L is conic if it is exterior conic or interior conic. The constant c is called the center parameter and r is called the radius parameter of L.

The conic relation L is said to be inside the sector $\{a, b\}$, if $a \leq b$ and if it satisfies

$$\langle (Lx)_t - ax_t, (Lx)_t - bx_t \rangle \leq 0 \quad \forall x \in \mathrm{Do}(L)\ \&\ \forall t \in T. \tag{6.14}$$

Additionally, L is said to be outside the sector $\{a, b\}$, if $a \leq b$ and if the sign in the inequality in Eq. (6.14) is reversed.

These definitions can be extended to incrementally conic relations as follow. A relation L in $\mathcal{R}_0$ is incrementally interior conic if there are real constants $r \geq 0$ and c for which satisfy

$$\|(Lx - Ly)_t - c(x - y)_t\| \leq r\|(x - y)_t\| \quad \forall x, y \in \mathrm{Do}(L)\ \&\ \forall t \in T. \tag{6.15}$$

Additionally, L is incrementally exterior conic if the sign of inequality in Eq. (6.15) is reversed. Moreover, an incrementally conic relation L is incrementally inside the sector $\{a, b\}$, if $a \leq b$ and if it satisfies

$$\langle (Lx - Ly)_t - a(x - y)_t, (Lx - Ly)_t - b(x - y)_t \rangle \leq 0 \quad \forall x, y \in \mathrm{Do}(L)\ \&\ \forall t \in T. \tag{6.16}$$

Additionally, an incrementally conic relation L is incrementally outside the sector $\{a, b\}$, if $a \leq b$ and the sign of inequality of Eq. (6.16) is reversed.

If L is incrementally interior (exterior) conic with center c and radius r, then L is incrementally inside (outside) the sector $\{c - r, c + r\}$. On the other hand, if L is incrementally inside (outside) the sector $\{a, b\}$, then L is incrementally interior (exterior) conic with center $\frac{a+b}{2}$ and radius $\frac{b-a}{2}$.

Definitions Related to the Concept of Positivity: A relation L in $\mathcal{R}_0$ is positive if it satisfies

$$\langle x_t, (Lx)_t \rangle \geq 0 \quad \forall x \in \mathrm{Do}(L)\ \&\ \forall t \in T. \tag{6.17}$$

Additionally L is incrementally positive if it satisfies

$$\langle (x - y)_t, (Lx - Ly)_t \rangle \geq 0 \quad \forall x, y \in \mathrm{Do}(L)\ \&\ \forall t \in T. \tag{6.18}$$

Instantaneous Conditions: Conicity and positivity definitions can be extended to include the instantaneous conditions, as

(i.) The relation L is instantaneously inside the sector $\{a, b\}$, if $a \leq b$ and if it satisfies

$$a \leq \frac{Lx(t)}{x(t)} \leq b \quad x \in L_{2e}, t \geq 0, x(t) \neq 0. \tag{6.19}$$

(ii.) The relation L is instantaneously positive if it satisfies

$$x(t).Lx(t) \geq 0 \quad x \in L_{2e}, t \geq 0. \tag{6.20}$$

(iii.) The relation L is instantaneously incrementally inside the sector $\{a, b\}$, if $a \leq b$ and if it satisfies

$$a \leq \frac{Lx(t) - Ly(t)}{x(t) - y(t)} \leq b \quad x \in L_{2e}, t \geq 0, x(t) - y(t) \neq 0. \tag{6.21}$$

(iv.) The relation L is instantaneously incrementally positive if it satisfies

$$(x(t) - y(t)).(Lx(t) - Ly(t)) \geq 0 \quad x, y \in L_{2e}, t \geq 0. \tag{6.22}$$

6.2.2 Main Theorems

Consider the general feedback loop as shown in Figure 6-2.

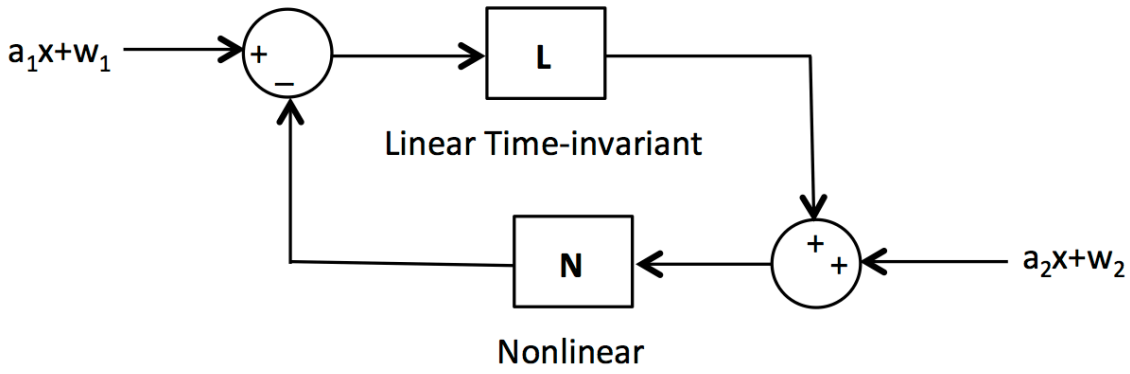

Figure 6-2 General Nonlinear Feedback Control System with External Inputs.

In Figure 6-2 L represents a linear time-invariant relation, and N represents a nonlinear relation that is not necessarily time-invariant. A single input, x, multiplied by two real constants, a_1 and a_2, is added into the systems at two points. This is to consider a more general configuration. By setting either a_1 or a_2 to zero, a single input system can be obtained. Additionally, w_1 and w_2 in Figure 6-2 are fixed bias functions, and are used to account for initial conditions.

The objective is to present the satiability conditions for the closed-loop system shown in Figure 6-2. For this, the following theorems and lemmas have been formulated in [75, 76].

6.2.2.1 Circle Conditions

Suppose N is a nonlinear relation, that could be memoryless or with memory, and is inside a sector $\{\delta_1, \delta_2\}$. Assume $\delta_1 \leq \delta_2$, $\delta_2 > 0$, $\varepsilon \geq 0$ are real constants. $L(j\omega)$ is said to satisfy the circle conditions for the sector $\{\delta_1, \delta_2\}$, with offset ε, if the following conditions hold:

Case a: If $\delta_1 > 0$, then

$$\left|L(j\omega) + \frac{1}{2}\left(\frac{1}{\delta_1} + \frac{1}{\delta_2}\right)\right| \geq \left|\frac{1}{2}\left(\frac{1}{\delta_1} - \frac{1}{\delta_2}\right)\right| + \varepsilon \quad \forall\omega, \tag{6.23}$$

and the Nyquist diagram of $L(j\omega)$ does not encircle the point $\frac{-1}{2}\left(\frac{1}{\delta_1} + \frac{1}{\delta_2}\right)$.

Case b: If $\delta_1 < 0$, then

$$\left|L(j\omega) + \frac{1}{2}\left(\frac{1}{\delta_1} + \frac{1}{\delta_2}\right)\right| \leq \left|\frac{1}{2}\left(\frac{1}{\delta_2} - \frac{1}{\delta_1}\right)\right| - \varepsilon \quad \forall\omega. \tag{6.24}$$

Case c: If $\delta_1 = 0$, then

$$Re\{L(j\omega)\} \geq -\frac{1}{\delta_2} + \varepsilon \quad \forall\omega. \tag{6.25}$$

Conditions presented in cases a through c divide the complex plane into two regions. These regions shape either like a circular disk and its compliment or like two half planes (which can be viewed as a circular disk with the radius being infinity). One of these regions is called the "permissible" region and the other one is called the "critical" region.

It can be shown that if $L(j\omega)$ does not enter or encircle the critical region, then the closed loop is bounded. In addition, if N is incrementally inside sector $\{\delta_1, \delta_2\}$, then the closed loop is continuous as well. These results can be formulated in a theorem as follow.

6.2.2.2 Circle Theorem

Suppose that

(i.) N is a relation in $\mathcal{R}_0$, and is (incrementally) inside the sector $\{\delta_1 + \tau, \delta_2 - \tau\}$, where $\delta_2 > 0$,

(ii.) L is an operator in $\mathcal{L}$, which satisfies the circle conditions for the sector $\{\delta_1, \delta_2\}$ with offset ε, and

(iii.) ε and τ are non-negative constants, at least one of which is greater than zero,

then, the closed loop is L_2-bounded (L_2-continous).

Proof: See refernce [76].

The Circle Theorem can be considered as a generalization of the sufficient part of the Nyquist's criterion, in which the critical region is replaced by the critical instability point, i.e., $0 + j(-1)$. From this theorem, for any given N, there are two critical regions, one for boundedness and one for continuity. Due to the stricter conditions imposed for the continuity, the critical region for the continuity is smaller than the critical region for the boundedness.

6.2.2.3 Main Result: Corollary 1

The Circle theorem is served as the generating theorem for the following results that is presented as a corollary to the Circle theorem by imposing additional requirements on N.

Corollary 1: Suppose that (i.) N in $\mathcal{R}_0$, and is instantaneously (incrementally) inside the sector $\{\delta_1 + \tau, \delta_2 - \tau\}$, where $\delta_2 > 0$, and conditions (ii.) and (iii.) of the Circle theorem hold, then, the closed loop is L_2-bounded (L_2-continous).

The nonlinearities considered in Corollary 1 include a wide range of functions, i.e., time-varying nonlinearity with or without memory. This results in producing a relatively large critical region. In other words, the stability assessment based on Corollary 1 is vey conservative.

To reduce this conservativeness, one way is to make the critical region smaller and this can be achieved by imposing more limitations on N. In this regard, more corollaries are formulated such as Popov's conditions and the Factorization method [76]. In these formulations, the requirements imposed on N will limit the class of nonlinearities to the single-valued nonlinearities. Moreover, they only provide the boundedness (and not continuity) results for the closed loop system. Since the nonlinear controllers designed in Chapter 5 include both single-valued and double-valued nonlinearities, therefore the Popov's conditions and the Factorization method are not desirable. Therefore, Corollary 1 will be used to assess the stability of feedback systems presented in Chapter 5. In the next section, it will be shown how Corollary 1 can be utilized to evaluate the stability of the designed nonlinear feedback systems.

6.3 Applications of Corollary 1

From the results presented in Chapter 4 and Chapter 5, the open loop linear element in the feedback loop can be simplified as

$$L(s) = \frac{10.99s^2 + 47.64s + 43.99}{0.00134s^4 + 0.3403s^3 + 1.75s^2 + 4.096s + 5.62}. \tag{6.26}$$

The Nyquist plot of the linear open loop transfer function is shown in Figure 6-3.

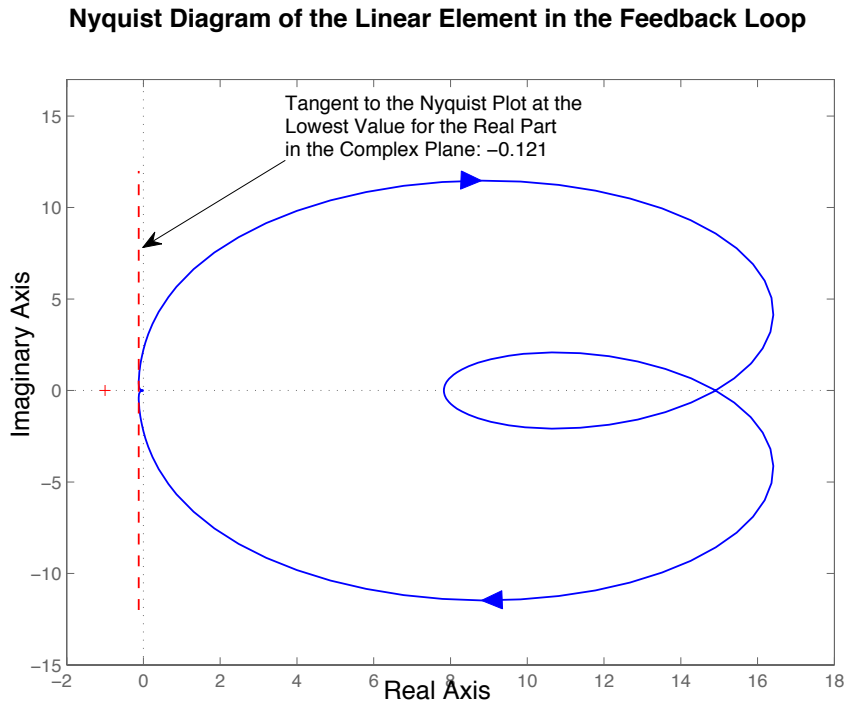

Figure 6-3 Nyquist Diagram of the Linear Element in the Feedback Loop.

In the following sections, the stability of the nonlinear feedback systems for the nonlinear controllers designed in Case 1 and Case 2 in Chapter 5 are evaluated.

6.3.1 Stability of the Feedback System with the Nonlinear Controller in Case 1

To evaluate the stability of the feedback system with the nonlinear controller in Case 1, three conditions of the Corollary 1 must be checked:

(i.) Consider $f_1(x)$ shown in Figure 6-4.

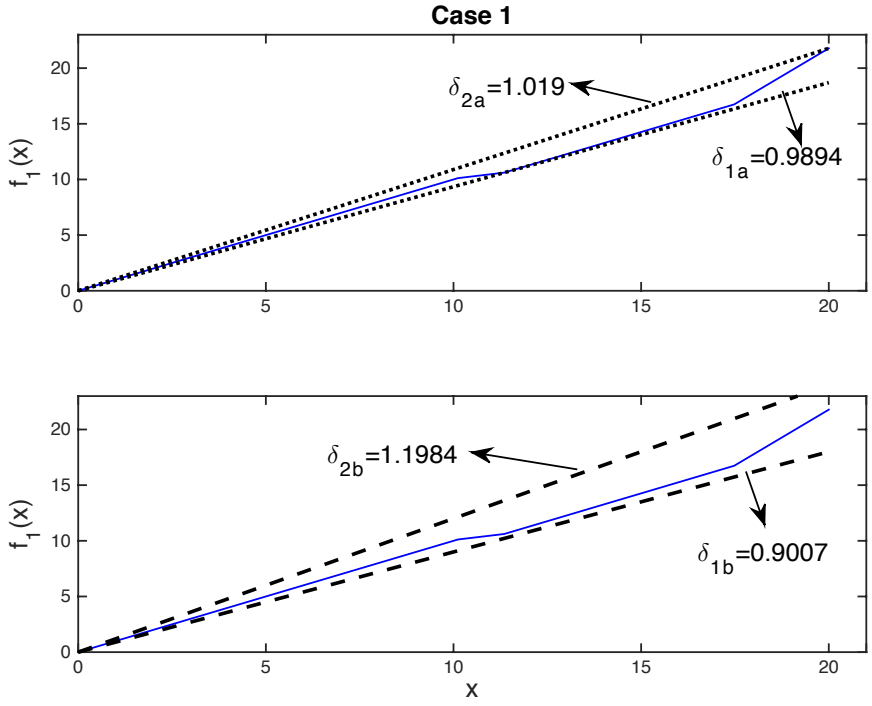

Figure 6-4 Nonlinearity in Case 1: (top) Boundedness Condition, (bottom) Continuity Condition.

From Figure 6-4, it can be verified that $f_1(x)$ belongs to $\mathcal{R}_0$. Moreover, based on Eq. (6.19), it can be verified that $f_1(x)$ is instantaneously inside $\{\delta_{1a} + \tau, \delta_{2a} - \tau\}$, where $\delta_{1a} = 0.9894$, $\delta_{2a} = 1.019$, and $\tau = 0$. In other words $f_1(x)$ is instantaneously inside $\{0.9894,1.019\}$. Moreover, based on the definition in Eq. (6.21), $f_1(x)$ is instantaneously incrementally $\{\delta_{1b} + \tau, \delta_{2b} - \tau\}$, where $\delta_{1b} = 0.9007$, $\delta_{2b} = 1.1984$, and $\tau = 0$. In other words $f_1(x)$ is instantaneously incrementally inside $\{0.9007,1.1984\}$.

(ii.) Consider L in Eq. (6.26). Since L is a linear and time-invariant transfer function, it obviously belongs to $\mathcal{L}$. Next step is to check if L satisfies the circle conditions for the sectors $\{\delta_{1a}, \delta_{2a}\}$ and $\{\delta_{1b}, \delta_{2b}\}$ with offsets $\varepsilon_a, \varepsilon_b \geq 0$ for boundedness and continuity, respectively.

Since $\delta_{1a} = 0.9894 > 0$ and $\delta_{1b} = 0.9007 > 0$, therefore Eq. (6.23) must satisfy for positive constants ε_a and ε_b. In other words, for the boundedness

$$|L(j\omega) + 0.9965| \geq 0.0152 + \varepsilon_a \quad \forall\omega, \tag{6.27}$$

must be satisfied, and for the continuity

$$|L(j\omega) + 0.9723| \geq 0.1379 + \varepsilon_b \quad \forall\omega, \tag{6.28}$$

must be satisfied. For this, consider the graphical representation of the left hand side of Eqs. (6.27) and (6.28) as shown in Figure 6-5.

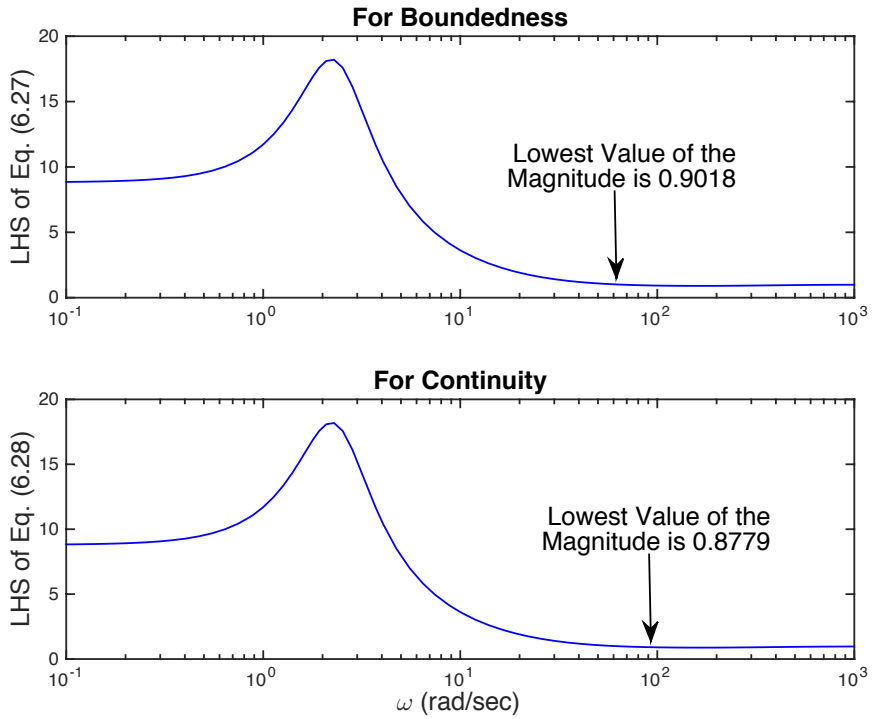

Figure 6-5 Graphical Representaion of the LHS of Eqs. (6.27) and (6.28).

Form Figure 6-5, if $0.0152 + \varepsilon_a$ is set to be equal to 0.9018 then Eq. (6.27) is satisfied. This mean $\varepsilon_a = 0.8866$, which is a positive value. Moreover, if $0.1379 + \varepsilon_b$ is set to be

equal to 0.8779 then Eq. (6.28) is satisfied. This mean $\varepsilon_b = 0.74$, which is also a positive value.

Additionally, the Nyquist diagram of $L(j\omega)$ does not encircle the points $\frac{-1}{2}\left(\frac{1}{\delta_{1a}} + \frac{1}{\delta_{2a}}\right) = -0.9965$ and $\frac{-1}{2}\left(\frac{1}{\delta_{1b}} + \frac{1}{\delta_{2b}}\right) = -0.9723$, since as shown in Figure 6-3, these points are not contained in the Nyquist diagram of $L(j\omega)$. Therefore, the second condition in Corollary 1 is satisfied for both continuity and boundedness

From circle conditions, the critical region for boundedness and continuity can also be obtained. Since δ_{1a} and δ_{1b} are non-zero, the complex plane is divided into two regions, one is a circular disk (which is the critical region) and the other one is the compliment of the circular disk (which is the permissible region). The center and radius parameters for the critical boundedness disk are $\frac{-1}{2}\left(\frac{1}{\delta_{1a}} + \frac{1}{\delta_{2a}}\right)$ and $\left|\frac{1}{2}\left(\frac{1}{\delta_{1a}} - \frac{1}{\delta_{2a}}\right)\right|$, respectively. The center and radius parameters for the critical continuity disk are $\frac{-1}{2}\left(\frac{1}{\delta_{1b}} + \frac{1}{\delta_{2b}}\right)$ and $\left|\frac{1}{2}\left(\frac{1}{\delta_{1b}} - \frac{1}{\delta_{2b}}\right)\right|$, respectively. For the closed loop to be bounded and continuous, the Nyquist plot of $L(j\omega)$ should not enter or encircle the critical regions for boundedness and continuity. This is shown in Figure 6-6 and Figure 6-7.

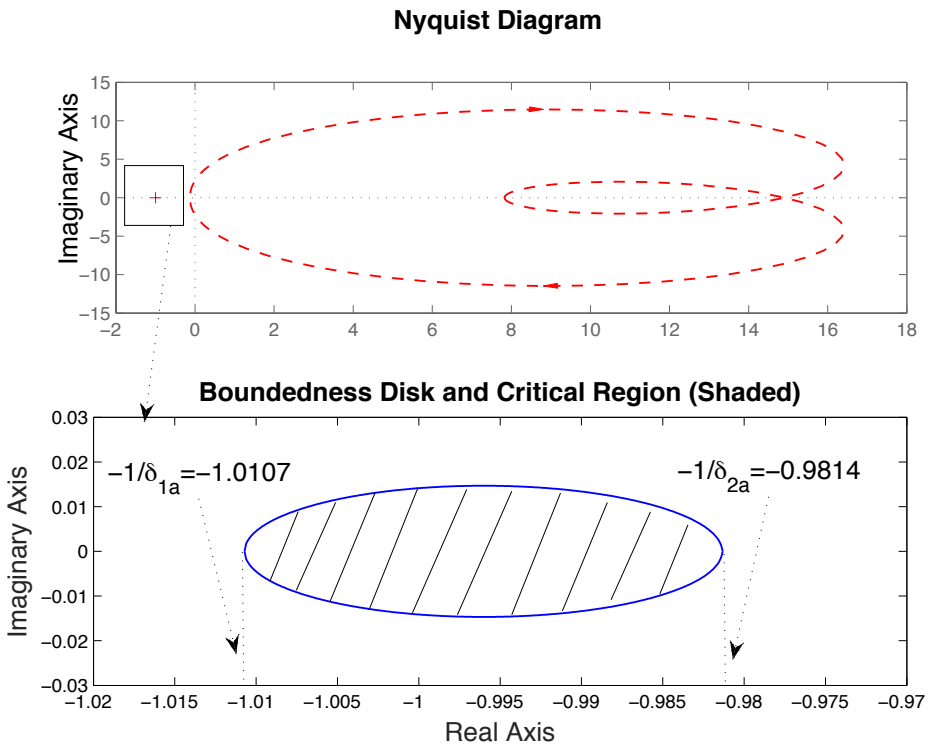

Figure 6-6 Boundedness Disk and Critical Region for Case 1.

In the top plot of Figure 6-6, the Nyquist plot of $L(j\omega)$ and the critical boundedness disk are shown together. It can be seen that $L(j\omega)$ does not enter or encircle the critical region. Since the disk is very small comparing to the Nyquist plot of $L(j\omega)$, to better visualize the critical region, the boundedness disk is shown separately in the bottom plot of Figure 6-6. The critical region is the shaded area inside the disk.

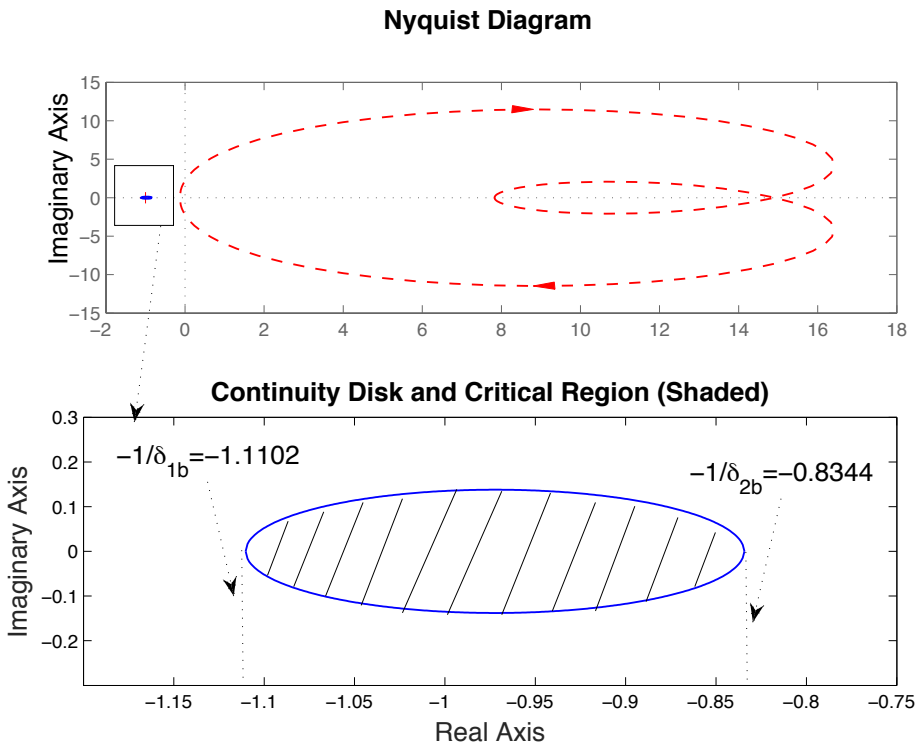

Figure 6-7 Continuity Disk and Critical Region for Case 1.

In the top plot of Figure 6-7, the Nyquist plot of $L(j\omega)$ and the critical boundedness disk are shown together. It can be seen that $L(j\omega)$ does not enter or encircle the critical region. Since the disk is very small comparing to the Nyquist plot of $L(j\omega)$, to better visualize the critical region, the boundedness disk is shown separately in the bottom plot of Figure 6-7. The critical region is the shaded area inside the disk. Moreover, shown in Figure 6-8 are the continuity and the boundedness disks together. The continuity disk has larger size than the boundedness disk; therefore the critical region for the continuity is also larger than the critical region for the boundedness.

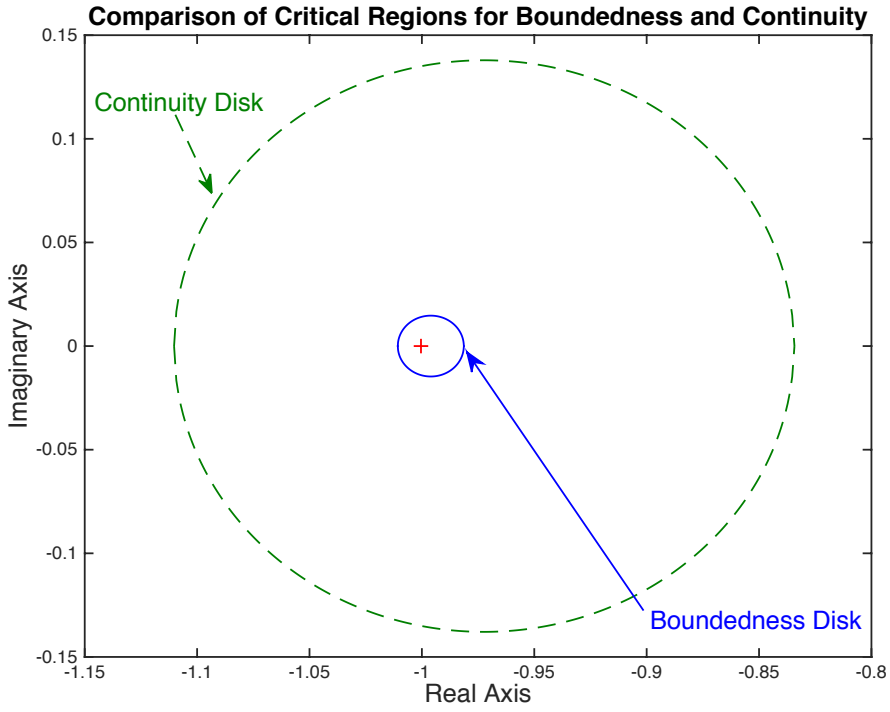

Figure 6-8 Comparison of Critical Regions for Boundedness and Continuity for Case 1.

(iii.) Since $\varepsilon_a = 0.8866$, $\varepsilon_b = 0.74$, and $\tau = 0$ are all non-negative constants and ε_a and ε_b are greater than zero, the last condition in Corollary is also satisfied.

Form (i.), (ii.) and (iii.), and based on Corollary 1, it can be concluded that the closed loop is L_2-bounded and also L_2-continuous. This can also be interpreted as the BIBO stability criterion.

6.3.2 Stability of the Feedback System with the Nonlinear Controller in Case 2

To evaluate the stability of the feedback system with the nonlinear controller in Case 2, three conditions of the Corollary 1 must be checked:

(i.) Consider $f_2(x)$ shown in Figure 6-9.

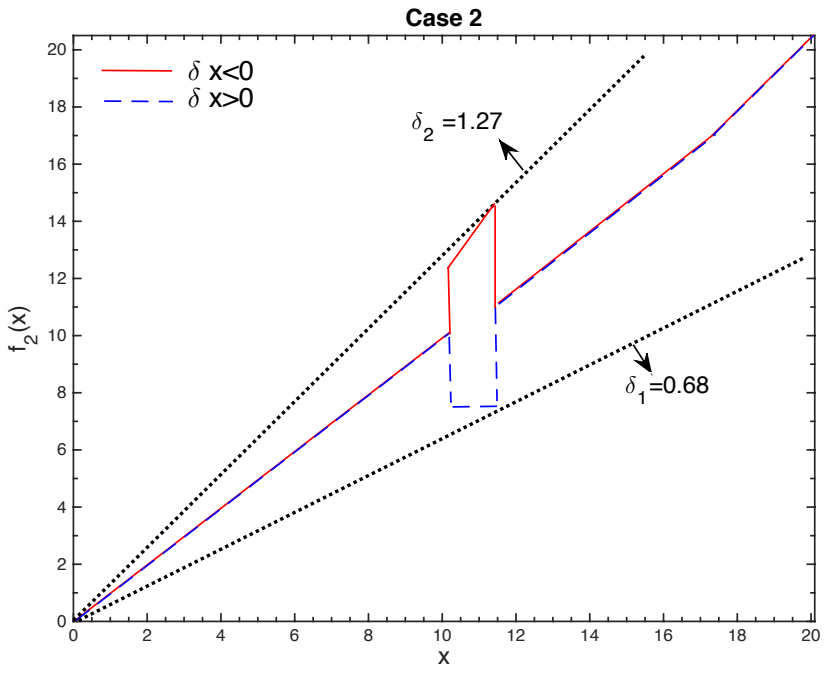

Figure 6-9 Nonlinearity in Case 2: Boundedness Condition.

From Figure 6-9, it can be verified that $f_2(x)$ belongs to $\mathcal{R}_0$. Moreover, from Eq. (6.19) it can be verified that $f_2(x)$ is instantaneously inside $\{\delta_1 + \tau, \delta_2 - \tau\}$, where $\delta_1 = 0.68$, $\delta_2 = 1.27$, and $\tau = 0$. In other words $f_2(x)$ is instantaneously inside $\{0.68,1.27\}$. However, since $f_2(x)$ is double-valued, and based on the definition in Eq. (6.21), N is not instantaneously incrementally inside any sectors. Therefore, no continuity conclusions can be drawn from Corollary 1 for this case.

(ii.) As mentioned in previous section, L belongs to $\mathcal{L}$. Next step is to check if L satisfies the circle condition for the sector $\{\delta_1, \delta_2\}$ with offset $\varepsilon \geq 0$. Since $\delta_1 = 0.68 > 0$, therefore Eq. (6.23) must satisfy for a positive constant ε. In other words, for the boundedness condition

$$|L(j\omega) + 1.129| \geq 0.3416 + \varepsilon \quad \forall\omega, \tag{6.29}$$

must be satisfied. For this, consider the graphical representation of the left hand side of Eq. (6.29) shown in Figure 6-10.

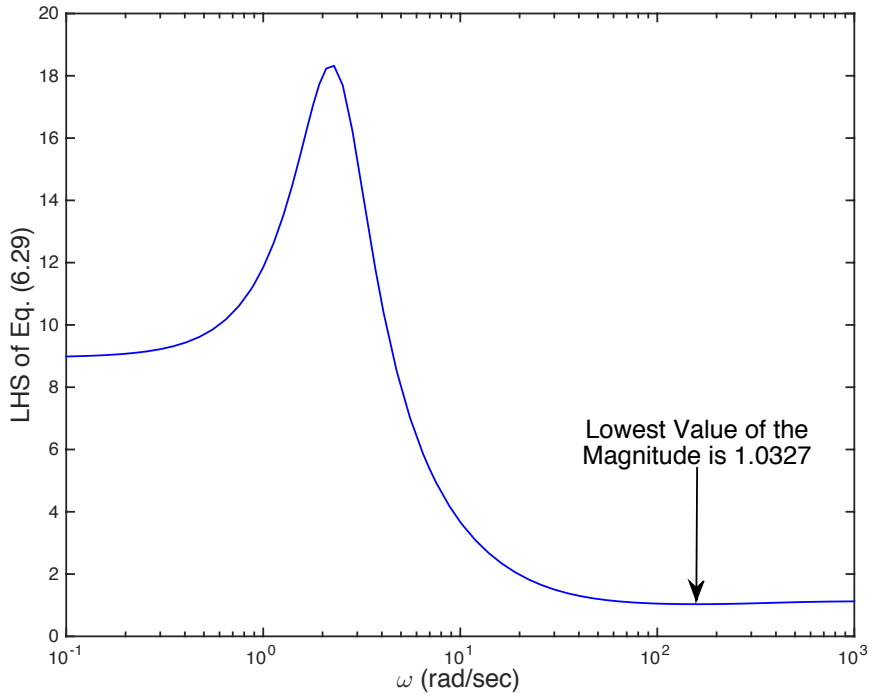

Figure 6-10 Graphical Representaion of the LHS of Eq. (6.29).

Form Figure 6-10, if $0.3416 + \varepsilon$ is set to be equal to 1.0327, then Eq. (6.29) is satisfied. This mean $\varepsilon = 0.6911$, which is a positive value.

Moreover, the Nyquist diagram of $L(j\omega)$ does not encircle the point $\frac{-1}{2}\left(\frac{1}{\delta_1} + \frac{1}{\delta_2}\right) = -0.129$, since as shown in Figure 6-3, this point is not contained in the Nyquist diagram of $L(j\omega)$. Therefore, the second condition in Corollary 1 is satisfied.

From circle conditions, the critical region for the boundedness can also be obtained. Since δ_1 is non-zero, the complex plane is divided into two regions, one is a circular disk (which is the critical region) and the other one is the compliment of the circular disk (which is the permissible region). The center and radius parameters for the critical boundedness disk are $\frac{-1}{2}\left(\frac{1}{\delta_1}+\frac{1}{\delta_2}\right)$ and $\left|\frac{1}{2}\left(\frac{1}{\delta_1}-\frac{1}{\delta_2}\right)\right|$, respectively. For the closed loop to be bounded, the Nyquist plot of $L(j\omega)$ should not enter or encircle the critical region. This is shown in Figure 6-11.

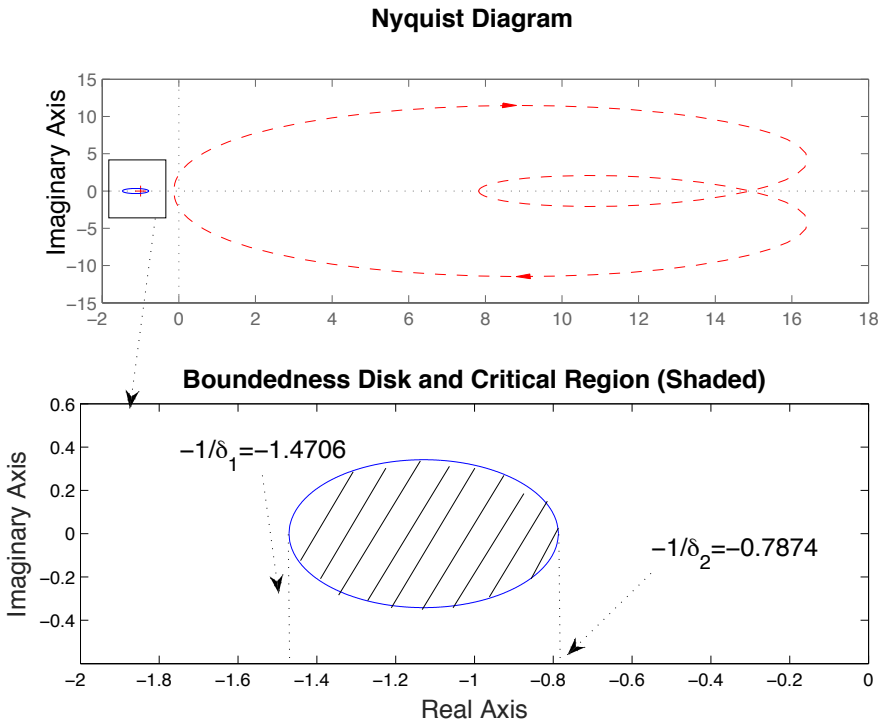

Figure 6-11 Boundedness Disk and Critical Region for Case 2.

In the top plot of Figure 6-11, the Nyquist plot of $L(j\omega)$ and the critical boundedness disk are shown together. It can be seen that $L(j\omega)$ does not enter or encircle the critical region. Since the disk is very small comparing to the Nyquist plot of $L(j\omega)$, to better

visualize the critical region, the boundedness disk is shown separately in the bottom plot of Figure 6-11. The critical region is the shaded area inside the disk. As mentioned earlier, since the nonlinear element is double-valued and hence not incrementally in any sector, no continuity disk can be obtained in this case.

(iii.) The last step is to check the third condition in Corollary 1. $\varepsilon = 0.6911$ and $\tau = 0$ are both non-negative constants and at-least one of them (ε) is greater than zero.

Form (i.), (ii.) and (iii.), and based on Corollary 1, it can be concluded that the closed loop is L_2-bounded. This can be interpreted as the BIBO stability criterion. However, as mentioned in (i.) no continuity conclusions can be made due to the double-valued nature of the nonlinearity in the feedback loop

It should be noted that the selection of ε and τ as mentioned above are not unique. In other words, different values of these two parameters can result in the same conclusion for the boundedness of the closed loop system. But this does not mean that any values can end up with conclusion that the closed loop is L_2-bounded. For example, by selecting a non-zero value for τ, same conclusion can be made for $\varepsilon = 0$. Doing this, the values of δ_1 and δ_2 must also be altered. More specifically, a smaller value for δ_1 and a larger value for δ_2 must be selected, to ensure that N lies instantaneously inside the sector $\{\delta_1 + \tau, \delta_2 - \tau\}$. These modifications in δ_1 and δ_2 make the critical region relatively larger comparing to what was shown in Figure 6-11, which can end up with more conservative results. The values that are presented above are for the tightest critical regions, and thereby the least conservative results drawn from Corollary 1.

6.4 Chapter Summary

Presented in this chapter is a theorem developed in [75, 76] that formulates sufficient conditions for the stability of the nonlinear feedback systems subject to external inputs. In particular, conditions on the open loop linear and nonlinear relations are found that result in the closed loop stability in the sense of BIBO. The results are used to evaluate the stability of nonlinear feedback systems designed in Chapter 5. For the feedback system with single-valued nonlinear controller, it is shown that the nonlinear feedback system satisfies sufficient conditions for both BIBO stability and continuity. For the second feedback system with double-valued nonlinear controller, on the other hand, only BIBO stability is concluded and no continuity conclusion can be made, due to the double-valued nature of the nonlinear controller.

Chapter 7. Conclusions and Future Works

In this dissertation a novel nonlinear controller design methodology is proposed. This controller design is conducted in the frequency domain. The class of the systems considered is the SISO linear regulating systems subject to time domain constraints. The proposed nonlinear controller design methodology is aimed to improve the closed loop performance of the system by increasing the allowable disturbance step size beyond what is obtained by a linear controller for a given level of disturbance step size.

The dissertation can be separated into two major sections. First, it is assumed that the gain and phase distortions of the nonlinear controller are known, and a discussion on the identification of the nonlinear controller to implement in the feedback loop is investigated. This is addressed in Chapters 2 and 3. The second part of the dissertation addresses a method for obtaining the required gain and phase distortions for the nonlinear controller that is covered in Chapters 4 and 5. A discussion to assess the stability of the closed loop nonlinear system is presented in Chapter 6.

The identification of the nonlinear controller from its gain and phase distortions information is based on the sinusoidal input describing function (SIDF) method. The SIDF method is a quasi-linearization of the nonlinear system that effectively minimizes the mean square error between the nonlinear system response and its linear description. The formulation for the SIDF is presented in Chapter 2. It is shown that the SIDF

representation of a nonlinear system can be considered as the gain and phase distortions in the response of the nonlinearity to the harmonic input signal.

An algorithm for identifying a nonlinear function from its gain and phase distortions information is developed in Chapter 3. This algorithm formulates a numerical solution to the inverse SIDF problem. Assuming that the gain and phase distortions of the nonlinear controller are known, a method for numerically solving the inverse SIDF problem is proposed that can identify an isolated static nonlinearity with or without memory. A major advantage of the developed algorithm is that, it does not require *a priori* knowledge or information of the class of the nonlinearity to initiate the identification process. The proposed solution provides a non-parametric representation of the static nonlinearity. The characteristics of the identified nonlinear function can be estimated from the non-parametric solution by LSE method. The proposed computational inverse SIDF algorithm is validated through different case studies in Chapter 3.

To obtain the gain and phase distortions of the nonlinear controller, first the issue of translating the time domain specifications in to the frequency domain characteristics is addressed. It is shown in Chapter 4 that the time domain performance requirements of the class of system considered in this research can be formulated in terms of lower and upper amplitude bounds on the open loop transfer function in the frequency domain. These lower and upper amplitude bounds create an acceptable design region for the frequency response of the open loop transfer function. Based on the intersection point of the lower an upper amplitude bounds, a method for predicting the level of performance prior to the controller design is also discussed, therefore, a linear controller can be designed through

H_∞ controller design approach. Additionally, a method of maximizing the disturbance step size achievable via a linear controller through H_∞ controller design approach is proposed in Chapter 4.

The proposed nonlinear controller methodology in the frequency domain is formulated in Chapter 5. The design goal is to improve regulating performance beyond what is achievable by a linear control for a given level of disturbance step size. The controller design is executed by imposing required gain and phase distortions on the frequency response of linear open loop transfer function to enforce the time domain constraint. A method is proposed that translates the increase in the disturbance step size to the gain and phase distortions due to the nonlinearity. The inverse SIDF algorithm developed in Chapter 3 is employed to identify an isolated explicit nonlinearity that is associated with the obtained gain and phase distortions.

The proposed deign technique is validated on the idle speed control of a V-6 fuel injected engine model subject to an external torque load disturbance. In Chapter 4, the allowable disturbance step size for this system is estimated and a linear controller is designed for this level of disturbance step size. In Chapter 5, a four percent increase in the step distance size is considered and a nonlinear controller is designed such that all the performance requirements of the system are satisfied for the resultant modified (augmented with nonlinear controller) feedback system.

At the end, a discussion to assess the stability of the closed loop systems containing nonlinear elements, such as those designed in Chapter 5 is presented in Chapter 6. The stability assessment provides sufficient conditions for the BIBO stability of the nonlinear

feedback systems subject to nonzero external inputs. Similar to the proposed controller design methodology, the discussed stability analysis tool is in the frequency domain and it provides closed loop stability guarantees using the Circle theorem.

7.1 Contributions

The major outcome of this work is a novel approach for designing nonlinear controllers in the frequency domain for SISO linear regulating systems subject to time domain constraints. The following achievements are accomplished:

- *Inverse Sinusoidal Input Describing Function Algorithm:* A computational inverse SIDF algorithm to identify (estimate) the nonlinear functions based on their gain and phase distortions information is developed that identifies an isolated static nonlinearity in the range of the amplitude of the input signal. The output solution is a non-parametric model of the nonlinearity, from which a parametric model can be obtained via LSE method.
- *Disturbance Step Size Maximization through H_∞:* By introducing two scalars in the weighting functions in the mixed sensitivity H_∞ optimization problem, an iterative process in proposed by which the disturbance step size achievable by linear controllers can be maximized.
- *Defining the SIDF Gain and Phase Distortions of the Nonlinear Controller:* A method of obtaining the gain and phase distortions of the nonlinear controller is formulated with the goal to improve the closed loop performance for a regulating system subject to time domain constraints. For this, three different options for

defining nonlinear control laws are formulated. The nonlinear controller designed will be augmented to an already designed linear controller to increase the capability of the closed loop system for handling larger external disturbances. From the proposed methodology, both single-valued and double-valued nonlinear controllers can be designed. One main advantage of the proposed technique is that the structure of the nonlinear controller is not preconceived and will be determined by the developed inverse SIDF solution.

- *Amplitude Calculations:* To use the inverse SIDF algorithm to identify the nonlinear controller, the amplitude of the input signal must be obtained. For nonlinear functions, this amplitude is depended on the SIDF representation of the nonlinearity. The calculation of this amplitude becomes more complicated in the feedback loop. A method to overcome this challenge is formulated in this dissertation.
- *Performance Improvement via Nonlinear Control:* To illustrate the proposed methodology, the idle speed control of a V-6 fuel injected engine model subject to an external torque load disturbance is considered. It is shown that for the linear feedback system, nonlinear controllers can be designed such that the augmented closed loop system can maintain system performance requirements for larger values of step disturbance. Two nonlinear controllers (single-valued and double-valued) are designed for the example problem considered.
- *Stability Analysis:* The sufficient conditions for the linear and nonlinear elements in the feedback loop that result in the BIBO stability and continuity of the closed loop are presented in the form of a theorem and a corollary. From this, the BIBO stability

of the designed nonlinear feedback systems is concluded. It is shown that the continuity results cannot be made for the systems with double-valued nonlinearities, since this class of nonlinearities does not incrementally instantaneously belong to any sectors.

7.2 Recommendations for Future Works

From the results presented in Chapter 4 and Chapter 5, if the nonlinear controllers were built around G_{C2} instead of G_{C1}, higher closed loop performances would have been achieved. For this, the actual impact of the time domain parameters $\widetilde{k_1}$ and $\widetilde{k_2}$ in the frequency domain (i.e., upper and lower bounds) must be determined. In other words, the relationship between $\widetilde{k_1}$, $\widetilde{k_2}$ and Λ_u, Λ_y defined in Eqs. (4.17) and (4. 22) must be specified in order to impose required gain and phase distortions on the linear open loop transfer function. In fact, introducing $\widetilde{k_1}$ and $\widetilde{k_2}$ in the performance weighting functions in H_∞ mixed sensitivity optimization problem can be viewed as relaxing the assumption of setting Λ_u and Λ_y to one, as discussed in Chapter 4. Unfortunately, the actual relationship between these pairs of parameters are not clear, due to the intrinsic incompatibilities between time and frequency domains. Without this relationship, the values of Λ_u and Λ_y cannot be obtained $\widetilde{k_1}$ and $\widetilde{k_2}$, hence the gain and phase distortion cannot be defined. Formulating this relationship is an interesting subject for future research.

The formulation presented in Chapter 3 considers a numerical solution for inverse SIDF problem for static (explicit) nonlinearities. Extensions of this approach for

dynamics (implicit) nonlinearities further extend inverse SIDF applications. A dynamic nonlinearity can be represented by

$$y = y(x, \dot{x}, \ddot{x}, \dots). \tag{7.1}$$

From Eq. (7.1), it can be inferred that the describing function of a dynamic nonlinearity is a function of both frequency and amplitude of the input signal ($x(t)$). Consequently, the coefficients of the Fourier expansion of the nonlinear function response to the harmonic input are also function of both amplitude (A) and frequency (ω) of the input signal. This makes the modified integral transformations from presented in Chapter 3 more complicated. One possible approach to formulate a numerical solution for inverse SIDF problem for dynamic nonlinearities is to generate gain-phase plots for varying input amplitudes and consider the input frequency as a free parameter. This could be a research area of considerable interest.

The application of the proposed nonlinear control design methodology can be extended to uncertain systems. This can be achieved by modifying the formulations presented in Chapter 5 such that they account for the parametric uncertainty in the system dynamics. If a compact set of parametric uncertainties in the system are represented by $\alpha \in \Omega$, then the upper and lower amplitude bounds define in Chapter 4 must be determined for all values of $\alpha \in \Omega$ at any given frequency. These bounds can be used to form a composite upper and lower amplitude bounds on the nominal open loop transfer function, $L_0(j\omega_k) = G_C(j\omega_k)G_{U_0}(j\omega_k)$, where $G_{U_0}(j\omega_k)$ is the nominal plant transfer function, i.e., $G_{U_0}(j\omega_k) = G_U(j\omega_k, \alpha = \alpha_0)$. This can be accomplished by some

modifications in the gain and phase of the upper and lower bounds. The gain modification can be written as [68]

$$\left|\frac{G_{U_0}(j\omega)}{G_U(j\omega_k,\alpha_i)}\right|, \tag{7.2}$$

and the phase modification can be expressed by

$$\angle\left(\frac{G_{U_0}(j\omega)}{G_U(j\omega_k,\alpha_i)}\right). \tag{7.3}$$

The composite upper and lower bounds can be developed by modifying the formulations presented in Chapter 4 using Eqs. (7.2) and (7.3). The acceptable design region at each frequency will also be developed based on these composite bounds. To satisfy the performance requirements, the nominal open loop transfer function, $L_0(s)$, must be contained in the acceptable composite design region [68]. Consequently, the nonlinear control law as presented in Chapter 5, must be defined such that the frequency response of the modified nominal open loop transfer function is contained in the composite acceptable design region.

The method for calculating the amplitude of the input signal to the nonlinearity in the feedback loop, as described in Chapter 5, can be improved. Due to the approximation nature of the SIDF method and because of the assumptions made in calculating the amplitude of the input signal to the nonlinearity, it was observed that in some cases the formulation for the amplitude derivation in the feedback loop fails to work. For example, if the disturbance step size is larger than a threshold and the objective is to define the

nonlinear control law for options one or three (i.e., cases involving phase distortions), then the resultant gain and phase distortions of the nonlinear controller will not have a monotonous trend, which is physically infeasible. Therefore it is important to investigate a more exact way to obtain the amplitude of the input signal to the nonlinearity in the feedback loop.

REFERENCES

[1] J. W. Glass, "Frequency Based Nonlinear Controller Design for Regulating Systems Subject to Time Domain Constraints," PhD Dissertaion, Purdue University, December 2000.

[2] K. Ogata, "Modern Control Engineering," *Prentice Hall, Upper Saddle River, New Jercy,* 4th ed., 2001.

[3] B. J. Lurie, "Feedback Maximization," *Artech House Inc.,* 1986.

[4] J. E. Slotine and W. Li, "Applied Nonlinear Control," *Prentice Hall, Englewood Cliffs, New Jercy,* 1991.

[5] K. J. Astrom and B. Wittenmark, "Adaptive Control," *Addison-Wesley, New York,* 1995.

[6] G. Gu, A. G. Sparks, and S. S. Banda, "Bifurcation Based Nonlinear Feedback Control of Rotating Stall in Axial Flow Compressors," *Proceeding of the American Control Conference,* pp. 1524-1528, 1997.

[7] D. Liaw and E. H. Abed, "Active Control of Compressor Stall Inception: A Bifurcation Theoretic Approach," *Automatica,* vol. 32, no. 1, pp. 109-115, 1996.

[8] J. W. Glass and M. A. Franchek, "Frequency-based Nonlinear Controller Design for Regulating Systems Subject to Time-Domain Constraints," *Int. J. Robust Nonlinear Control,* vol. 10, pp. 39-57, 2000.

[9] A. Gelb and W. E. Vander Velde, "Multiple Input Describing Functions and Nonlinear System Design," *McGraw-Hill Book Co. New York*, 1968.

[10] J. C. Hsu and A. U. Meyer, "Modern Control Principles and Applications," *McGraw-Hill Book Co. New York,* 1968.

[11] D. P. Atherton, "Nonlinear Control Engineering," *Van Nostrand Reinhold Co,* 1975.

[12] D. P. Atherton, "Design of Nonlinear Controllers using Harmonic Balance Plant Models," *American Control Conference,* pp. 5115-3116, Green Valley, AZ, 1994.

[13] O. Nanka-Bruce and D. P. Atherton, "Design of Nonlinear Controllers for Nonlinear Plants," *11th IFAC World Congress*, Tallinn, vol. 6, pp. 75-80, August 13-17, 1990.

[14] M. Zhuang and D. P. Atherton, "CAD of Nonlinear Controllers for Nonlinear Systems," *UKACC International Conference on Control*, pp. 545-550, September 2-5, 1996.

[15] J. H. Taylor, "Robust Nonlinear Control Based on Describing Function Methods," *ASME IMECE, Dynamic Systems and Control Division*, Anaheim, CA, vol. 64, November, 1998.

[16] A. Nassirharand and H. Karimi, "Nonlinear Controller Synthesis Based on Inverse Describing Function Technique in the MATLAB Environment," *Advances in Engineering Software,* vol. 37, no. 6, pp. 370-374, 2006.

[17] J. W. Glass and M. A. Franchek, "Stability of Nonlineat Feedback Systems in a Volterra Representaion," *Int. J. Robust Nonlinear Control,* vol. 10, pp. 799-819, 2000.

[18] J. W. Glass and M. A. Franchek, "H_∞ Synthesisz of Nonlinear Feedback Systems in a Volterra Representation," *J. Dyn. Sys., Meas., Control (ASME)*, vol. 124, pp. 382-389, September, 2002.

[19] P. Herman and M. A. Franchek, "Performance Enhancement of Fixed Regulating Systems via Actuator Saturation," *J. Dyn. Sys., Meas., Control (ASME),* vol. 121, no. 1, pp. 34-40, March, 1999.

[20] M. A. Franchek, "Robust Linear Control Design," Lecture Notes, University of Houston, Fall 2012.

[21] C. Goldfarb, "On Some Nonlinear Phenomena in Regulatory Systems," *Automatika i Telemekhanika*, vol. 8, no. 5, pp. 359-383, Sep-Oct, 1947.

[22] W. Opplet, "Locus Curve Method for Regulators with Friction," *J. Inst. Elect. Eng. London,* vol. 94, part II A, no.1 and 2, May, 1947.

[23] A. Tustin, “The Effects of Backlash and Speed Development Friction on the Stability of Closed-Cycle Control Systems,” *J. Inst. Elect. Eng. London*, vol. 94, part II A, no. 1, 1947.

[24] J. Dutilh, “Theorie des Servomecanismes a Relais,” *L’Onde Electrique,* vol. 30, pp. 438-445, 1950.

[25] C. Ecary, “Etude Graphique du Regime Transitoire d’un System Non-lineaire,” *C. E. M. V., Service Technique Aeronautique,* no. 10, 1950.

[26] R. Kochenburger, “Frequency Response Method for Analysis of a Relay Servomechanism,” *Trans. AIEE*, vol. 69, pp. 270-283, 1950.

[27] R. C. Booton, “Nonlinear Control Systems with Random Inputs,” *IEEE Transactions on Circuit Theory, IRE*, vol. 1, no. 1, pp. 9-18, March,1954.

[28] R. L. Haussler, “Stabilization of Nonlinear Systems by Means of a Second Nonlinearity,” Control and information system lab report, Purdue Univerity.

[29] S. R. Sanddres, “On Limit Cycle and Describing Function Method in Periodiacally Swithced Circuits,” *IEEE Transactions on Circuits and Sytesm, Fundamental Theory and Applications,* vol. 40, no. 9, September, 1993.

[30] X. Wei and J. E. Mottershead, “Limit Cycle Assignment in Nonlinear Aeroelastic System Using Describig Functions and the Receptance Method,” *Conference Proceedings of the Society for Exprimental Mechanics Series,* pp. 701-713, June, 2013.

[31] A. R. Bergen and R. L. Franks, "Justification of the Describing Function Method," *SIAM J. Conrol,* vol. 9, no. 4, November, 1971.

[32] A. Udrea, C. Lupu, and D. Popescu, "Hysteresis Control of a (Ba/Sr)Tio3 Based Actuator: A Comparison of Prandtl-Ishlinskii and Nonlinear Compensator Numerical Methods," *Proceeding of the 18th IFAC World Congress,* vol. 18, pp. 12733-12738, Milano, Italy, August 28-September 2, 2011.

[33] J. M. Giron-Sierra, J. Recas, and S. Esteban, "Iterative Method Based on CFD Data for Assesment of Seakeeping Control Effects, Considering Amplitude and Rate Saturation," *Int. J. Robust. Nonlinear Control*, vol. 21, pp. 1562-1573, 2011.

[34] T. Tain-Sou, "Model Based Adaptive Piecewise Linear Controller for Complicated Control Systems," *Journal of Applied Mathematics,* Atricle ID 120419, 2014.

[35] S. H. Teh, S. Malawaraarachci, W. P. Chan, and A. Nassirharand, "Design and Instrumnetation of a Benchmark Multivariable Nonlinear Control Laboratory," *International Conference on Intelligent Control System Engineering, World Academy of Science, Engineering and Technology,* vol: 4, 2010.

[36] T. Tain-Sou, "Adaptive Piecewise Linear Controller for Servo Mechanical Control Systems," *Journal of Applied Mathematics and Physics,* vol. 1, pp. 85-92, 2013.

[37] S. C. Li and A. Nassirharand, "Nonlinear Proportional-Integral-Derivative Synthesis for Unstable Non-Linear System Using Describing Function Inversion with

Exprimental Verification," *Journal of Systems and Control Engineering*, vol. 226, no. 2, pp. 145-153, 2012.

[38] D. P. Atherton, "Comment on Describing Function Inversion," *Electronics Letters*, vol. 6, pp. 779-780, 1970.

[39] D. P. Atherton, "Inverse Random Descrbing Function," *Electronics Letters*, vol. 10, no. 6, pp. 82-83, 1974.

[40] D. P. Atherton, "The Inverse Multiple Input Descrbing Function Problem," *Int. J. Control*, vol. 21, no. 3, pp. 385-390, 1975.

[41] A. Nassirharand, "Matlab Software for Inversion of Describing Function," *Advances in Engineering Software,* vol. 40, pp. 600-606, 2009.

[42] L. A. Zadeh, "On the Identification Problem," *IRE Trans. On Circuit Theory*, vol. CT-3, pp. 277-281, December, 1956.

[43] J. E. Gibson, E. S. DiTada, J. C. Hill, and E. S. Ibrahim, "Describing Function Inversion: Theory and Computational Techniques," Control & Information Systems Lab., TR-EE62-1D, Purdue University, Lafayette, IN, December 1962.

[44] J. E. Gibson, "Nonlinear Automatic Control," *McGraw-Hill Book Co.,* 1963.

[45] J. E. Gibson and E. S. DiTada, "On the Inverse Descrining Function Problem," *2nd IFAC Conference,* Basle, 1963.

[46] D. P. Atherton, "The Evaluation of the Response of Single-Valued Nonlinearities to Several Inputs," *The Institution of Electrical Engineers,* Monograph no. 474M, pp. 146-157, October, 1961.

[47] M. J. Somerville and D. P. Atherton, "Multi-gain Representation for a Single-Valued Nonlinearity with Several Inputs, and the Evaluation of Their Equivalent Gains by a Cursor Method," *The Institution of Electrical Engineers*, pp. 537-549, July, 1958.

[48] J. L. Douce, "A Note on the Evaluation of the Response of a Nonlinear Element to Sinusodial and Random Signals," *The institution of Electrical Engineers*, pp. 88-92, October, 1957.

[49] M. Vidyasagar, "Optimal Rejection of Persistent Bounded Disturbances," *IEEE Trans Automatic Control*, vol AC-31, pp. 527-534, June, 1986.

[50] S. Jayasuria S and M. A. Franchek, "Frequency Domain Design for Prespecified State and Control Constraints Under Persistent Bounded Disturbances," *Proceeding of the 27th IEEE Conference in Decision and Control*, Austin, TX, December, 1988.

[51] S. Jayasuria S and M. A. Franchek, "Frequency Domain Design for Maximal Rejection of Persistent Bounded Disturbance," *Jorubnal of Dynamics, Systems, Measuremtns, and Control*, vol. 113, no. 2, pp. 195-205, 1991.

[52] M. Sobhani and S. Jayasuria, "Incorporating Right Half-Plane Poles and Zeros in a Frequency Domain Design Technique," *Jorubnal of Dynamics, Systems, Measuremtns, and Control*, vol. 116, no.4, pp.593-601, 1994.

[53] Y. Zhao and S. Jayasuria, "Stabilizability of Unstable Linear Plants Under Bounded Control," *Jorubnal of Dynamics, Systems, Measurements, and Control*, vol. 117, no. 1, pp. 63-73, 1995.

[54] I. Horowitz and M. Sidi, "Synthesis of Feedback Systems with Large Plant Ignorance for Prescribed Time Doiman Tolerance," *International Journal of Control*, vol. 16, no. 2, pp. 278-309, 1972.

[55] O. Yaniv and I. Horowitz, "Quantitative Feedback Theory: Reply to Criticisms," *International Journal of Control*, vol. 46, no. 3, pp. 945-962, 1987.

[56] I. Horowitz, "Survey of Quantitative Feedback Theory (QFT)," *International Journal of Control*, vol. 53, no. 2, pp. 255-291,1991.

[57] I. Horowitz, "Quantitative Feedback Design Theory (QFT)", vol. 1, *QFT Publications, Boulder. CO*, 1993.

[58] I. Horowitz and M. Sidi, "Optimum Synthesis of Non-Minimum Phase Feedback Systems with Plant Uncertainty," *International Journal of Control*, vol. 27, no. 3, pp. 361-386, 1978.

[59] G. Amos and I. Horowitz, "Optimization of the Loop Transfer Fucntion," *International Journal of Control*, vol. 31, no. 2, pp. 389-398, 1980.

[60] S. Jayasuria, "QFT Type Design for Maximizing Tolerable Disturbances in Structered Uncertain Systems," *International Journal of Control*, vol. 56, no. 1, pp. 67-85, 1992.

[61] M. A. Franchek, P. Herman, and O. Nwokah, "Robust Non-Diagonal Controller Design for Uncertain Multivariable Regulating Systems," *ASME Journal of Dynamic Systems Measurement and Control*, vol. 119, pp. 80-85, 1997.

[62] M. Shah and M. A. Franchek, "Frequency Based Controller Design for a Class of Hammerstein Type Nonlinear Systems," *Int. J. of Robust and Nonlienar Control*, vol. 9, no. 12, pp. 825-840, 1999.

[63] G. K. Hamilton and M. A. Franchek, "Designing Robust Speed Controllers for Internal Combustion Engines," *ASME International Mechanical Engineering Congress and Exposition Proceeding Dynamics Systems and Control Division*, vol. 57-1, pp. 275-282, 1995.

[64] J. W. Glass and M. A. Franchek, "NARMAX Modeling and Robust Control of Interal Combstion Engine," *Int. J. of Control,* vol. 72, no. 4, pp. 289-304, 1999.

[65] M. A. Franchek, "Selecting the Performance Weights for the μ and H_∞ Synthesis Methods for SISO Regulating Systems," *J. Dyn. Syst., Meas., Control (ASME),* vol. 118, pp. 126-131, 1996.

[66] J. M. de Bedout and M. A. Franchek, "Stability Conditions for Sequential Design of Non-Diagnol Multivariable Feedback Controllers," *International Journal of Control*, vol. 75, no. 12, pp. 910-922, 2002.

[67] S. Jayasuriya and J. W. Song, "On the Synthesis of Compensators for Nonovershooting Sterp Response," *J. Dyn. Sys., Meas., Control (ASME),* vol. 118, pp. 757-763, 1996.

[68] M. A. Franchek and P. Herman, "Direct Connection Between Time-Domain Performance and Frequency-Domain Characteristicts," *Int. J. Robust Nonlinear Control,* vol. 8, no. 12, pp. 1021-1042, October, 1998.

[69] M. Sobhani and S. Jayasuriya, "On the Application of Frequency Domain Controller Design Methodology to Non-Minimum Phase and Unstable Systems," *In the Proccedong of the ACC*, pp. 632-638, 1990.

[70] R.E. Nordgren, M. A. Franchek, and O. D. I. Nwokah, "A Design Procedure for the Exact H_∞ SISO Robust Performnace Problem," *Int. J. Robust Nonlinear Control,* vol. 5, no. 2, pp. 107-118, 1995.

[71] J. C. Doyle, B. A. Francis, and A. R. Tannenbaum, "Feedback Control Theory," *Macmillan, New York,* 1992.

[72] S. J. Williams, D. Hrovat, C. Davey, D. Maclay, J. W. VanCrevel, and L. F. Chen, "Idle Speed Control Design Using an H_∞ Approach," *In the Proceeding of ACC, IEEE,* pp. 1950-1956, Pittsburgh, PA, USA, 1989.

[73] H. W. Bode, "Network Analysis and Feedback Amplifier Design," *D. Van Nostrand Co., New York,* 1945.

[74] D. P. Atherton, "Stability of Nonlinear Systems," *John Wiley, Research Studies Press,* 1981.

[75] G. Zames, "On the Input-Output Stability of Time-Varying Nonlienar Feedback Systems Part I: Conditions Derived using Concepts of Loop Gain, Conicity, and Positivity," *IEEE Trans Automatic Contol,* vol. AC-11, pp. 228-238, April, 1966.

[76] G. Zames, "On the Input-Output Stability of Time-Varying Nonlienar Feedback Systems Part II: Conditions Involving Circles on the Frequency Plane and Sector Nonlinearities," *IEEE Trans Automatic Contol*, vol. AC-11, pp. 456-476, July, 1966.

[77] A. M. Lyapunov, "Stability in Nonlinear Control Systems," *Princeton University Press*, Princeton, N. J., 1961.

[78] V. M. Popov, "Absolute Stability of Nonlinear Control Systems of Automatic Control," *Automatic and Remote Control*, vol. 22, pp. 857-858, 1962.

[79] W. Kaplan, "Advanced Calculus," *Addison-Wesley*, 4th ed., Reading, MA, 1992.

Appendix A.

Solution of $Q(x)$: Volterra's Integral Equation of the 1st Kind

Presented in this appendix are the details on the derivation of Eq. (3.27) from Eq. (3.24). For this, first consider Eq. (3.24) as follow

$$C(A) = \frac{2}{\pi A^2} \int_0^A \frac{xQ(x)}{\sqrt{A^2 - x^2}} dx. \tag{A.1}$$

Equation (A.1) can be rearranged as

$$\frac{\pi A^2}{2} C(A) = \int_0^A \frac{xQ(x)}{\sqrt{A^2 - x^2}} dx. \tag{A.2}$$

Next step is to multiply both sides of Eq. (A.2) by $H(A, \xi)$ and integrate both sides with respect to A. This results in

$$\int_0^\xi \frac{\pi A^2}{2} C(A)\, H(A, \xi) dA = \int_0^\xi dA \int_0^A \frac{xQ(x)}{\sqrt{A^2 - x^2}} H(A, \xi) dx. \tag{A.3}$$

The order of the integrals in the right hand side of Eq. (A.3) can be changed. This yields

$$\int_0^\xi \frac{\pi A^2}{2} C(A)\, H(A, \xi) dA = \int_0^\xi xQ(x) dx \int_x^\xi \frac{H(A, \xi)}{\sqrt{A^2 - x^2}} dA. \tag{A.4}$$

Equation (A.4) can be simplified, if $H(A,\xi)$ is selected such that $I = \int_x^{\xi} \frac{H(A,\xi)}{\sqrt{A^2-x^2}}\,dA$ becomes a constant value. For this consider the change of variables as $A^2 = y$ (that results in $dA = \frac{dy}{2\sqrt{y}}$) and $x^2 = \eta$. Using these in I as define above, produces

$$I = \frac{1}{2}\int_y^{\xi^2} \frac{H\left(\sqrt{y},\xi\right)}{\sqrt{y}} \frac{dy}{\sqrt{y-\eta}}. \tag{A.5}$$

Next, let define $G(y,\xi) \triangleq \frac{H(\sqrt{y},\xi)}{\sqrt{y}}$ and apply the change of variables $t = \frac{y-\eta}{\xi^2-\eta}$ (that results in $dt = \frac{dy}{\xi^2-\eta}$) and $1-t = \frac{\xi^2-y}{\xi^2-\eta}$ in Eq. (A.5). This yields to

$$I = \frac{1}{2}\int_0^1 G(y,\xi)t^{\frac{-1}{2}}(1-t)^{\frac{-1}{2}} \frac{dt}{(\xi^2-y)^{\frac{-1}{2}}}. \tag{A.6}$$

In Eq. (A.6), if $G(y,\xi)$ is set to be equal to $(\xi^2-y)^{\frac{-1}{2}}$, then I will be reduced to

$$I = \frac{1}{2}\int_0^1 t^{\frac{-1}{2}}(1-t)^{\frac{-1}{2}}dt. \tag{A.7}$$

Equation (A.7) can be solved by considering the definition of the Beta function. This functions is defined as

$$B(x,y) = \int_0^1 t^{x-1}(1-t)^{y-1}dt = \frac{(x-1)!\,(y-1)!}{(x+y-1)!} \quad \text{for } \mathrm{Re}(x), \mathrm{Re}(y) > 0. \tag{A.8}$$

Using Eq. (A.8) in Eq. (A.7) results in

$$I = B\left(\frac{1}{2},\frac{1}{2}\right) = \frac{1}{2}\frac{\left(\frac{-1}{2}\right)!\left(\frac{-1}{2}\right)!}{(0)!} = \frac{1}{2}\sqrt{\pi}\sqrt{\pi} = \frac{\pi}{2}. \tag{A.9}$$

Now, returning to the original variables yields

$$H(A,\xi) = A(\xi^2 - A^2)^{\frac{-1}{2}}. \tag{A.10}$$

Next, substituting Eq. (A.10) in to Eq. (A.4) results in

$$\int_0^{\xi} \frac{\pi A^3}{2} \frac{C(A)}{(\xi^2 - A^2)^{\frac{1}{2}}} dA = \frac{\pi}{2}\int_0^{\xi} xQ(x)dx. \tag{A.11}$$

Equation (A.11) can be rearranged as

$$\int_0^{\xi} \frac{A^3 C(A)}{(\xi^2 - A^2)^{\frac{1}{2}}} dA = \int_0^{\xi} xQ(x)dx. \tag{A.12}$$

Finally, taking derivative of both sides of Eq. (A.12) with respect to x, results in the solution of $Q(x)$ as

$$Q(x) = \frac{1}{x}\frac{d}{dx}\int_0^{\xi} \frac{A^3 C(A)}{(\xi^2 - A^2)^{\frac{1}{2}}} dA. \tag{A.13}$$

QED.

It is to be noted that Eq. (3.26) can be obtained from Eq. (3.23) by following the same procedure.

Appendix B.

Derivation of Equation (3.31)

Presented in this appendix are the details on the derivation of Eq. (3.31). First consider the followings:

Primer: Integration by Parts: In mathematical analysis, the integration by parts is used to transform one form of integral to another form, which is easier to analyze [79]. Let u and v be functions of x, i.e., $u = u(x)$ and $v = v(x)$, then

$$\int_{x_1}^{x_2} u\,dv = (uv)\Big|_{x_1}^{x_2} - \int_{x_1}^{x_2} v\,du, \tag{B.1}$$

where x_1 and x_2 are two arbitrary end points for integration.

Primer: Leibniz Integral Rule: In mathematical analysis, the Leibniz integral rule is used for differentiation under integration [79]. Let $f(x, y)$ be a function such that $\frac{\partial f(x,y)}{\partial y}$ exists and is continuous, then

$$\frac{d}{dy}\left(\int_{a(y)}^{b(y)} f(x,y)dx\right) = \int_{a(y)}^{b(y)} \frac{\partial f(x,y)}{\partial y}dx + f(b(y),y)\frac{db}{dy} - f(a(y),y)\frac{da}{dy}, \tag{B.2}$$

where a and b are functions of y.

Derivation of Eq. (3.31): Consider the integral in the left hand of side of Eq. (3.31). Using integration by parts, this integral can be written as

$$\int_0^x \frac{z^3 C(z)}{\sqrt{x^2 - z^2}}\, dz = -C(z) z^2 \sqrt{x^2 - z^2}\Big|_0^x + \int_0^x \sqrt{x^2 - z^2}\, d\big(z^2 C(z)\big). \tag{B.3}$$

The first term at the right hand side of Eq. (B.3) vanishes at both ends; therefore Eq. (B.3) reduces to

$$\int_0^x \frac{z^3 C(z)}{\sqrt{x^2 - z^2}}\, dz = \int_0^x \sqrt{x^2 - z^2}\, d\big(z^2 C(z)\big). \tag{B.4}$$

The next step is to utilize Leibniz integral rule to calculate the deravative of Eq. (B.4). This produces

$$\begin{aligned} &\frac{d}{dx}\int_0^x \sqrt{x^2 - z^2}\, d\big(z^2 C(z)\big) \\ &\qquad = \int_0^x \frac{x}{\sqrt{x^2 - z^2}}\, d\big(z^2 C(z)\big) + \sqrt{x^2 - x^2}\,.1 - \sqrt{x^2 - 0^2}.\,0. \end{aligned} \tag{B.5}$$

The second and third terms at the right hand side of Eq. (B.5) vanish. Moreover, x parameter in the first term at the right hand side of Eq. (B.5) can be moved outside the intergral, since it is not dependent on z. Therefore Eq. (B.5) can be simplified as

$$\frac{d}{dx}\int_0^x \sqrt{x^2 - z^2}\, d\big(z^2 C(z)\big) = x \int_0^x \frac{d\big(z^2 C(z)\big)}{\sqrt{x^2 - z^2}}\,. \tag{B.6}$$

QED.

Appendix C.

Numerical Data for the Nonlinear Controllers

The numerical data for the nonlinear controllers designed in Chapter 5 are presented in this appendix.

1. Definition of nonlinear control law for Case 1: The results are listed in Table C. 1.

Table C. 1. Defining Nonlinear Control Law for Case 1.

$\boldsymbol{\omega}\ \left(\frac{\boldsymbol{rad}}{\boldsymbol{sec}}\right)$	$\lvert\boldsymbol{L}\rvert\ (\boldsymbol{dB})$	$\measuredangle\boldsymbol{L}$ (°)	$\lvert\hat{\boldsymbol{L}}\rvert\ (\boldsymbol{dB})$	$\measuredangle\hat{\boldsymbol{L}}$ (°)
0	17.873085	0	17.9027	0
0.5	18.660700	8.855616791	18.660700	8.855616791
2	24.562354	-13.94886185	24.562354	-13.94886185
3	23.287996	-51.77861006	23.287996	-51.77861006
4	20.187304	-69.06950422	19.3066	-69.06950422
5	17.681929	-76.50537921	16.8036	-76.50537921
6	15.733216	-80.42513513	15.1572	-80.42513513
7	14.15860	-82.84876087	14.0553	-82.84876087
8	12.840305	-84.52362967	12.840305	-84.52362967
9	11.706232	-85.77617733	11.706232	-85.77617733
10	10.710438	-86.76856642	10.710438	-86.76856642
12	9.0199333	-88.29196556	9.0199333	-88.29196556

2. Definition of nonlinear control law for Case 2: The results are listed in Table C. 2.

Table C. 2. Defining Nonlinear Control Law for Case 2.

$\boldsymbol{\omega}\ \left(\frac{\boldsymbol{rad}}{\boldsymbol{sec}}\right)$	$\lvert\boldsymbol{L}\rvert\ (\boldsymbol{dB})$	$\measuredangle\boldsymbol{L}$ (°)	$\lvert\hat{\boldsymbol{L}}\rvert\ (\boldsymbol{dB})$	$\measuredangle\hat{\boldsymbol{L}}$ (°)
0	17.87308544	0	17.9027	0
0.25	18.07780338	4.905279259	18.09780338	4.905279259
0.5	18.66070015	8.855616791	18.660700	8.855616791
1	20.62398843	11.16362318	20.62398843	11.16362318
1.5	22.94449392	3.609747956	22.94449392	3.609747956
2	24.56235478	-13.94886185	24.56235478	-13.94886185
3	23.2879963	-51.77861006	23.2879963	-51.77861006
4	20.18730441	-69.06950422	19.45	-67
5	17.68192962	-76.50537921	17.04	-75.32
6	15.73321674	-80.42513513	15.385	-79.85
7	14.15860429	-82.84876087	14.042	-82.697
8	12.8403056	-84.52362967	12.8403056	-84.52362967
9	11.7062326	-85.77617733	11.7062326	-85.77617733
10	10.71043836	-86.76856642	10.71043836	-86.76856642
12	9.019933305	-88.29196556	9.019933305	-88.29196556
14	7.615068435	-89.46097648	7.615068435	-89.46097648

3. The SIDF gain and phase distortions of the nonlinear controller for Case 1: The results are listed in Table C. 3.

Table C. 3. SIDF Gain and Phase Distortions for the Nonlinear Controller in Case 1.

$\omega \left(\frac{rad}{sec}\right)$	A	$\rho_N = C(A)$
100000	0	1
10000	0.035	1
1000	0.335	1
100	3.575	1
40	6.925	1
20	8.85	1
18	9.045	1
16	9.24	1
14	9.43	1
12	9.63	1
10	9.85	1
9	9.975	1
8	10.125	1
7	10.315	0.999678676
6	10.595	0.996539929
5	10.965	0.995323474
4	11.53	0.995665404
3	12.455	1
2	14.265	1
1.5	15.69	1
1	17.48	1
0.5	19.25	1.000214862
0.25	19.84	1.000152179
0	20.05	1.000414079

4. The SIDF gain and phase distortions of the nonlinear controller for Case 2: The results are listed in Table C. 4.

Table C. 4. SIDF Gain and Phase Distortions for the Nonlinear Controller in Case 2.

$\omega\ \left(\frac{rad}{sec}\right)$	A	ρ_N	θ_N (°)	$C(A)$	$S(A)$
100000	0	1	0	1	0
10000	0.035	1	0	1	0
1000	0.335	1	0	1	0
100	3.575	1	0	1	0
40	6.925	1	0	1	0
20	8.85	1	0	1	0
18	9.045	1	0	1	0
16	9.24	1	0	1	0
14	9.43	1	0	1	0
12	9.63	1	0	1	0
10	9.85	1	0	1	0
9	9.975	1	0	1	0
8	10.125	1	0	1	0
7.8	10.16	1	0	1	0
7.6	10.195	1	0	1	0
7.4	10.23	1	0	1	0
7.2	10.27	1	0	1	0
7	10.315	0.9991	0.1518	0.9991	0.0026
6	10.58	0.9962	0.5751	0.9961	0.0099
5	10.95	0.9943	1.18538	0.9941	0.0206
4	11.525	0.9930	2.0695	0.9923	0.0359
3.9	11.555	0.9925	0	0.9925	0
3.8	11.635	0.9924	0	0.9924	0
3.7	11.715	0.9923	0	0.9923	0
3.5	11.895	0.9921	0	0.9921	0
3.4	11.995	0.992	0	0.992	0
3.3	12.1	0.9919	0	0.9919	0
3.2	12.21	0.9918	0	0.9918	0
3.1	12.33	0.9917	0	0.9917	0
3	12.455	0.9916	0	0.9916	0
2	14.265	0.9915	0	0.9915	0
1.5	15.69	0.9914	0	0.9914	0
1	17.48	0.9913	0	0.9913	0
0.5	19.25	1.001	0	1.001	0
0.25	19.84	1.002	0	1.002	0
0	20.05	1.004	0	1.004	0